UNIVERSIDAD DE PAVIA

FACULTAD DE INGENIERÍA

DEPARTAMENTO DE ELECTRÓNICA

GENERACIÓN DE SEÑALES DE RADIOFRECUENCIA CON DISPOSITIVOS FOTÓNICOS INTEGRADOS

SUPERVISORES:

Ing.Guido Giuliani

D.Jose Victor Rodríguez Rodríguez

Realizado por:

Mª Carmen Matencio Hernández

2009/2010

INDEX

FIGURE INDEX

CHAPTER 1

INTRODUCTION

Today's wireless communication systems are constantly increasing their penetration in everyday life, thanks to the prompt technology response to the increasing needs for bandwidth and mobility, with examples like mobile telephones, PDAs and indoor wireless communication systems. To allow for larger bandwidth of unlicensed parts of the RF spectrum, new systems are to be operated at frequencies centered around 40 GHz or 60 GHz. Hence, the need arises for new and compact sources for mm-wave signals, that must have high spectral purity (linewidth < 100 kHz, phase noise < 100 dBc @ 100 kHz offset), tuneability, compactness, low power consumption and low cost. Other important applications are in the fields of:

i)anti-collision car-borne radars (60 GHz)

ii)local oscillators for astronomic investigations (100-900 GHz range)

iii)THz applications (300-3000 GHz range).

iiii) Meteorology where these frequencies can be used to atmospheric monitoring due to the fact that the oxygen has a resonance frequency equal to 60GHz.

Among the possible technologies for mm-wave signal generation, the microelectronic approach can provide oscillators at 60 GHz (and up to a few hundreds GHz) that can be realized onto a single chip, the main disadvantage being the modest tuneability, and the poor scalability, i.e. a design suitable for 60 GHz cannot be easily pushed beyond 100 GHz.

.

The optoelectronic approach based on photomixing can be of great interest for its versatility, summarized by tuneability and scalability, and by the possibility of propagating the optical signals along an optical fiber to allow for remote generation of the mm-wave signal. The photomixing technique consist of generation of continuous wave mm-wave or terahertz radiation from two lasers, the beams are mixed together and focused onto a photomixer device which generates the mm-wave or terahertz radiation which frequency is equal to the difference of two laser frequencies ($|\nu 1 - \nu 2|$). One limitation of the basic photomixing approach lies in the spectral purity of the generated signal (which depends on the linewidths of the laser oscillators) that can be hardly reduced below 1 MHz. For applications that require a better spectral purity, more complex photomixing systems shall be used, including a reference RF signal source and an optoelectronic feedback loop (optical PLL) to stabilize the generated signal.

The present project is part of a research project funded by the Cariplo Foundation which principal goal is to demonstrate a new approach for the optoelectronic generation of mm-wave signals with high spectral purity, based on a modification of the photomixing scheme. The main idea is that two DFB lasers emitting at ν_1 and ν_2 can be phase-locked via mutual injection assisted by a Four-Wave-Mixing process that takes place in a third auxiliary DFB emitting at $\nu_{AUX} = (\nu_1+\nu_2)/2$. The first part of the project is devoted to the study of this technique, implemented by a single integrated photonic chip which includes different laser devices. First, the characterization of the integrated devices which have three DFB lasers has been done just as the experimental research of the Four-Wave-Mixing and Injection locking phenomenon as via to produce the phase-locked between two lasers. The other one is dedicated to the study of phase-locking between the modes of a Fabry-Perot laser without an externally injected signal measuring the contrast of the generated interferometric signal and also the linewidth of a Fabry Perot laser mode with an heterodyning method. We report on experiments that confirmed these research lines.

CHAPTER 2

GENERATION OF mm-WAVE SIGNALS USING MUTUALLY-COUPLED DFB LASERS

The main idea of the generation of mm-wave signals using coupled DFB is that two DFB lasers emitting at v1 and v2 frequencies can be phase locked via mutual injection assisted by a Four Wave Mixing (FWM) process that takes place in a third auxiliary DFB emitting at $v_{aux}=(v_1+v_2)/2$.

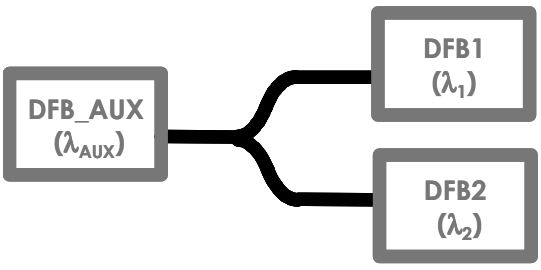

Figure 1: Scheme of mutual injection-locking assisted by FWM.

A conceptual scheme is shown in figure 1 where DFB1 and DFB2 are injected into DFB_AUX taking place FWM and clones of DFB1 and DFB2 are generated at the idler frequencies of, respectively, $v_{1'}=2v_{aux}-v_1$ and $v_{2'}=2v_{aux}-v_2$ (as is depicted in figure 2). When proper conditions are satisfied, DFB2 is

injection-locked by the clone signal of DFB1 and laser DFB1 is injection-locked by the clone signals of DFB2. In this condition the two lasers DFB1 and DFB2 are mutually coupled and it is expected that the beat signal generated by DFB1 and DFB2 is indeed spectrally pure radiofrequency (RF) signal.

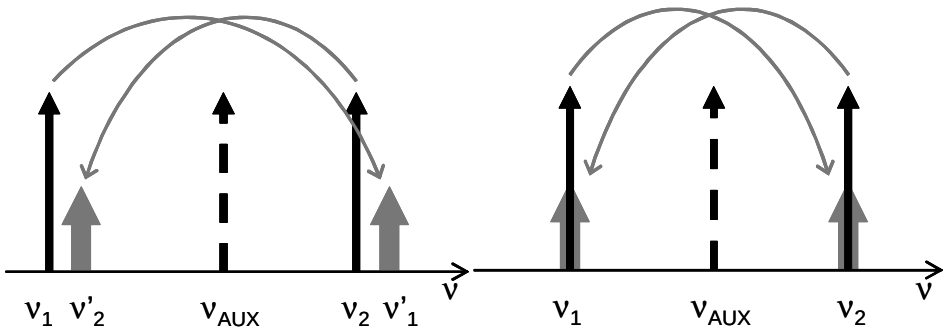

Figure 2 a) unlocking condition. b) mutual injection locking condition

The FWM is realized inside the DFB_AUX due to the non linear characteristic of semiconductor material. As has been explained, if the condition $f_{AUX}=(f_1+f_2)/2$ is fulfilled a phase locking between the lasers 1 and 2 is produced for mutual injection locking through FWM. The injection is mutual because the lasers 1 and 2 are coupled between themselves through their clone signal generate by FWM, and in laser 1 and 2 an external signal is injected, with an emission frequency equal to the frequency of the own laser, this effect is shown in the figure.

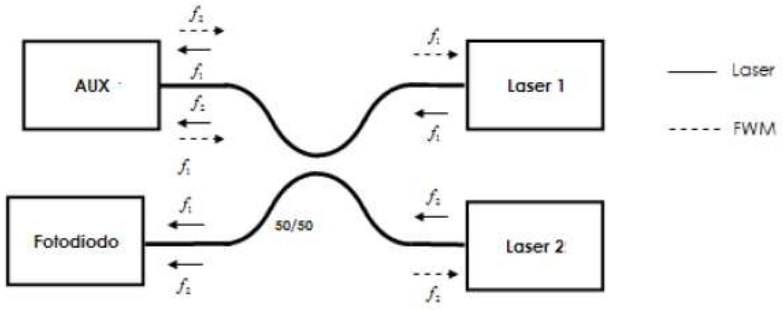

Figure 3: Schematic of mutual injection locking

The injection between lasers is reciprocal at all, and for this reason, it isn't possible to distinguish a master laser or a slave laser.

If the signals of lasers 1 and 2 are beating on a photodiode they produce an electrical signal at the frequency $f_{RF}=|f_1-f_2|$. As in this configuration the lasers are constantly injected by other lasers, in order to avoid a chaotic regime an optical attenuation in the path between lasers is needed. If this attenuation is variable it is possible to optimize it according to the detuning and emitting power of the lasers.

The RF signal will have a very high spectral purity, due to the fact that the laser 1 and 2 will have a constant phase difference, thanks to the mutual injection locking. Another advantage of this configuration is the behavior of DFB-AUX as optical amplifier when it is injected by lasers 1 and 2, thus partially compensating the attenuation underwent by the signal before being injected into DFB-AUX.

2.1. Results from hybrid setup

To demonstrate that an mm-wave signal can be generated with the above scheme, some previous experiments have been done in [1] with two experimental setups which are shown in figure 4 and 5.

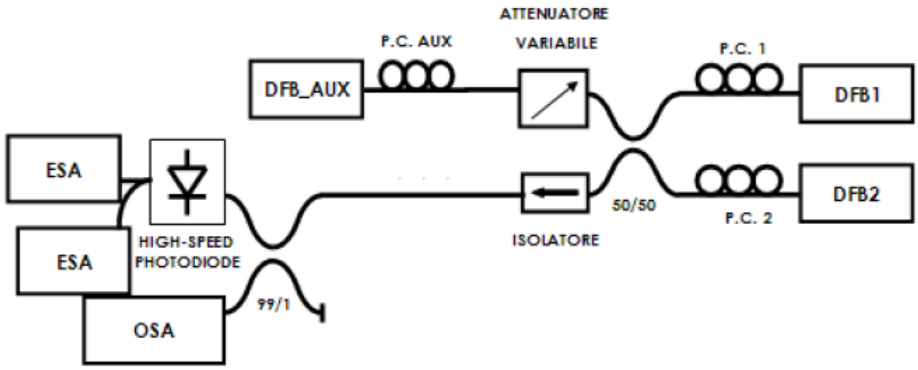

Figure 4: Experimental reciprocal setup

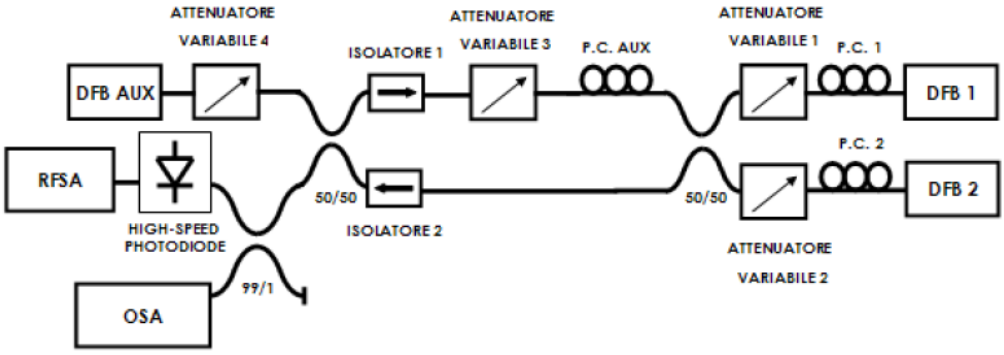

Figure 5: Experimental non reciprocal setup.

The principal advantage of reciprocal setup with respect to the non-reciprocal setup is that there exists only one way for all laser signals with the consistent reduction in the number of components and the possibility to integrate the system in a chip. This setup is composed of an only coupler, an attenuator before laser AUX, an isolator before the exit coupler to avoid the read instrument reflection and, finally, two polarization controllers because the polarization is a sensitive parameter of locking.

In these experimental setups a characterization of lasers DFB has been done giving special attention to its use as non-linear optical amplifier of externally injected signals. For a detuning of 10GHz the injected signals are amplified by 5dB while, for the same detuning, the FWM signals are amplified by 10dB with respect to the input signal.

Then, RF signals have been generated by the locking of two DFB lasers with a non reciprocal setup. The technique to check the locking condition is based on the observation of the spectrum of the electrical signals generated by the beating on a fast photodiode. For a moderated detuning, the beating between laser DFB_AUX and laser DFB1 or DFB2 has been observed, and the locking took place when the beating between DFB1-DFB_AUX and DFB2-DFB_AUX were perfectly overlapped (degenerating into one single signal). For larger detunings the beating between DFB2 and the generated clone by FWM of DFB1 has been observed. When the beating disappears, it means that the signals are at the same frequency and the locking has been produced. Then the locking range (the difference frequency range where lasers are locked) was analyzed.

Then the setup was changed to realize a reciprocal setup and the locking experiments were repeated. In the experiments done using this setup the possibility of mm-wave signal generation has been demonstrated up to 100 GHz, being impossible to explore other top frequencies due to measurement instruments. The locking effect over the beating signals between lasers DFB1 and DFB2 has been checked too, and it has been demonstrated that, with respect to an unlocking situation when the phase noise is added to one of the locked lasers, the signal generated over the spectrum analyzer screen

presents fewer disturbances in the adjacent frequencies and the linewidth is reduced to 50%.

All the results obtained in these experiments demonstrate that the photonic technology for the generation of mm-wave signals up to 100GHz (and beyond) is valid and it is going to be studied with more attention in this project. Therefore, the idea of generation of radiofrequency signals by the mutual coupling of DFB lasers assisted by FWM is an interesting technique also from a commercial point of view and its integration onto a single chip is the goal of the present project.

2.2. Integrated device

The requirements of modern wireless systems ask for the development of new integrated devices for the generation of mm-wave signals with a high spectral purity and potential low cost.

The production of photonic integrated semiconductor chip today is based on photolithography. In photolithography a high energy UV-light is shone through a mask onto a slice of III-V semiconductor covered with a photosensitive film. The mask defines the parts of the chip and the UV-light will only hit the areas not covered by the mask. When the film is developed, the areas hit by light are removed. Now the chip has unprotected and protected areas forming a pattern that is the first step to fabrication of the final components of the chip.

Next, the unprotected areas are processed so their geometrical and physical properties change. When all the components have been made and the circuit is complete a layer of metal is added. Just as before, a layer of photosensitive film is applied and exposed through a mask. However, this time the mask used describes the layout of the wires connecting all the

parts of the chip. The film is developed and the unexposed parts are removed. Next, the metal not protected with film is removed to form the wires. Finally, the chip is tested and packaged.

In the present project the integration of the experimental setup in a single chip has been done by the University of Glasgow. Its manufacture is done with lithographic techniques of high precision. This layout of the chip is shown in figure 6: it is composed by three DFB lasers, one coupler and three optical attenuators.

A distributed-feedback laser is a laser where the whole resonator consists of a periodic structure, which acts as a distributed reflector at a specific wavelength, and contains a gain medium. Typically, the periodic structure is realized with a $\lambda/4$ phase shift in its middle. This structure is essentially the direct concatenation of two Bragg gratings with internal optical gain. It has multiple axial resonator modes, but there is typically one mode which is favored in terms of losses. (This property is related to the above-mentioned phase shift.) Therefore, single-frequency operation is often easily achieved. Due to the large free spectral range, wavelength tuning without mode hops may be possible over a range of several nanometers. The tuning mechanism is thermal.

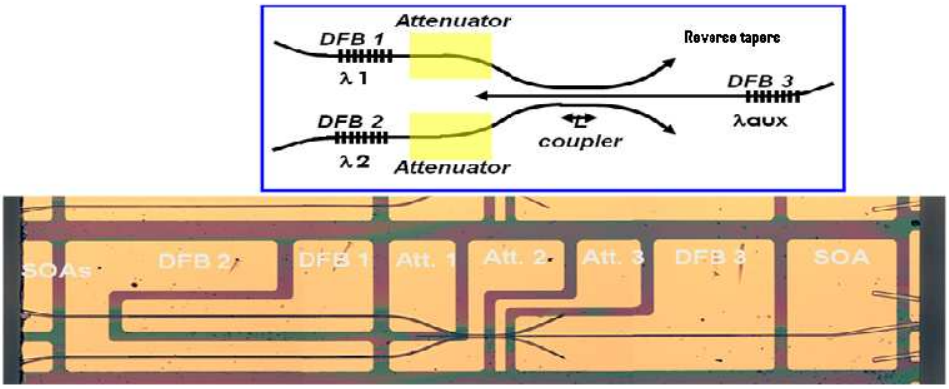

Figure 6: layout of the integrated device

For the design and fabrication of the chip a lot of steps have been realized which will be explained with more detail in the next section of the project.

2.2.1 Device design and fabrication

Previous measurements have demonstrated that a very high level of power injected in a laser produce a chaotic regime, for this, the coupler used in this experimental setup guarantee a coupling of the order of 0.1% in power.

The attenuators 1 and 2 of figure 6 have the goal of controlling the power injected in the DFB lasers. The presence of Down-Tapers is very important because it avoids a big retroreflection into the DFB lasers, which can generate a chaotic regimen or multi-mode operation of the devices; These tapers are done by reducing to a few nanometers the width of the waveguide. Also output waveguides with up-tapers (the width of the waveguide reaches 10 μm) improve the coupling with optic fiber; Inclination of 10º respect to the axis avoids reflections that could, again, produce a bad operation of the device.

The waveguides are of the type *shallow etched ridge*; This type of guides have multiple vantages respect to the *"rib" deep etched guides*. The principal vantages are: low retroreflection in presence of curvatures, a better heat dissipation, and above all a better technological tolerance with respect to the *"rib" deep etched guides*.

The DFB lasers (depicted in figure 7) have been obtained by defining the Bragg grating by lateral excavation of the ridge guide (side etched DFBs), with a total length of 800 μm and a width of 2.4 μm. The Bragg wavelength (which determines the laser wavelength) is varied by changing the amplitude of the lateral recess with values between 450 nm and 575 nm,

while the period of the gratings is 242.5nm. The lasers have a coefficient k (coupling grating coefficient) of 245 cm^{-1}.

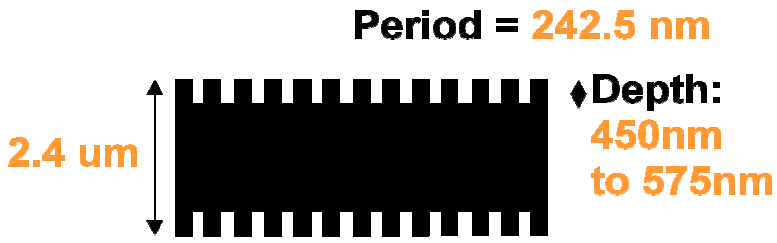

Figure 7: Experimental DFB lasers

Distributed feedback semiconductor lasers were developed during the 1980s. The feedback in DFB lasers as has been explained, is not localized at the facets but is distributed throughout the cavity length. This is achieved through an internal built-in grating that leads to a periodic variation of the mode index. Feedback occurs by means of Bragg diffraction, a phenomenon that couples the waves propagating in the forward and backward directions. Mode selectivity of DFB mechanism results from the Bragg condition: the coupling occurs only for wavelengths satisfying:

Where Λ is the grating period, is the average mode index, and the integer m represents the order Bragg diffraction. The coupling between the forward and the backward waves it is strongest for the first order Bragg diffraction (m=1).

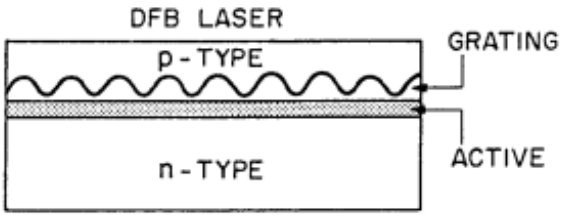

Figure 8: DFB laser

By other side the electrical field of the oscillating mode sees an effective diffraction index equal to:

$$\eta eff(z) = n_0 + n_1 \sin\left[\left(\frac{2\pi z}{\Lambda}\right) + \Phi\right]$$

Being ηeff periodic in z and Λ the grating period as has been explained.

For medium of the reflections provoked by the periodic structure of laser DFB the backwards and forwards waves are coupled as has been explained, only if the wavelength of the signal is equal to:

$$\lambda = \lambda_B = 2\langle \eta eff \rangle \Lambda$$

Con ⟨ηeff⟩ the average value of ηeff in z. To simplify can be assumed that ηeff(z) is a periodic function of squared wave of period Λ, this case is similar to a periodic sequence of mutistratum dielectric mirrors in which the constructive interference is produced when

$$(\langle \eta eff \rangle = \Lambda/2) = \Lambda/4$$

Therefore exists an only wavelength that satisfy the Bragg condition and it will indentify the only mode that will can oscillate.

The device fabrication has been done in the James Watt Nanofabrication Center of the University of Glasgow, using a state-of-the-art electronic beam lithography machine, which can obtain ultra-high resolution masks.

Therefore, the DFBs, the couplers and the tapers have been done with lithography by electronic beam and the successive attack of RIE (Reactive Ion Etching) type. RIE is an etching technology used in microfabrication. It uses chemically reactive plasma to remove material deposited on wafers. The plasma is generated under low pressure (vacuum) by an electromagnetic field. High-energy ions from the plasma attack the wafer surface and react with it.

For the fabrication of the integrated chip a series of necessary steps has been followed, including the definition of wave guide and coupler, planarization, definition and opening of contact window, definition of metal contacts.

Every microchip includes more than one device and is made of Al-quaternary material on InP substrate.

CHAPTER 3

CHARACTERIZATION OF INTEGRATED DFB LASERS

In this chapter all the experimental measurements necessary to the characterization of the lasers of every device will be presented. To summarize, several results have been obtained: the collection of several optical spectra, the wavelength-current plots, the current-SMSR (Side Mode suppression ratio) and the current-Power plots.

Other important measurement consists of operating two lasers simultaneously by changing the detuning between them, and to verify the gain and the efficiency of the Four-Wave-Mixing process, and whether locking or chaos are produced.

Finally, measurements on the couplers of every chip have been carried out to demonstrate that the coupling value is in effects corresponding the value defined in the specifications and the design of the device.

All the graphics plots have been done using the software Matlab, starting from data files created by the software Labview. The computer is connected to a laser diode combi-controller (temperature and current) and an OSA (Optical Spectrum Analyzer) with a PCMCIA card and GPIB interface. For all the measurements done a TEC (Temperature Electrical Controller) is needed, because the temperature of the chip has to be controlled to avoid overheating.

3.1 Experimental setup

At the beginning of the present project the experiments have been done using BAR-A, and then continued with BAR-B and BAR-E. All these photonic microchips are very similar in their basic structure with some differences in the lengths of the DFBs or in the devices number. BAR-A includes eight devices, as shown by the picture below. Every device is composed by 3 DFB lasers, 3 attenuators, a coupler and a 3 SOA (semiconductor optical amplifier).

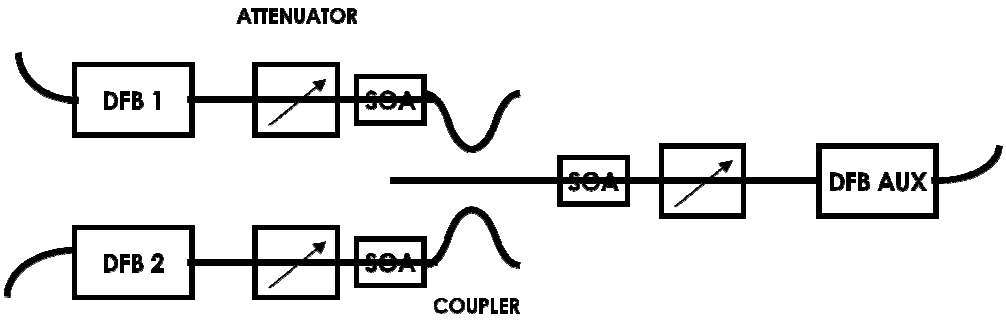

Figure 9: Experimental-setup

During the present work, the DFB lasers that have been characterized exhibited threshold current values between 10 and 12 mA, and were operated at a maximum current of 200 mA.

In the experiments are employed three DFB lasers, the laser that in the locking experiment works as pump for the generation of the Four-Wave-Mixing signals is called DFB_AUX (auxiliary laser) while the others are called DFB1 and DFB2.

The properties of every device are:

$L_{coupler}$=50µm (1% coupling); 0µm (point coupler) (0,1% coupling)

D coupler=1 µm

L DFB=200 µm, 800µm

L Taper out=100µm, 10º tilted

S-bend Radius=300µm

Af= 0GHz, 20GHz, 100GHz (nominal frequency detuning between lasers 1 and 2)

L attenuator= about 200 µm.

As it can be seen, two types of coupler exist with different coupling values and two types of DFB lasers with different lengths.

3.2 Power vs. current, SMSR vs. current and lambda vs. current plots

In this section the laser DFB1, DFB2 and DFB3 of BAR-A and BAR-B have been measured. For all measurements done in BAR-A the temperature was kept constant at 24 ºC (corresponding to a resistance of the thermistor of 10.530 KΩ). The injection current values changed between 5 and 140 mA with a wait time of 10 seconds. All measurements have been done using the Labview software.

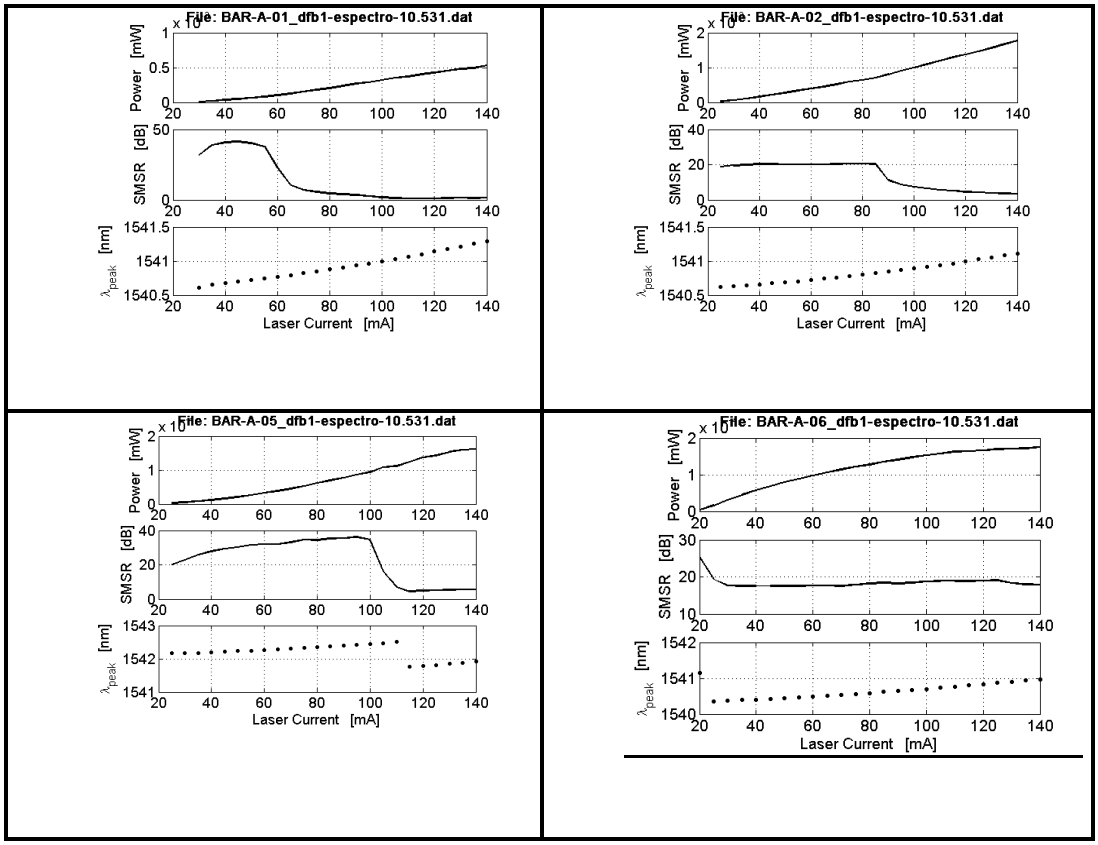

Figure 10: DFB1 plots for devices 1, 2, 5 and 6 respectively of BAR A.

In figure 10 plots for the wavelength peak, SMSR and power for the laser DFB1 of every valid device of the BAR-A are shown.

Perhaps the most basic parameter to be measured for these lasers is the amount of emitted light vs. the current is injected into the device. This generates the Output Light vs. Input Current curve. As the injected current is increased the laser first exhibits spontaneous emission which increases very gradually until it begins to emit stimulated radiation, which is the onset of laser action. The first parameter of interest is the exact current value at which this phenomenon takes place. This is typically referred to as the threshold current and is denoted by the symbol I_{th}. It is generally desirable that the threshold current be as low as possible, resulting in a more efficient device. Thus threshold current is one of the measurements used to quantify the performance of a laser diode. Threshold current is dependent on the

quality of the semiconductor material from which the device is fabricated and the general design of the structure of the device waveguide. The light has been collected by an optic fiber, measuring the power value from an OSA.

In this experiment the threshold currents are around 11 mA and the device 6 has the higher value of power for all current values.

Reference to the SMSR graphic, the single longitudinal modes (SLM) laser is often characterized by the SMSR which is defined as:

$$SMSR = P_{mm}/P_{sm}$$

Where P_{mm} is the main-mode power and P_{sm} is the power of the most dominant side mode. The SMSR should typically exceed 1000 (or 30dB) for a good SML laser.

In this case the device 5 has the higher value of SMSR and this is equal or higher to 30dB between 40 and 100 mA. For the present device, it si assumed that a SMSR of 10 dB is sufficient for a proper operation.

The temperature changes provoke changes in the wavelength emitted by the laser. In the figure 11 is shown the wavelength change with the temperature for a Fabry-Perot laser, in other words a gradual increase of wavelength while increase the temperature since is produced a jump to other longitudinal mode. The jump does not typically occur in a DFB laser.

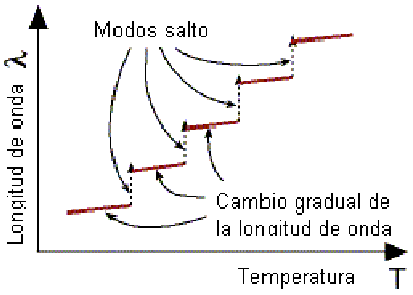

Figure 11: longitudinal mode jump

Therefore if we observe the lambda peak-current graphic of the device 5 it can be seen as such longitudinal jump mode is produced around 110 mA. In the other devices the wavelength is increased with the increase of current and the change is approximately of 1nm.

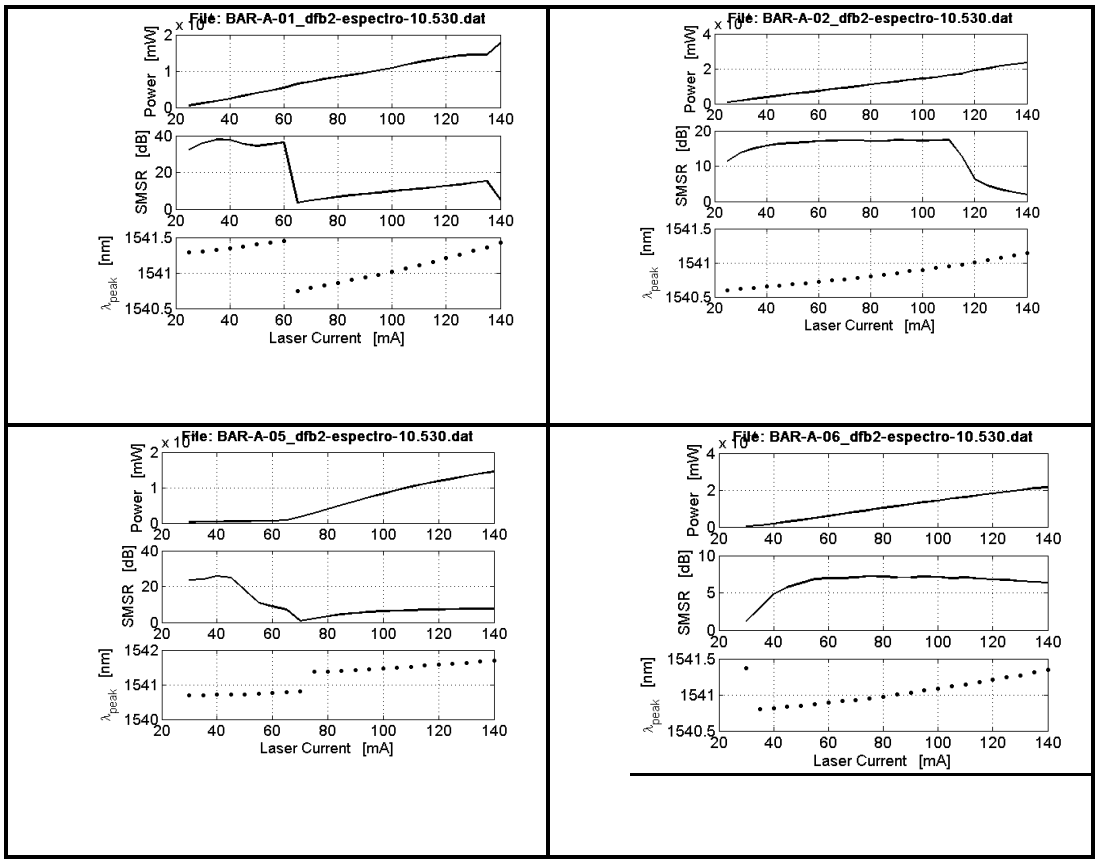

Figure 12: DFB2 plots for devices 1, 2, 5 and 6 respectively of BAR A.

Now in the DFB2 graphics is shown a similar power-current curve for all devices with a maximum power around 2mw. Then in the SMSR graphics the

device 1 reaches the higher value (40 dB) but only in the first values of current (even 65 mA), the device 2 has a SMSR of 17 dB for a wide range of current and the device 5 and 6 have a SMSR lower than 10 dB for almost every current values. If we analyze the graphs we can see a longitudinal mode jump too in all devices except in device 2, this is due to, as has been explained before, a temperature increase.

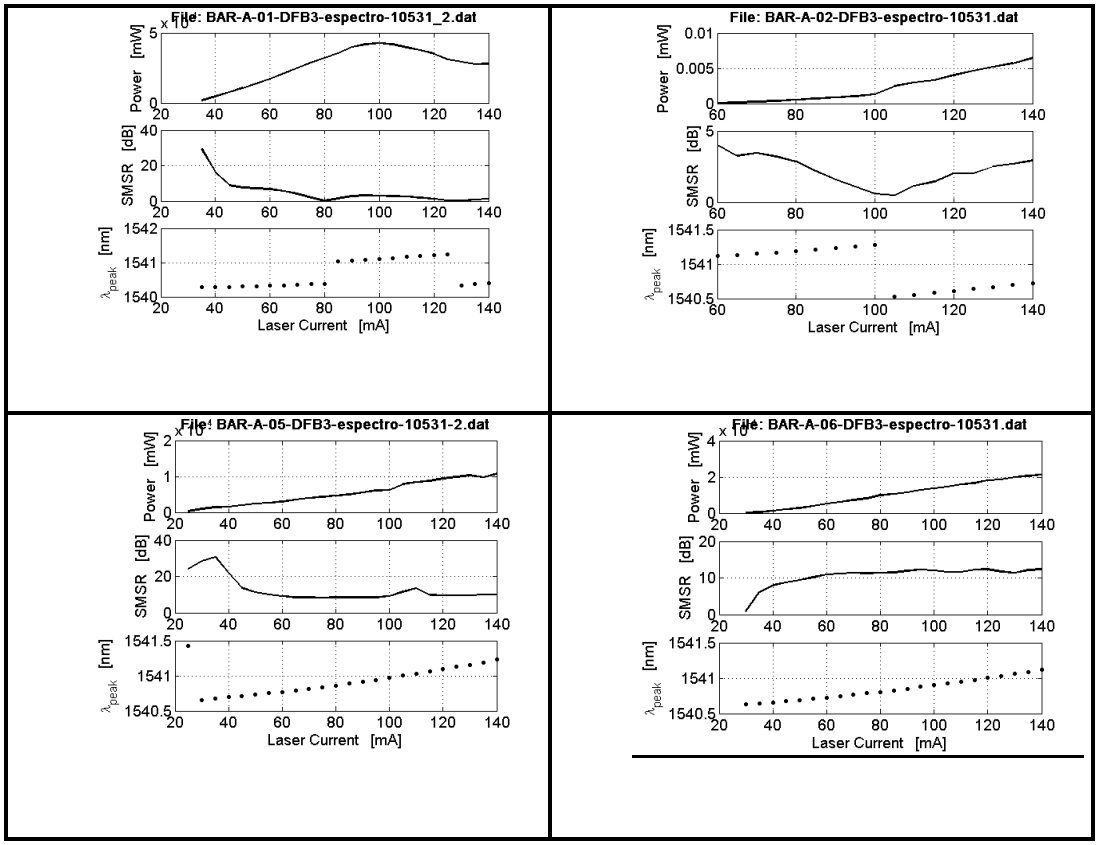

Figure 13: DFB3 plots for devices 1, 2, 5 and 6 respectively of BAR A.

The DFB3 graphs show that the DFB3 isn't working very well because the power isn`t very high in all devices, the SMSR is low which is an important factor in the DFB lasers, and there are longitudinal mode jump as consequence of temperature.

If we represent the SMSR vs current and the λ_{peak} vs current plot for each device of BAR-A we obtain the overlapped plots:

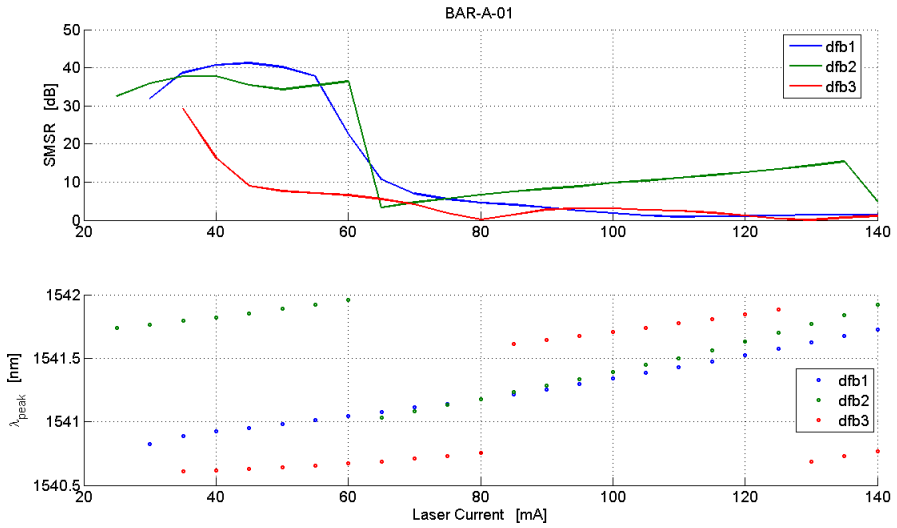

Figure 14: SMSR vs current and λ_{peak} vs current plots for device 1, of BAR-A chip

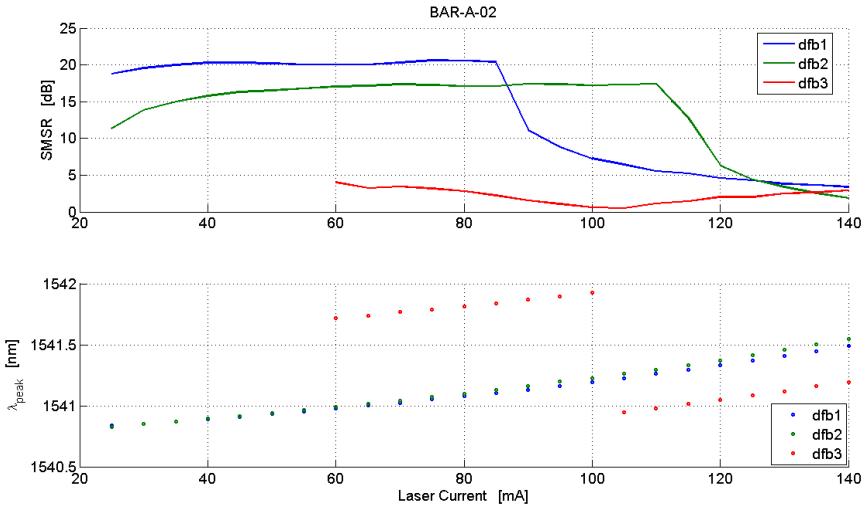

Figure 15: SMSR vs current and λ_{peak} vs current plots for device 2, of BAR-A chip

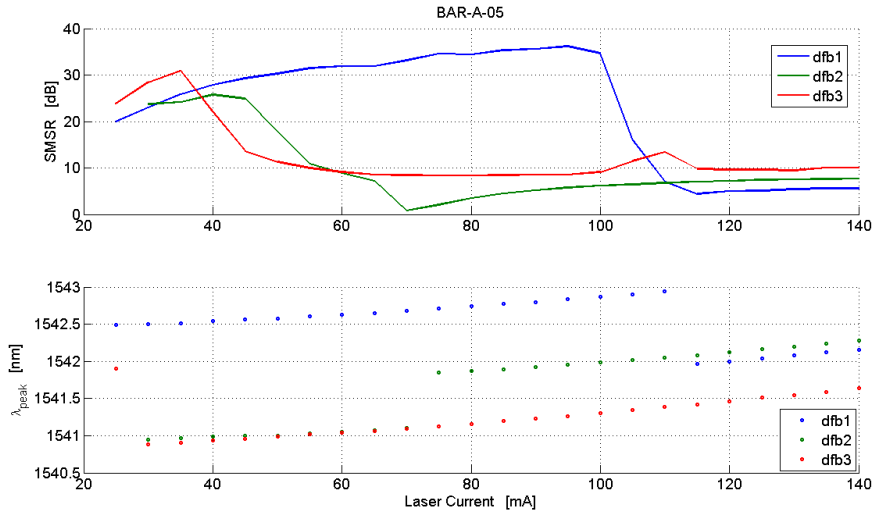

Figure 16: SMSR vs current and λ_{peak} vs current plots for device 5, of BAR-A chip

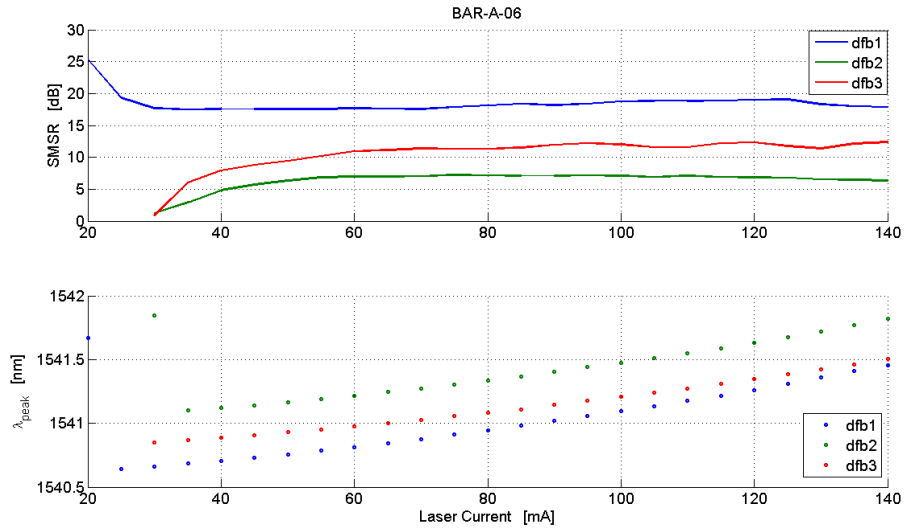

Figure 17: SMSR vs current and λ_{peak} vs current plots for device 6, of BAR-A chip

Then the BAR-B plots have been realized, as in the BAR-A the SMSR, Power and λ_{peak} graphs are plotted with Matlab. In this case the current value is change between 5mA and 160 mA with increases of 5 mA and a wait time of

15 seconds. We have done six measurements for the diferent devices of the chip BAR-B with a termoresistence of 12.509 kΩ.

The spectra have been acquired from the OSA(span of 5nm and resolution of 0.1nm) using LabView.

In figure 18, 19 and 20 a poor SMSR is observed, this is due to the fact that each integrated laser of the BAR-B emittes a lot of modes and the principal and secondary modes have a near level of power.

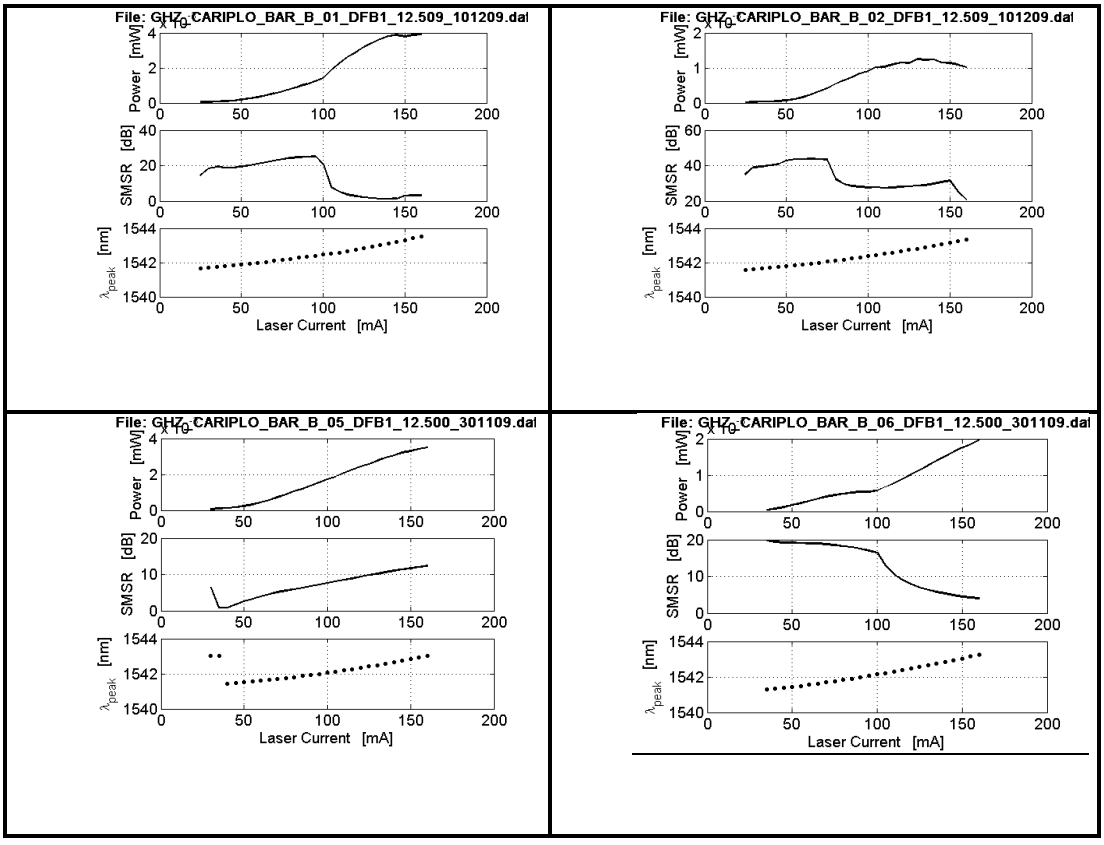

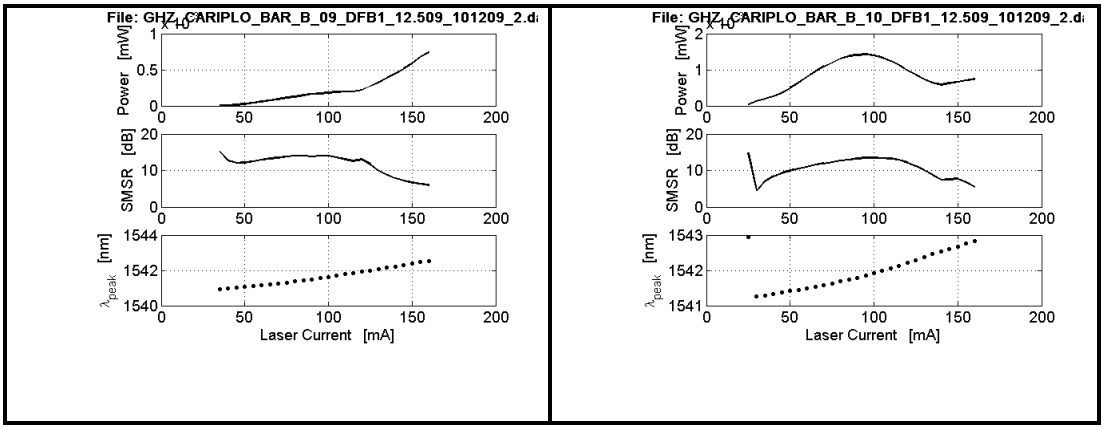

Figure 18: DFB1 plots for devices 1, 2, 5, 6, 9 and 10 of BAR B

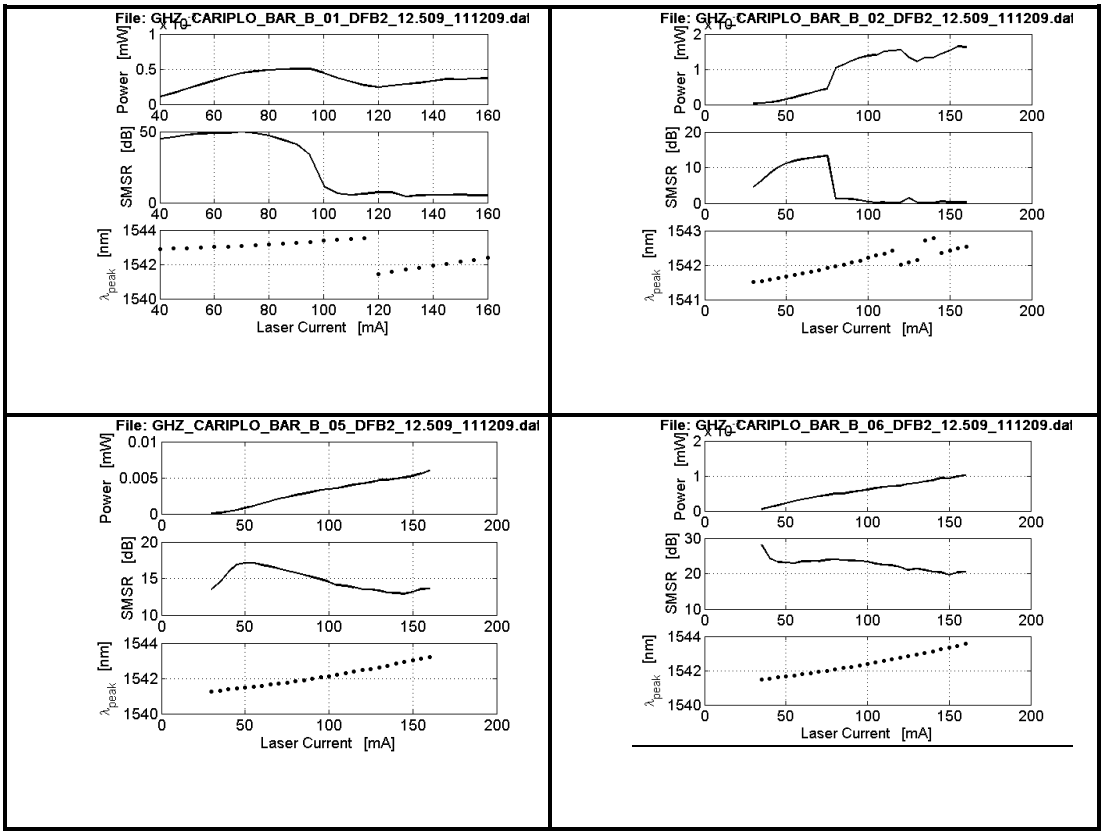

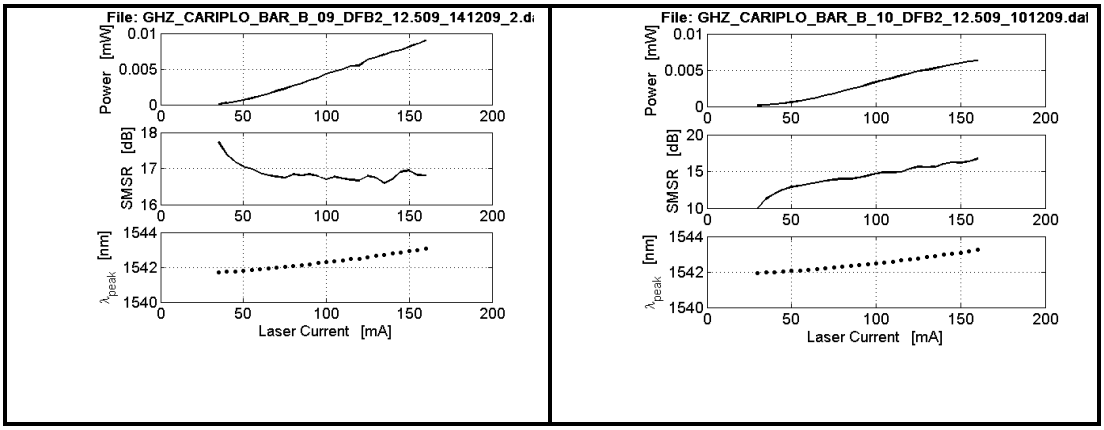

Figure 19: DFB2 plots for devices 1, 2, 5, 6, 9 and 10 of BAR B

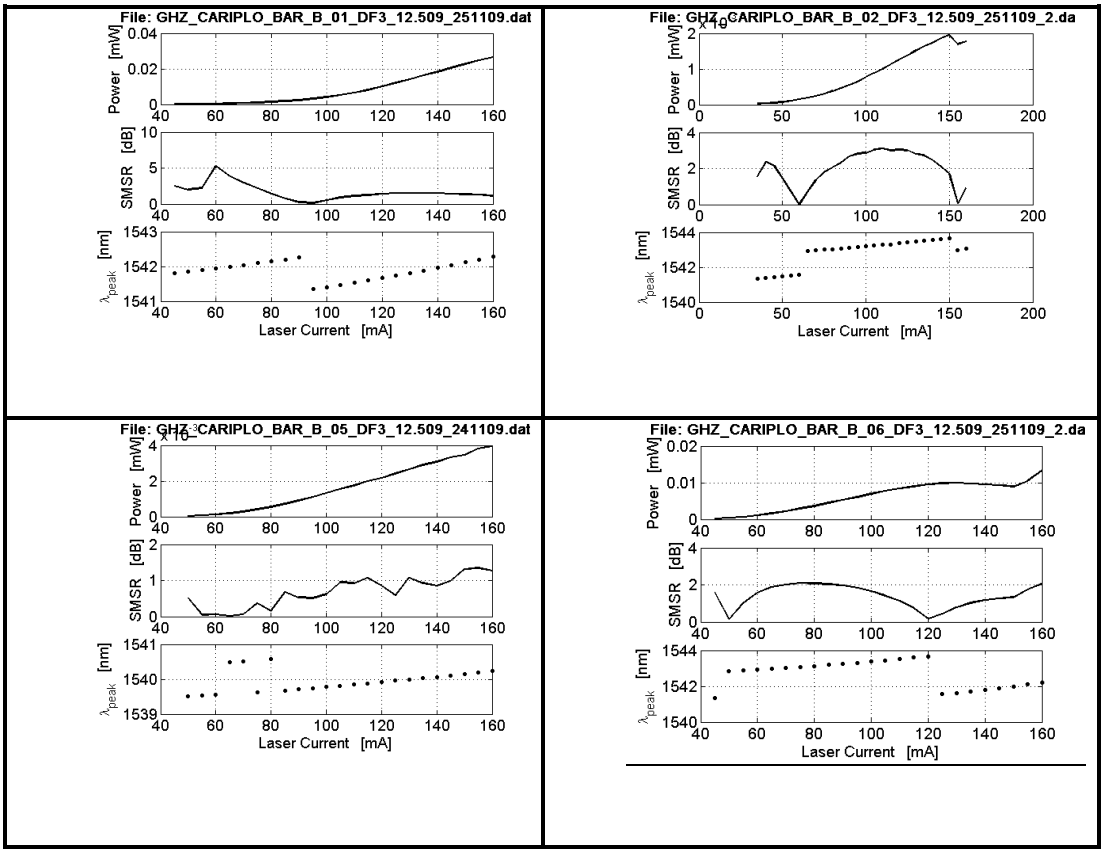

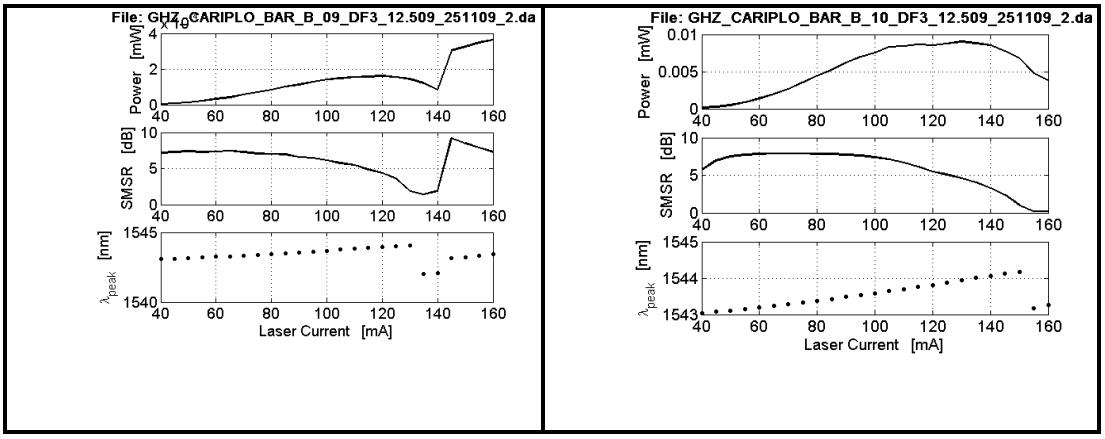

Figure 20: DFB3 plots for devices 1, 2, 5, 6, 9 and 10 of BAR B

3.3 Optical Spectra Measurement

Now in this point we are going to analyze the spectrum of the DFB lasers for the BAR-A and BAR-B. In the case of BAR-A the temperature is the equivalent to a resistance of 10.531KΩ and for the BAR-B it is 12.509KΩ.

In all the measurements done we have used a current between 5mA and 140 mA with increases of 5 mA and a wait time of 10 seconds. The spectra have been acquired from the OSA(span of 5nm and resolution of 0.1nm) using LabView and the graphs have been realized with the program Matlab.

We are going to begin the measurements with the DFB1 of the device one in the BAR-A chip. For this measure we feed the DFB1 laser with a current feeder that it is connected to the computer with a PCMCIA card, and by the software labview we can change the current value automatically and to do a simulation beginning with a current of 5 mA. In every step the current is changed in 5 mA and a sweep of the signal is done with an optical spectrum analyzer ANDO AQ6317C. The OSA is connected to the Computer too and to an optic fiber that it is put in front of the DFB1 laser with an angle of 36º

which allows a maximum level of coupling of the light in the fiber. The rest of measures are done in the same manner but changing the fiber position to see the DFB2 or DFB3 spectrum.

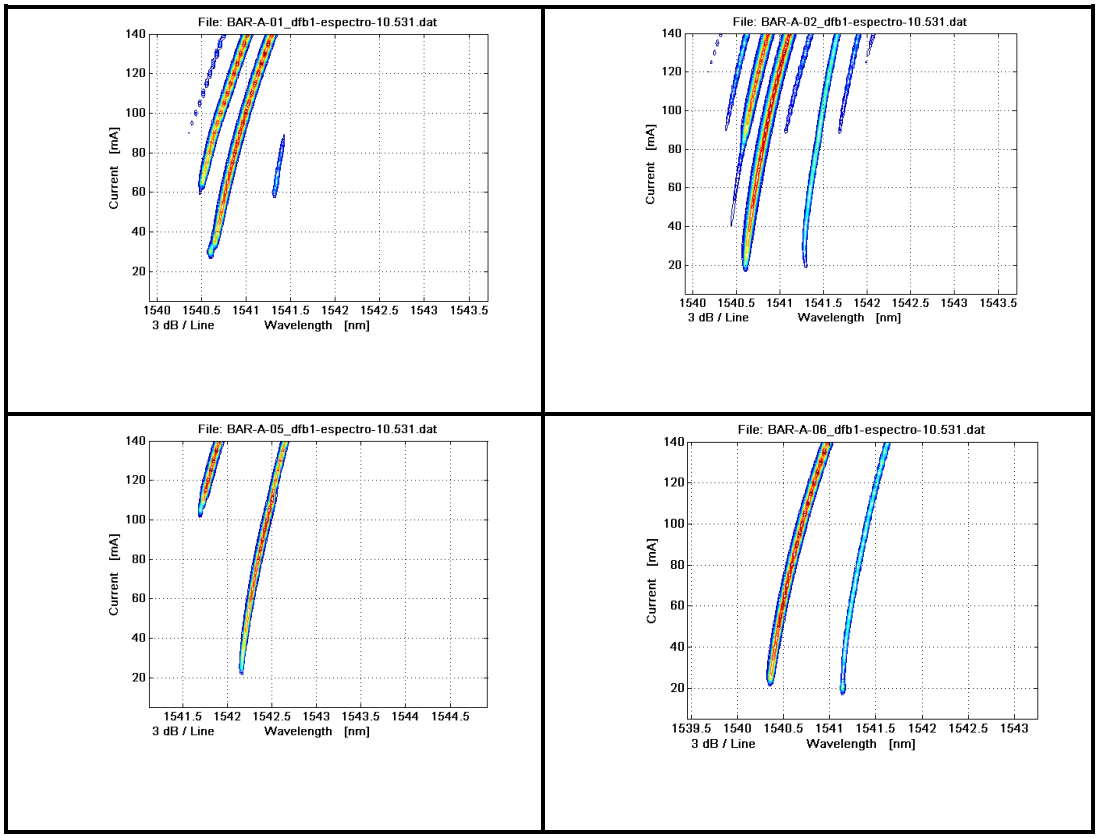

Figure 21: BAR-A_DFB1, device 1, 2, 5 and 6

In figure 21 the spectrum of the BAR-A DFB1 laser is shown, and as it can be seen the laser isn't working as a single mode laser. This is because DFB lasers behavior, in terms of emitted modes, is highly sensitive to reflections on the end facets. More particularly, if those facets are left untreated, the oscillation modes of the laser depend on the relative positions of the facets with respect to the grating spatial phase, which position is entirely casual, since it is impossible to exactly determine at which point a grating will be cut upon manufacturing the individual devices. If the laser facets are covered with antireflecting coatings, the laser will steadily oscillate on two modes symmetrical with respect to Bragg wavelength. In the latter case monomodality can be achieved by causing the rays propagating in the laser

to undergo a quarter-wave phase shift in the central grating zone. This phase shift is obtained by eliminating a groove of the grating in such a zone, which operation is rather complicated from the technological standpoint. The operations necessary to manufacture a grating presenting the phase shift and to apply the antireflecting coatings cause such a cost increase that generally, in the industrial production of such lasers, it is preferred to keep which are monomode by fabrication and to discard the others. Notwithstanding the elimination of a considerable proportion of the production, this approach is still advantageous from the economic standpoint. These lasers did not have the quarter-wave phase shift in the central grating zone but the new ones have it.

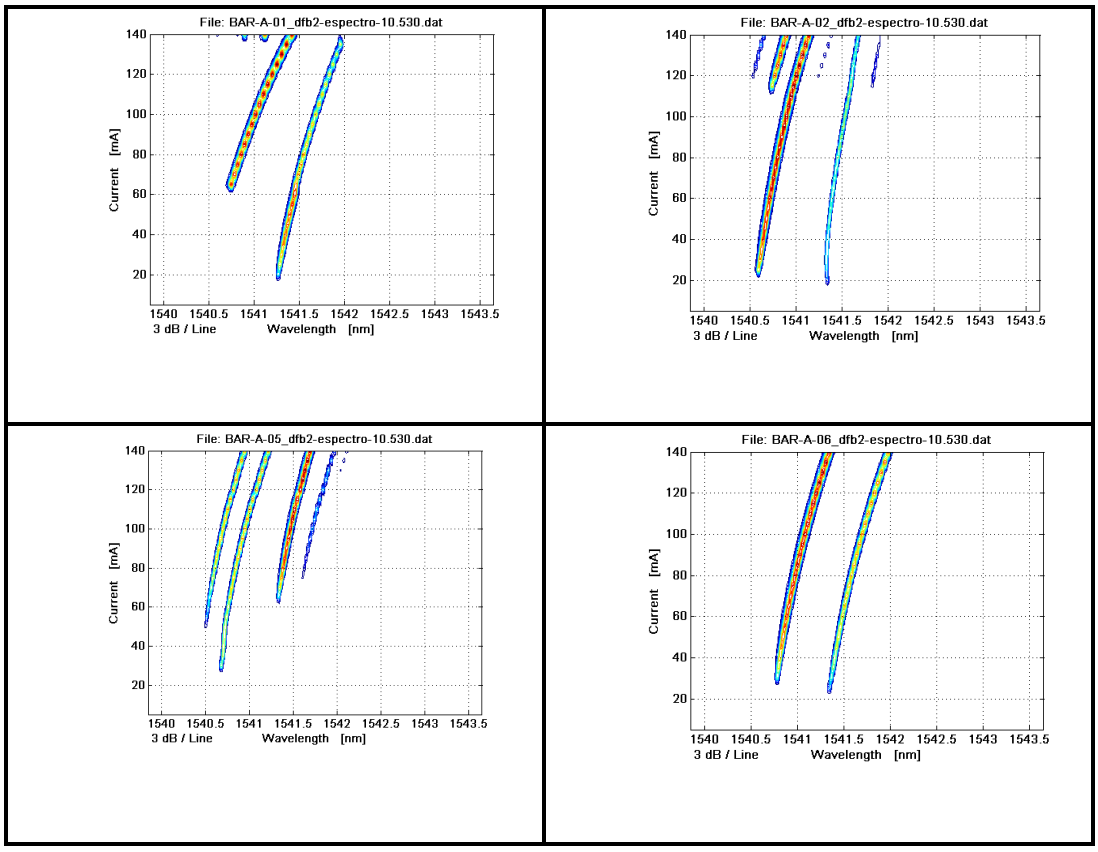

Figure 22: BAR-A_DFB2, device 1, 2, 5 and 6

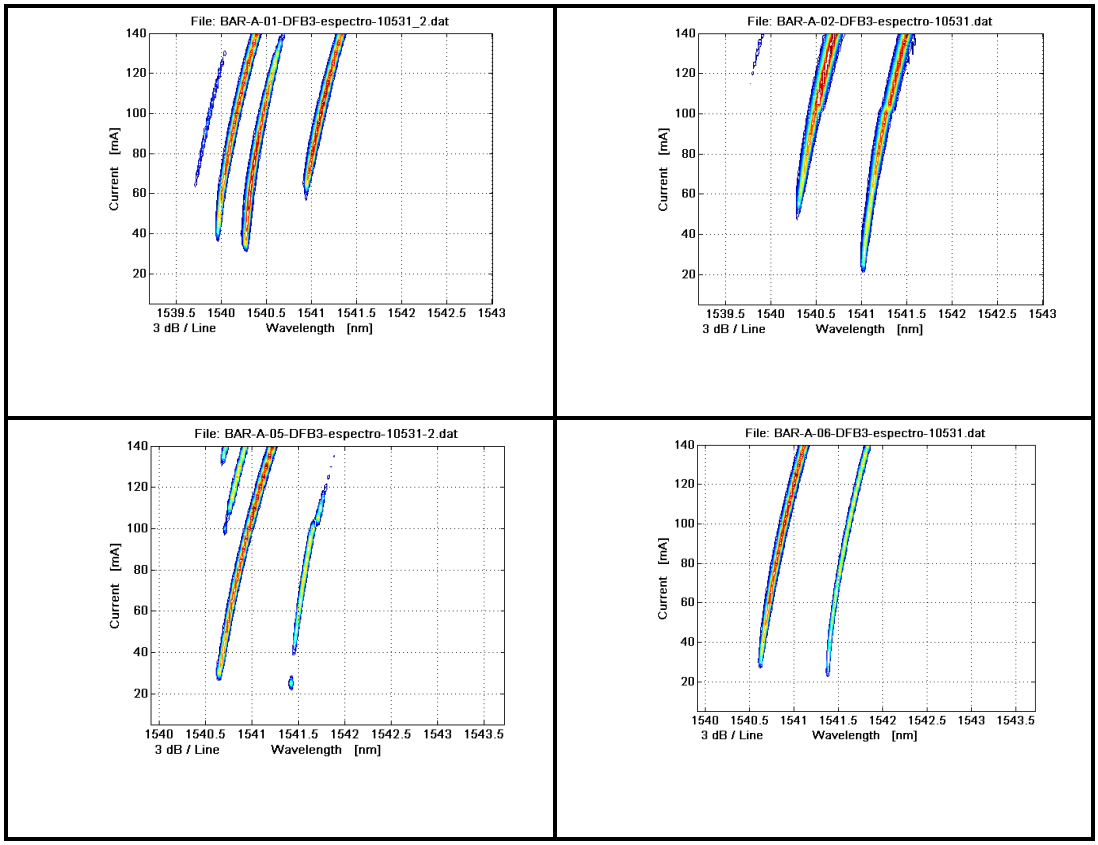

Figure 23: BAR-A_DFB3, device 1, 2, 5 and 6

For all DFB lasers in the BAR-A the central wavelength is between 1540 and 1541 nm as it is shown in the graphs. In other measurements done over the same laser by changing the temperature, it is observed that the central wavelength moves to larger values, which is a consequence of heating.

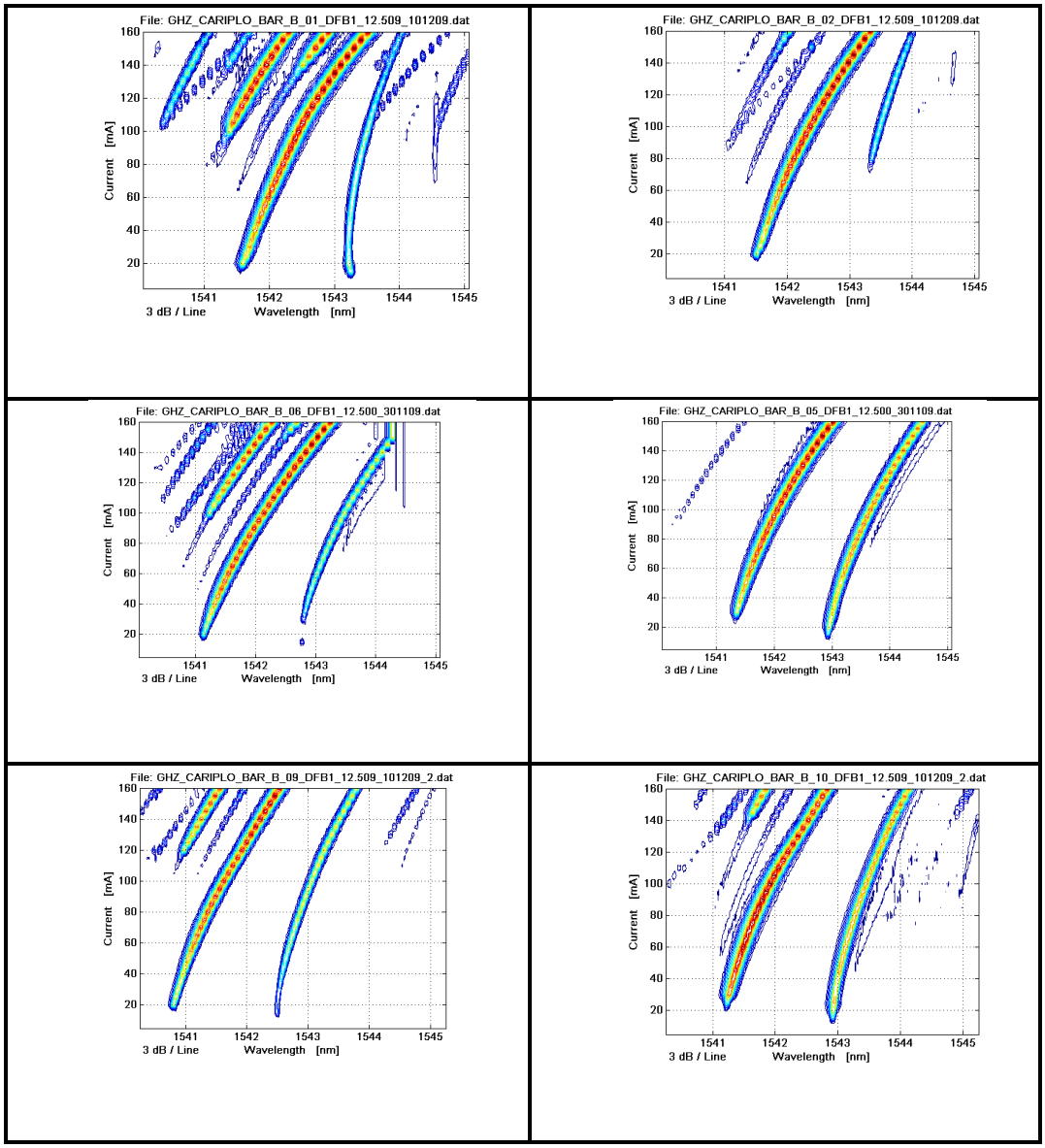

Figure 24: BAR-B_DFB1, device 1, 2, 5, 6, 9 and 10

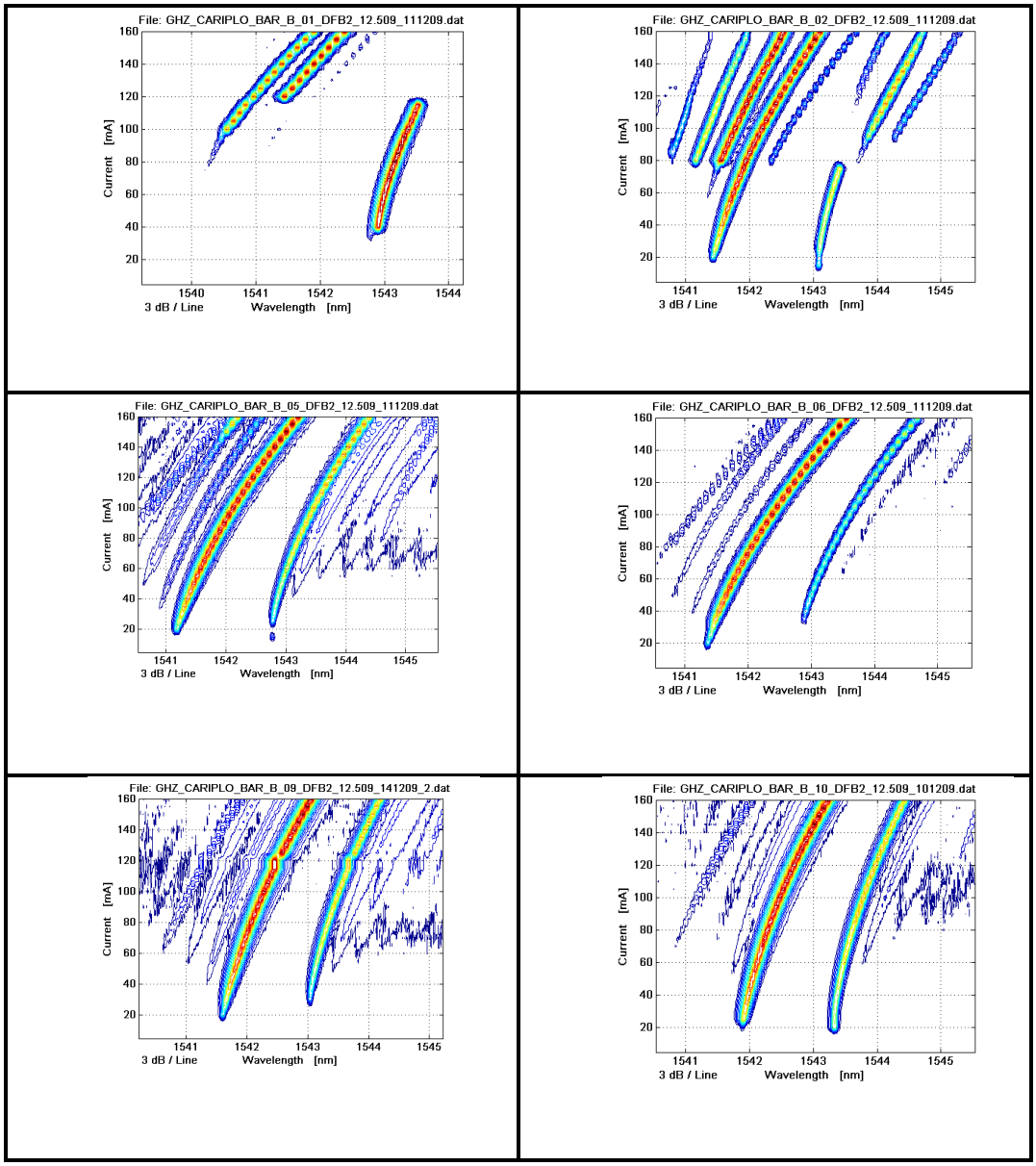

Figure 25: Bar-B_DFB2 device 1, 2, 5, 6, 9 and 10

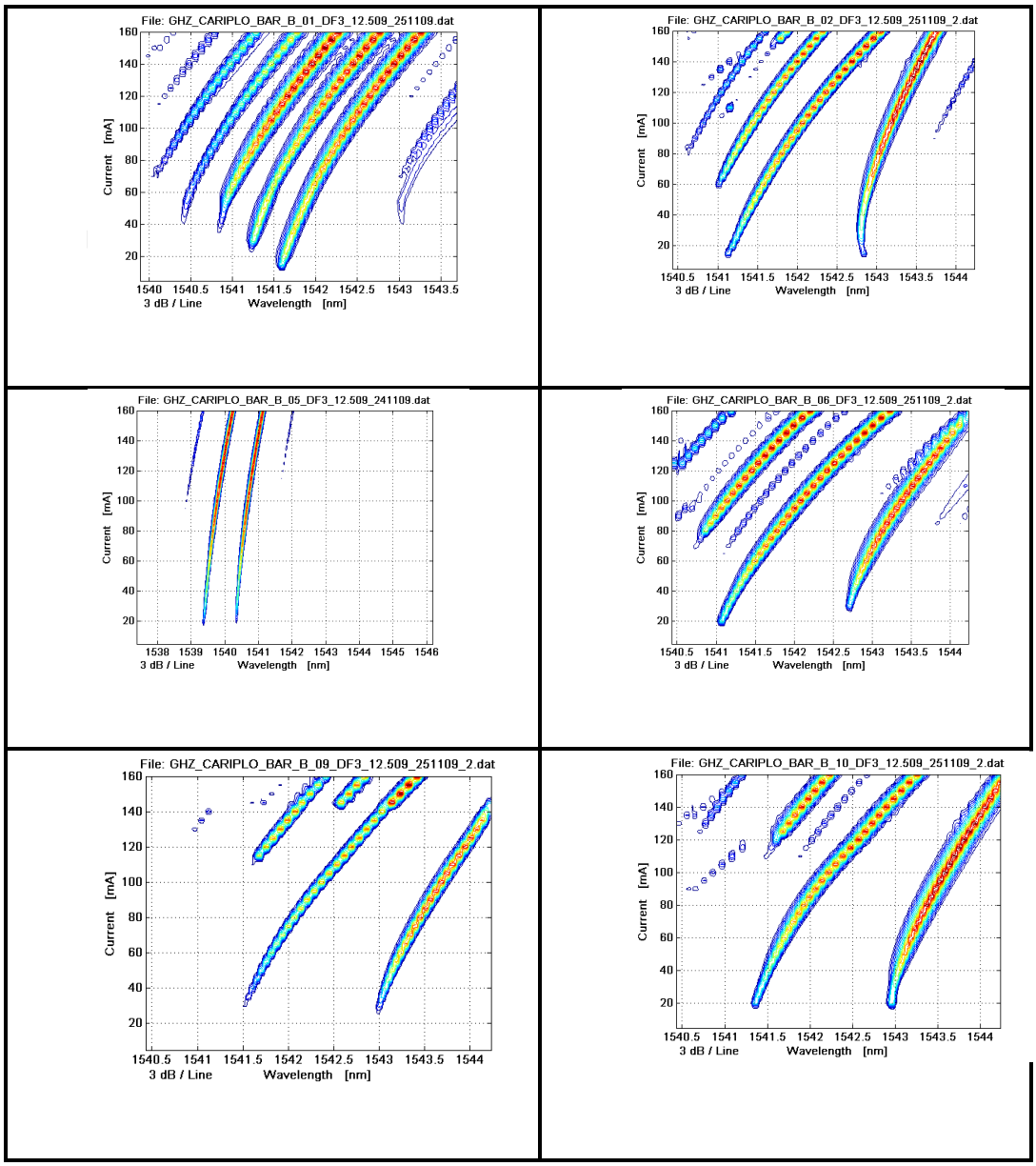

Figure 26: BAR-B_DFB3 device 1, 2, 5, 6, 9 and 10

In the case of BAR-B the central wavelength is between 1542 and 1543 nm and the current values vary between 5 and 160 mA for all DFB lasers in the chip. Other fact that can be seen observed in the graphs obtained it is that the number of modes is higher than in the BAR-A case.

3.4 Coupler

A Fiber Coupler is an Optical Fiber device with one or more input fibers and one or several output fibers. Light from an input fiber can appear at one or more outputs, with the power distribution potentially depending on the Wavelength and polarization. Such couplers can be fabricated in different ways, for example by thermally fusing fibers so that their cores get into intimate contact. If all involved fibers are single-mode (i.e., support only a single mode per Polarization direction for a given wavelength), there are certain physical restrictions on the performance of the coupler. In particular, it is not possible to combine two or more inputs of the same optical Frequency into one single-polarization output without significant excess losses. However, such a restriction does not occur for different input wavelengths: there are couplers which can combine two inputs at different wavelengths into one output without exhibiting significant losses. Such couplers are used e.g. in fiber amplifiers to combine the signal input and the pump wave. Other wavelength-sensitive couplers are used as multiplexers in wavelength division Multiplexing (WDM) telecom systems to combine several input channels with different wavelengths, or to separate channels.

In this section the characterization of the couplers of each BAR has been done to obtain the experimental value of coupling and to check if it is equal to the given value in its datasheet.

The coupler is a very important element due to the fact that the optic signal from laser DFB1 and laser DFB2 should be coupled in the wave guide of the laser DFB3 to be injected in itself and generates the Four-Wave-Mixing effect. The measurements have been started with the coupler of BAR-A device 6 which schematic is shown in figure 27.

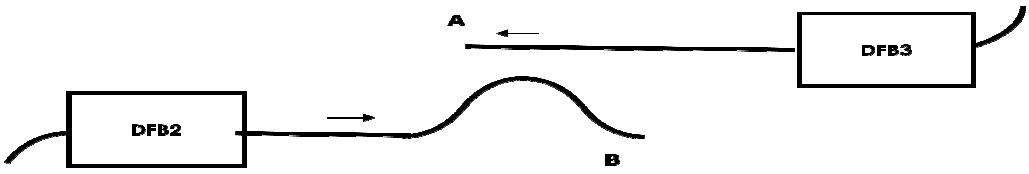

Figure 27: Schematic of the BAR-A, device 6 coupler

At first, it has been measured the variations of P2 (power of the principal mode of DFB2) and P3 (power of the principal mode of DFB3) collecting the light from the rear facet of DFB2, changing the bias current I2 (while I3=100mA).

In the second measure, P2 and P3 have been observed from the rear facet of DFB3, changing I3 (while I2=140mA). In this measure P3 is the power of the secondary mode of DFB3, significantly less powerful than the principal one.

It can be noticed that in the first measure, for small values of I2, P3 maintains a constant value of -60dBm, while in the second measure, for small values of I3 P2 keeps decreasing to -80dBm. That's probably due to an auxiliary coupling between the fiber positioned behind DFB2 and a portion of light coming from the point A, at the end of DFB3 guide, while in the second measure there can be no coupling between the fiber behind DFB3 and the point B, end of DFB2 guide.

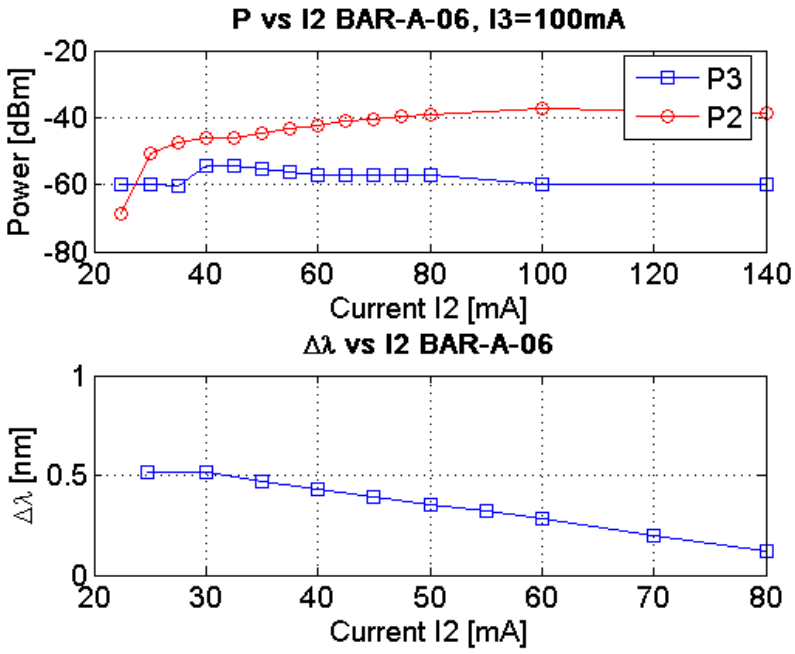

Figure 28: Power of the principal modes of DFB2 and DFB3 changing the DFB2 current with I3=100mA and variation of lambda with I2 current.

It is also observed that the difference between P3 and P2 at the same current in the first measure (graphic above) is 20 dB, giving a coupling value of 1% that is the given value in the specifications of the device.

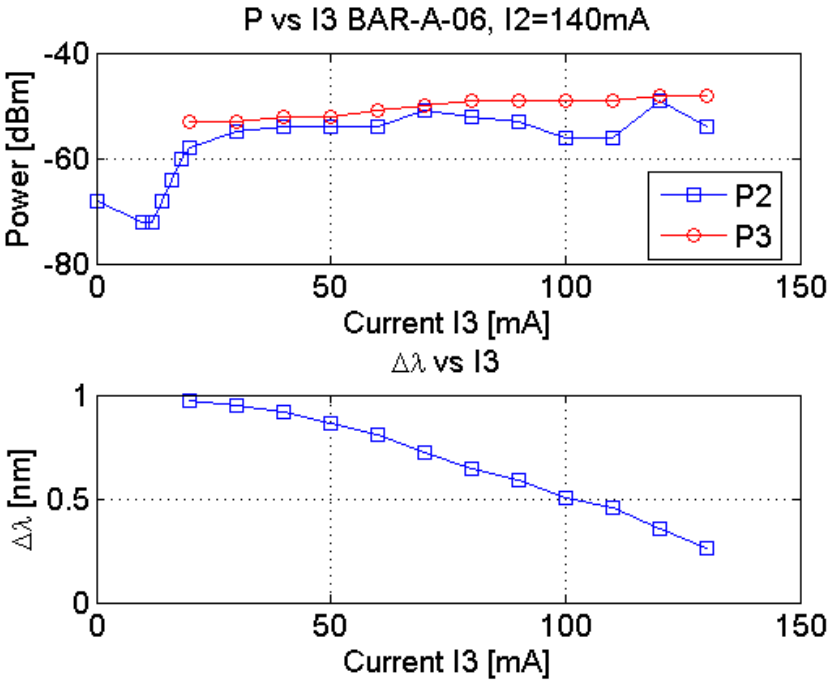

Figure 29: Power of the secondary modes of DFB2 and DFB3 changing the DFB3 current with I2=140mA and variation of lambda with DFB3 current.

The next measure has been done in the BAR-E, device proof which setup is shown in the next figure. This setup as can be noticed has the wave guide of DFB1 and DFB2 longer than the BAR-A and BAR-B devices. At first, it has been measured the coupling value with the laser DFB1 on, collecting the light from DFB3 side, then has been measured the coupling value with laser DFB2 on and collecting the light from DFB3 side again. The optic fiber put in the DFB3 side has been moved to collect the light of the different guides showed in the figure below with a respective coupling index of 99/0.1%, 1% and 99/0.1%.

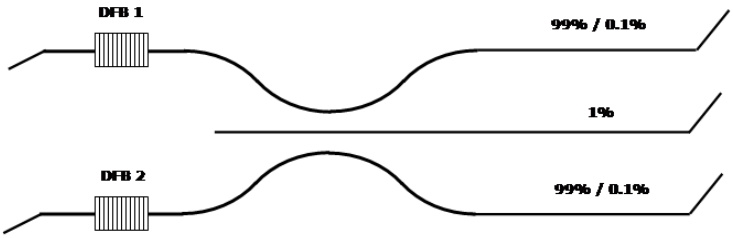

Figure 30: Device proof coupler

If the graphs obtained of the coupling value measure of this device are observed we can conclude saying that the central guide which go to the DFB3 laser has really a coupling value of 1%. It is seen in the graphics below due to the fact that when the laser DFB1 is on the guide that has a coupling value of 99% (guide directly connected to laser DFB1) receive a power value of approximately -27dBm while the central guide receives a power value of -47dBm. The difference of power between these values is 20dB and it means that the coupling value is 1%.

In the other measures done with laser DFB2 on, the results lead to the same conclusion verifying that the portion of light injected in DFB3 laser from DFB2 laser is the 1%.

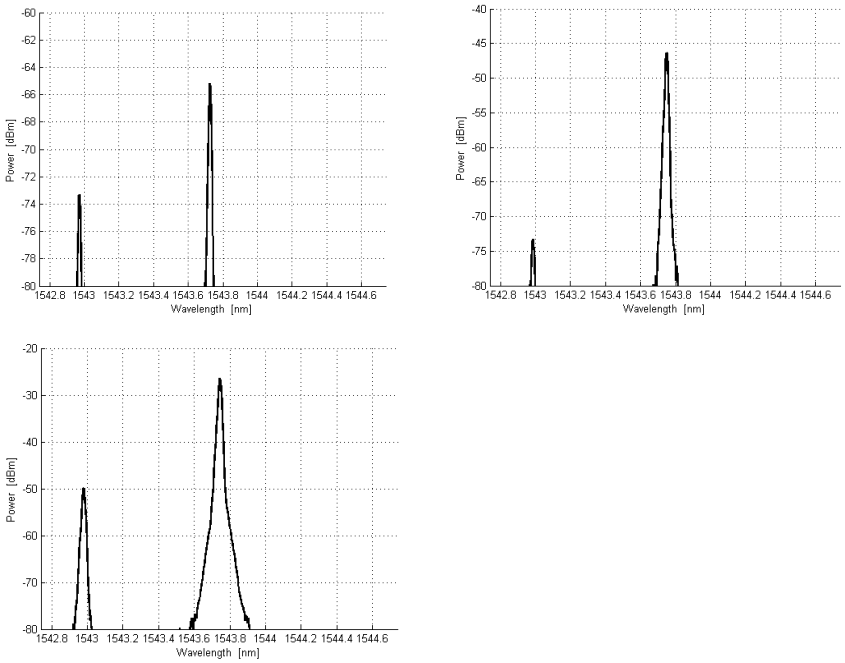

Figure 31: Measurement with coupler at 0.1%, 1% and 99% respectively with laser DFB1 on

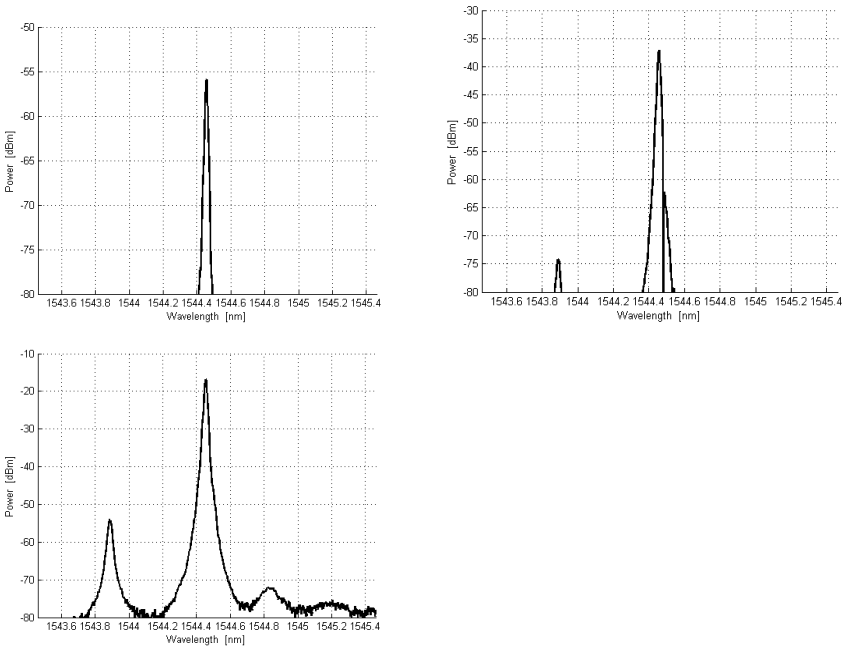

Figure 32: Measurement with coupler at 0.1%, 1% and 99% respectively with laser DFB2 on

3.5 Four-Wave-Mixing

In this section we will explain what the FWM phenomenon is and what the equations that govern its behavior are, to finally experimentally demonstrate how this phenomenon takes place in our integrated devices when the detuning value between 2 lasers achieves a certain value.

The Four-Wave Mixing is a third order effect generated by the interaction of two electromagnetic fields in a material with electromagnetic susceptibility of third order $\chi^{(3)}$. The polarization of a non-linear material induced by an electromagnetic wave can be expressed as:

$$\bar{P} = \chi^{(1)}.\bar{E} + \chi^{(2)}.\bar{E}\bar{E} + \chi^{(3)}.\bar{E}\bar{E}\bar{E} + \cdots$$

The expansion coefficients are known as susceptibilities in analogy to classical linear electromagnetic theory. This method assumes that the higher order susceptibilities grow progressively smaller so that power series expansion converges to a finite polarization.

In order to understand the Four-Wave-Mixing process, a closer examination of the third order non linear polarization must be made. The general form of the polarization may be written as:

$$P_i(v_4,\vec{r}) = \frac{1}{2}\chi^{(3)}_{ijkl}\left(-v_4, v_{1,}-v_2, v_3\right)E_j(v_1)E_k^*(v_2)E_l(v_3)\exp\left[i\left(\overline{k_1} - \overline{k_2} + \overline{k_3}\right).\vec{r} - iv_4t\right] + c.c$$

This non-linearity describes a coupling between four waves, each with its own direction of propagation, polarization, and frequency. Now, if this non-linear polarization is substituted into Maxwell´s equations, a set of four coupled wave equations is found for the fields. The form of the equations is simplified by defining non-linear scalar coupling coefficients and a wave vector mismatch.

$$\chi_{1234}^{NL} \equiv \hat{e_1}\hat{e_2^*}{:}\,\chi^{(3)}(-\omega_4, \omega_1, -\omega_2, \omega_3){:}\,\hat{e_3}\hat{e_4^*}$$

$$\chi_{ij}^{NL} \equiv \hat{e_i}\hat{e_i^*}{:}\,\chi^{(3)}\left(-\omega_i, \omega_i, -\omega_j, \omega_j\right){:}\,\hat{e_j}\hat{e_j^*}$$

$$\Delta kz \equiv \left(\overline{k_1} - \overline{k_2} + \overline{k_3} - \overline{k_4}\right).\bar{r}$$

Where e_i is the polarization vector of the i_{th} field. The equations for the field magnitudes may now be written in the following form:

$$\frac{dE_1}{dz} + \frac{1}{v_1}\frac{dE_1}{dt} = 2\pi\, i\,\frac{\omega_1}{n_1 c}\left[\chi_{1234}^{NL} E_2 E_3^* E_4 \exp(-i\Delta kz) + \sum_{j=1}^{4} \chi_{1j}^{NL} E_1 E_j E_j^*\right]$$

$$\frac{dE_2}{dz} + \frac{1}{v_2}\frac{dE_2}{dt} = 2\pi\, i\,\frac{\omega_2}{n_2 c}\left[\chi_{1234}^{NL} E_1 E_3^* E_4 \exp(+i\Delta kz) + \sum_{j=1}^{4} \chi_{2j}^{NL} E_2 E_j E_j^*\right]$$

$$\frac{dE_3}{dz}+\frac{1}{v_3}\frac{dE_3}{dt}=2\pi\, i\frac{\omega_3}{n_3 c}\left[\chi^{NL}_{1234}E_1E_2^*E_4\exp(-i\Delta kz)+\sum_{j=1}^{4}\chi^{NL}_{3j}E_3E_jE_j^*\right]$$

$$\frac{dE_4}{dz}+\frac{1}{v_4}\frac{dE_4}{dt}=2\pi\, i\frac{\omega_4}{n_4 c}\left[\chi^{NL}_{1234}E_1E_2^*E_3\exp(+i\Delta kz)+\sum_{j=1}^{4}\chi^{NL}_{4j}E_4E_jE_j^*\right]$$

In most of the common four-wave mixing processes, the equations are simplified since some of these frequencies, wave vectors, and polarizations are degenerate. The previous equations cannot be solved in general, so the usual approach taken is to assume plane wave solutions and that the energy transferred from the input fields to the fourth field is a negligible fraction of the total energy of the fields. With these assumptions, we may decouple the equations and solve for the four fields. This gives the equations for the field intensities:

$$I_{1j}=I_{1j}(0)\exp\,(-\alpha_1 L)$$

$$I_{2k}=I_{2k}(0)\exp\,(-\alpha_2 L)$$

$$I_{3l}=I_{3l}(0)\exp\,(-\alpha_3 L)$$

$$I_{4l}=\frac{L^2}{4}\exp\,(-\alpha_4 L)\left|\chi^{(3)}_{ijkl}(\omega_4)E_{ij}(0)E_{2k}(0)E^*_{3l}(0)\right|^2\times G(\Delta kL)$$

$$G(\Delta kL)=\frac{1+\exp(\Delta\alpha L)-2\exp\,(\frac{1}{2}\Delta\alpha L)\cos\,(\Delta kL)}{\frac{1}{4}L^2(\Delta k^2+\frac{1}{4}\Delta\alpha^2)}$$

Where $\alpha_i$is the absorption coefficient at wi, L is the effective length of overlap of the four fields, and $G(\Delta kL)$ is the phase matching factor. Notice

that the phase matching factor reduces to the familiar form $sinc^2(\frac{1}{2\Delta kL})$ when there is no absorption of the fields.

The assumption of plane wave solution limits the validity of field intensities equations since the fields use experimentally are invariably Gaussian. In order to apply this theory to Gaussian beams, the interaction length must be much smaller than the Rayleigh range so that phase fronts may be approximated as planar.

Efficient coupling between the four waves described may only occur when energy and momentum are both conserved: w4=w1-w2+w3, and k4=k1-k2+k3.

Another equivalent way of understanding these conditions is by realizing that since the energy transfer is a coherent process, all four waves must maintain a constant phase relative to the others in order to avoid any destructive interference. These constraints are embodied in the phase matching factor. $G(\Delta kL)$ only has an appreciable magnitude near ΔkL =0; thus, the output field is completely decoupled from the input fields for large phase mismatches. ΔkL =0 may be achieved by either having a very short overlap length, or choosing a small wave vector mismatch. Phase matching is the process of choosing the directions, and polarizations in birefringent media, in order to eliminate the wave vector mismatch. The figure below is a pictorial representation of the wave vector mismatch: situation (a) shows a finite wave vector mismatch, while (b) demonstrated the corresponding phase matched case. The constraints imposed by phase matching are responsible for the highly directional nature of the signals produced by four-wave-mixing and the ease of spatially separating the output fields.

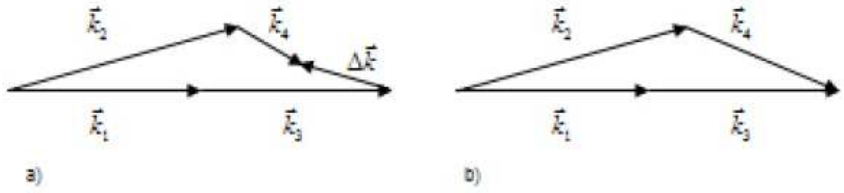

Figure 33: a) phase matching condition no checked, b) phase matching condition checked

The FWM can be used in the radiofrequency signals generation technique injecting a laser in a second semiconductor laser. The semiconductor material works as a non linear material and if it is present a bomb beam, the two beams generate by Four-Wave-Mixing two new signals a frequencies equals to $v_3=2v_1-v_2$ and $v_4=2v_2-v_1$.

One time the FWM has theoretically been explained we continue this section with the experiment reported at the beginning of this section.

To measure the Four-Wave-Mixing phenomena an experiment has been carried out on device 6 of BAR-A. In this experiment done with attenuation (attenuator 2 on) the lasers 2 and 3 are on and the DFB3 current is changed while the DFB2 current is fixed; by doing this we change the detuning between these two lasers and check when the FWM is produced.

To realize these measurements the device 6 has been used because it has a wavelength detuning between all the three lasers that is smaller than the other devices, and it has a higher SMSR. Therefore, there is more difference of power between the primary and secondary mode of each laser, and it can be easier to identify the new signal at a new frequency generated by FWM.

As usual, the spectra have been acquired using from the OSA (span of 1nm and resolution of 0.01nm) using LabView at different detuning values (30GHz, 25GHz, 20GHz, 17GHz, 15 GHz, 12GHz, 10GHz, 5GHz, 0GHz).

The results obtained are shown in the figures below:

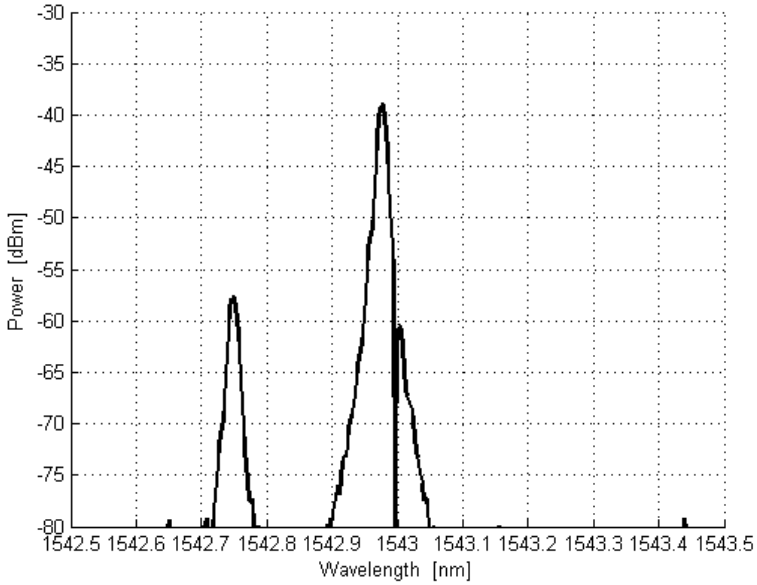

Figure 34: Detuning 30 GHz

In Figure 34 the left peak is the DFB3 and the other is the DFB2 peak. In this case the detuning value is of 30 GHz and in this case it isn´t produced a detectable FWM.

In the next measurements we are going to reduce the detuning value, so the DFB3 current is going to be increased.

If we observe the next graph we can see that for a detuning of 10 GHz the FWM signal can be detected, in the form of a fourth peak that can be seen in the spectrum: the DFB2 mode (194.4342546THz) the DFB3 mode (194.4236699THz) and the two FWM peaks that are generated at frequencies equal to $2V_2$-V_3 (194.4130863THz) and $2V_3$-V_2 (194.4452186 THz).

.

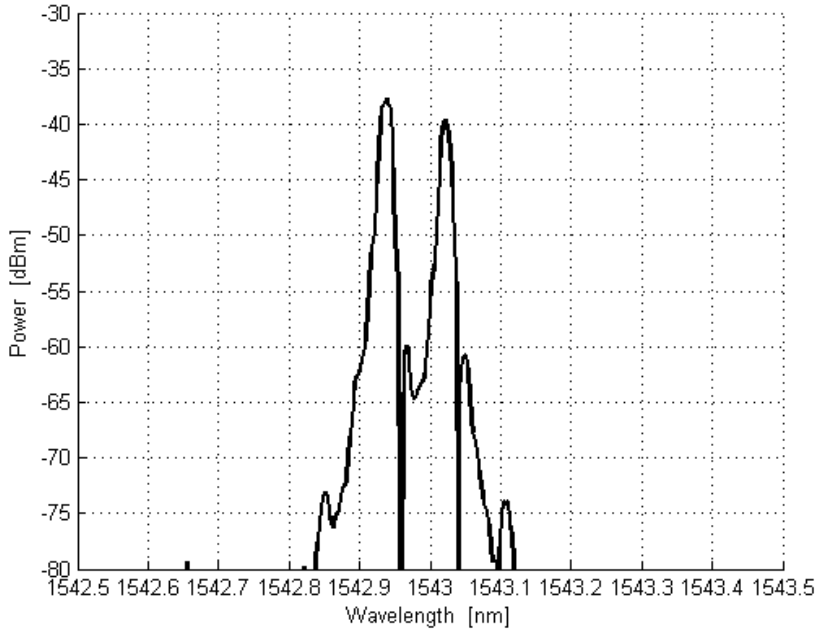

Figure 35: Detuning 10GHz

When the detuning is further reduced to 5GHz, the FWM signals cannot be observed, because a chaos situation occurs. The chaos is produced because in this case the portion of light of DFB3 that is injected in DFB2, and there amplified and backreflected into DFB3 is large, and it generates reflections to which laser DFB3 is extremely sensitive, and can bring the laser to chaos. In Figure 36, the peaks that appear around DFB2 are due to the excitation of the relaxation oscilations, at a frequency of about 4-7 GHz.

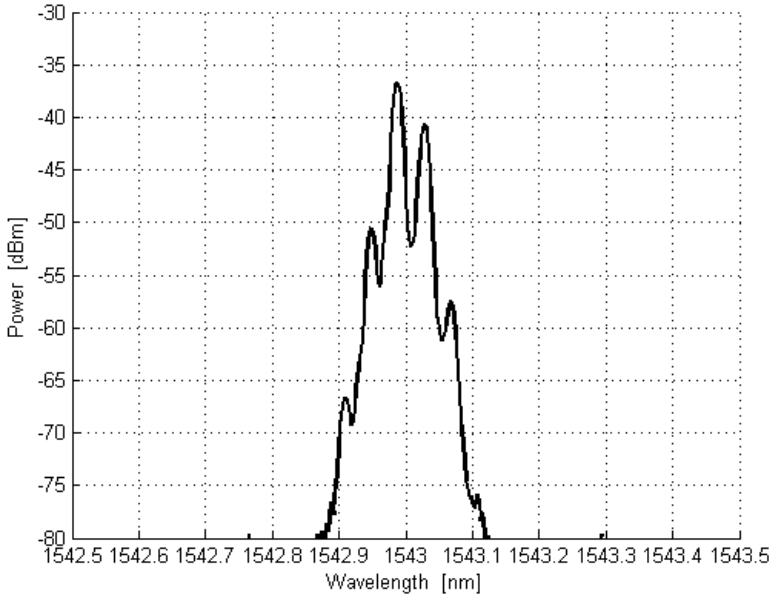

Figure 36: Detuning 5GHz

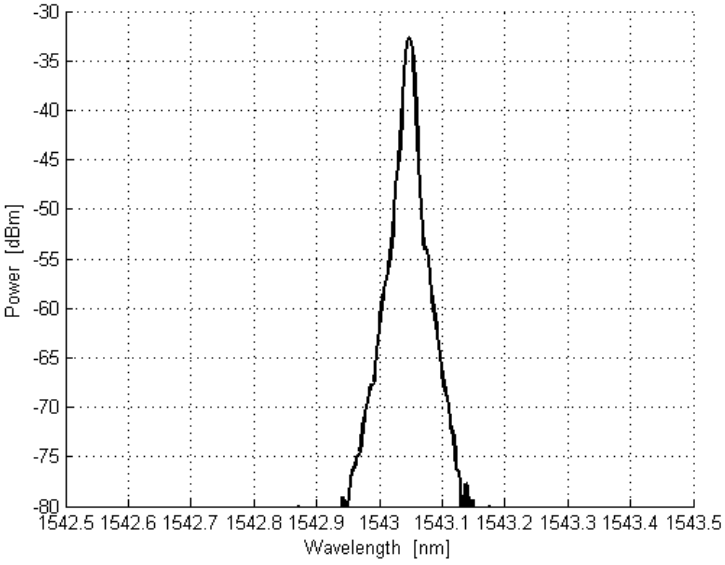

Figure 37: Detuning 0GHz

In Figure 37 a single peak is observed, this is due to the lasers 2 and 3 that are locking mutually together and therefore the two initial peaks observed are degenerate into a single peak, slightly increasing its power. To measure the locking range (the frequencies range where the two lasers are locked) it is required to keep on increasing the DFB3 current and check for what detuning value the two peaks of signal are again observed as separated; the difference of frequencies in this point between the modes of the two lasers is called locking range and for this case we reported a value of 2GHz.

The same measurement without attenuation has been also carried out. In this case the DFB3 current has been changed to obtain detuning values of 20GHz, 15 GHz, 10GHz, 9GHz, 5GHz and 0GHz. The spectra exhibited FWM from 20GHz to 10GHz, while at 9GHz the chaotic behavior started, and at 0GHz the lasers were locked, with a locking range of 4GHz.

In the FWM spectra for a detuning of 20GHz a single FWM peak is observed, however if we decrease the detuning value to 15 GHz a new peak arise as consequence of FWM, so we can observe the DFB2' peak (clone signal of the DFB2 laser) the DFB3 peak, the DFB2 peak and the DFB3' peak (clone signal of the DFB3 laser).

All these results are shown in the next plots:

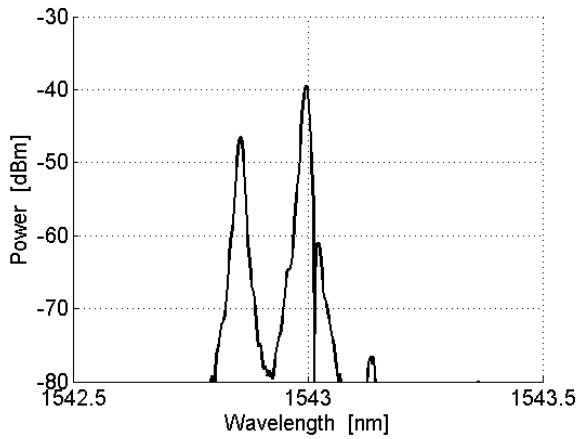

Figure 38: Detuning 20 GHz (from left to right: DFB3, DFB2, DFB3')

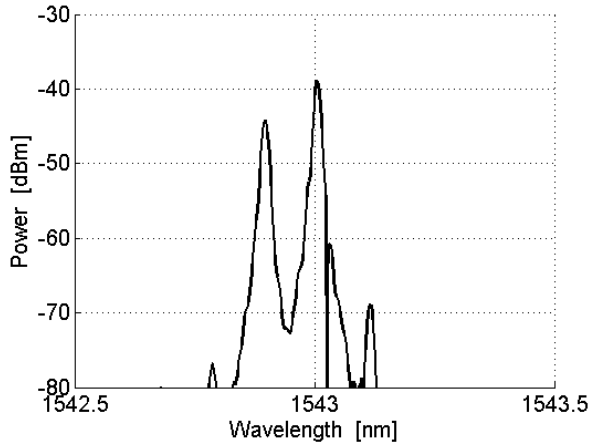

Figure 39: Detuning 15 GHz (from left to right: DFB2',DFB3, DFB2, DFB3')

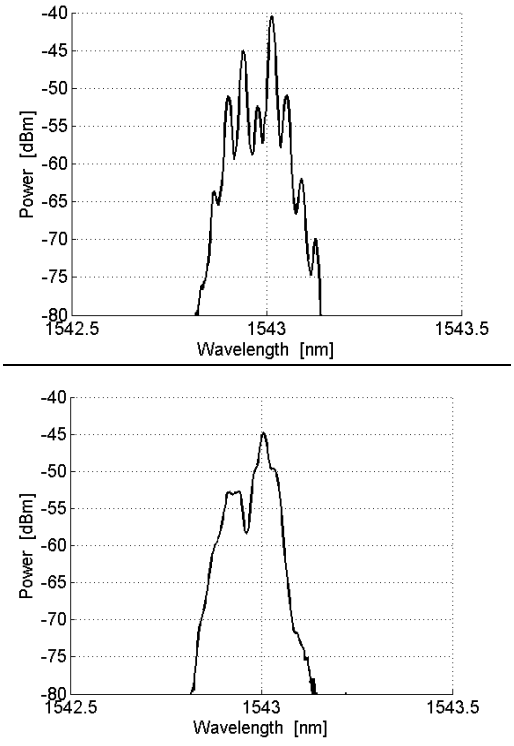

Figure 40: Chaos with a detuning of 9 and 5 GHz respectively

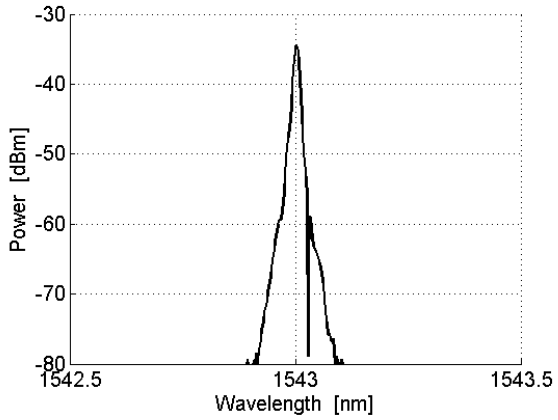

Figure 41: Detuning 0 GHz, locking

3.6 FWM Gain

Two parameters of the optical gain of the laser DFB-AUX used as optical amplifier in a reflection configuration can be measured. One of these parameters is the optical gain that can be measured as:

$G_{aux}=P_{out}/P_{in}$;

Where P_{in} is the power that is injected in DFB-AUX laser and P_{out} is the amplified signal at the same wavelength of P_{in} that is reflected back by DFB-AUX.

Another parameter that can be defined and measured is the FWM gain:

$G_{FWM}=P_{FWM}/P_{in}$

In this case the Pin is the same that in the Gaux measure and the P_{FWM} is the power of the Four wave mixing signal generated in DFB-AUX semiconductor laser.

The first measurement realized in this section is the FWM gain of the BAR-B, device 1. If we observe the Figure 42 where the FWM phenomenon is represented we can see four peaks corresponding to: The principal mode of laser 2 at frequency v2, the secondary mode of laser 2, the principal mode of laser 3 at frequency v3 and the peak corresponding to the FWM produced inside DFB3. The experiment has been realized with the DFB3 mode in the stop band and the DFB3 outside the stop band. The stop band is the distance between 2 modes of a DFB laser, this means the frequencies range where another modes can´t exist as consequence of the Bragg grating. As it can be seen from the measurement, the Four Wave Mixing gain is higher in the stop band case it means that when the principal mode of DFB3 laser is between the two modes of DFB2 laser the FWM gain is higher than in the other case.

In the other measurements, the DFB2 and DFB3 have been turned on and the DFB3 current has been changed between 140 and 160 mA, by increasing it in 2 mA steps with a constant value of DFB2 current (140 mA). The spectra have been acquired by collecting the light with an optical fiber from the DFB3 side. For each current value, the optical spectrum we have measured from the OSA: the DFB3 power, the DFB2 power, the DFB2' power (power of the FWM signal) and the detuning between the DFB3 laser and the FWM signal. The result concerning to this experiment is shown in the figure 44 in this figure R is the gain calculated as P_2/P_3. It can be observed that the gain decreases for increasing detuning: it means that when the distance in frequency between the DFB3 laser and the signal generated by FWM increases, the gain decreases. This is in agreement with the fact that the FWM gain is a decreasing function of the detuning.

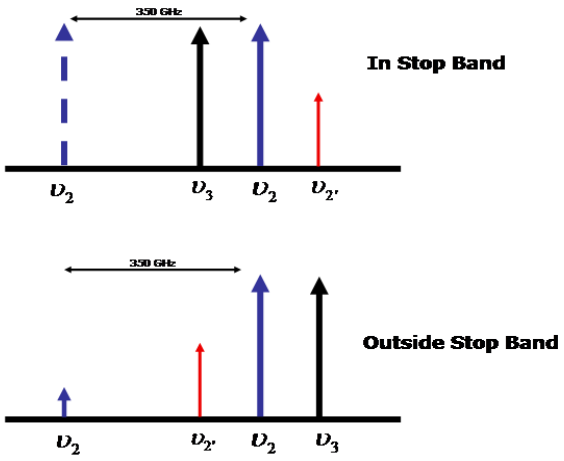

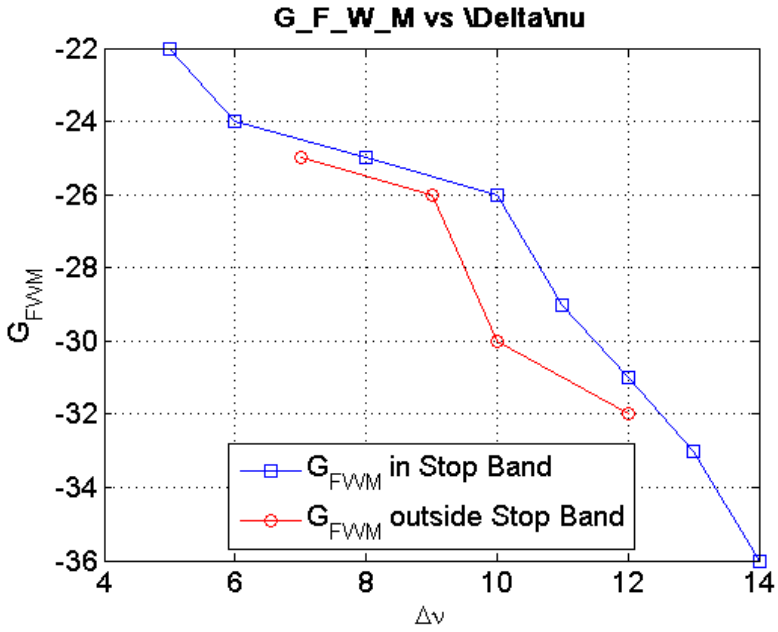

Figure 42: FWM Gain in BAR-B, device 1

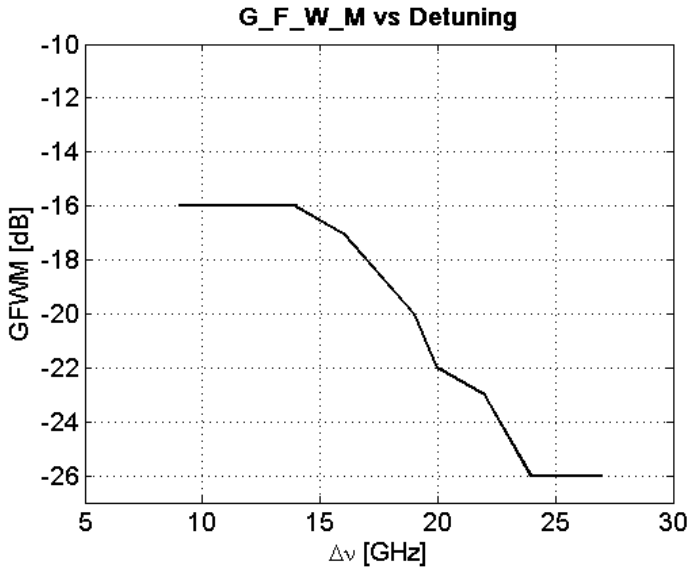

Figure 43: FWM Gain with laser 2 and 3 on

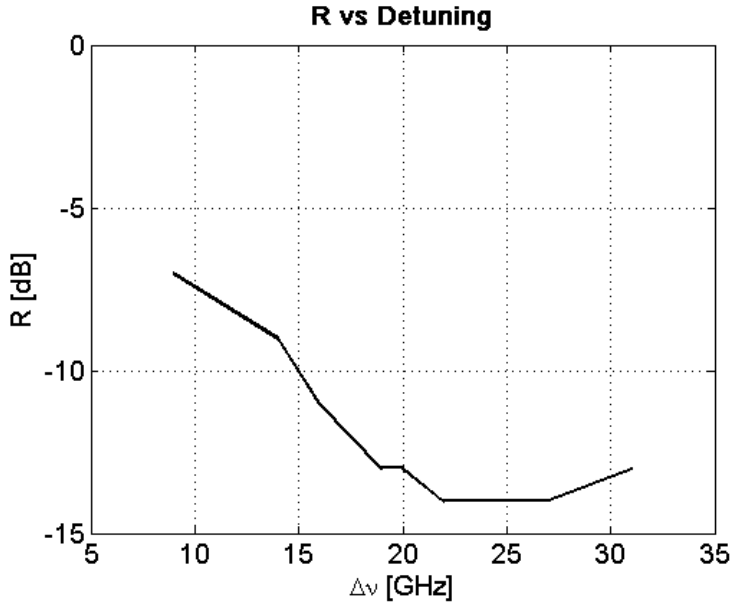

Figure 44: R with laser 2 and 3 on

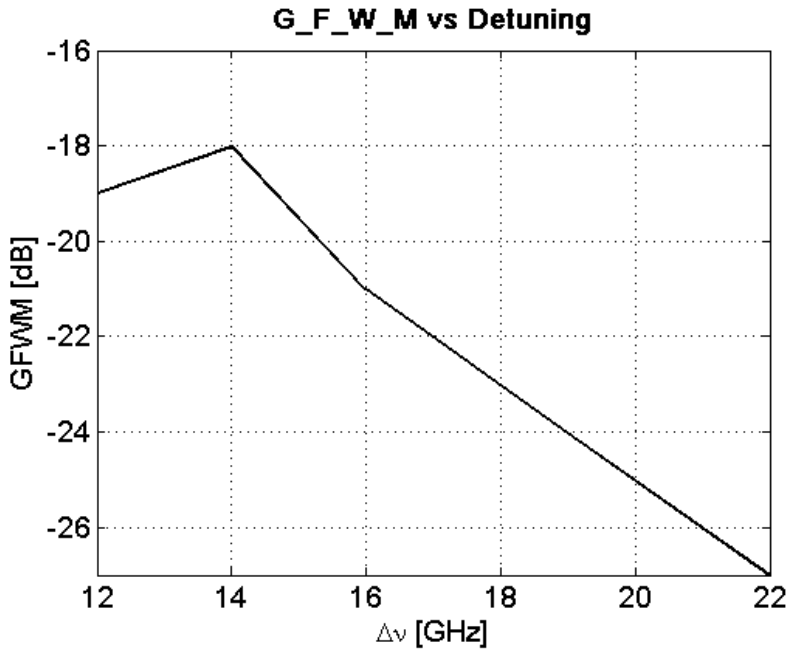

Figure 45: FWM Gain with laser 1 and 3 on.

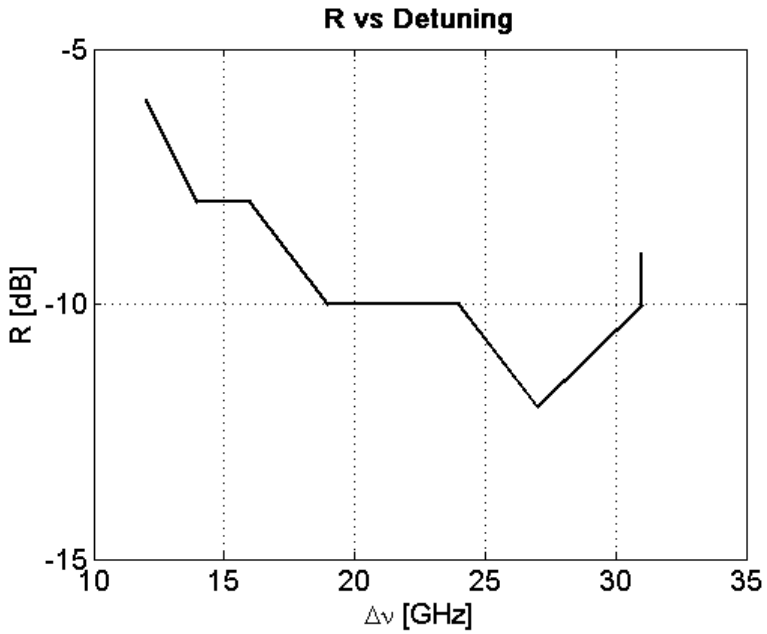

Figure 46: R with laser 1 and 3 on

In Figure 45 and 46 the DFB3 current is changed between 115 and 135 mA, and the power of DFB1 (current of 140 mA) is injected into DFB3. Now the values observed on the OSA are: the DFB3 power, the DFB1 power, the detuning between DFB3 and the signal generated by FWM and the signal generated by FWM as consequence of the power injected in DFB3. The graphics have been obtained using the software matlab as before and calculating:

$G_{FWM}=P_{1'}/P_1$;

$R=P_1/P_3$;

3.7 Injection locking regime

Another experiment to check the behavior of the principal modes of a laser in the injection-locking regime has been carried out. Injection locking and injection pulling refer to the frequency effects that can occur when a harmonic oscillator is disturbed by a second oscillator operating at a nearby frequency. When the coupling is strong enough and the frequencies close enough, the second oscillator can capture the first oscillator, causing it to have essentially the identical frequency of the second. This is called injection locking. When the second oscillator merely disturbs the first but does not capture it, the effect is called injection pulling. Injection locking and pulling effects are observed in numerous types of physical systems, however the terms are most often associated with electronic oscillators or laser resonators.

This technique can be used to synchronize a slave oscillator by a master oscillator injecting the emitted light of the master laser in the slave laser and, if adapted conditions are fulfilled, the slave laser emits light at the same frequency and a constant phase relation with master laser.

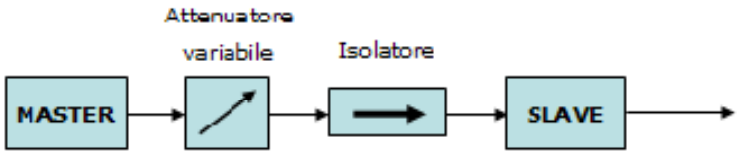

Figure 47: scheme of a master-slave configuration.

Fundamental parameters relevant to the injection locking are: the detuning (defined as the difference in frequency between the master laser frequency and the slave laser frequency when they aren´t locked) and the injection factor R (defined as the ratio between the injected power by the master laser and the power of the slave laser not locked). By observing the beating signals of two DFB lasers before and after the locking with an optical spectral analyzer, two peaks are seen at first: one of master laser and another of slave laser. When the locking is produced the two peaks disappear to show a single peak. A particular detuning value exists as a function of R for which the locking is produced. This characteristic is shown in the detuning-factor graphic that identify the locked regions.

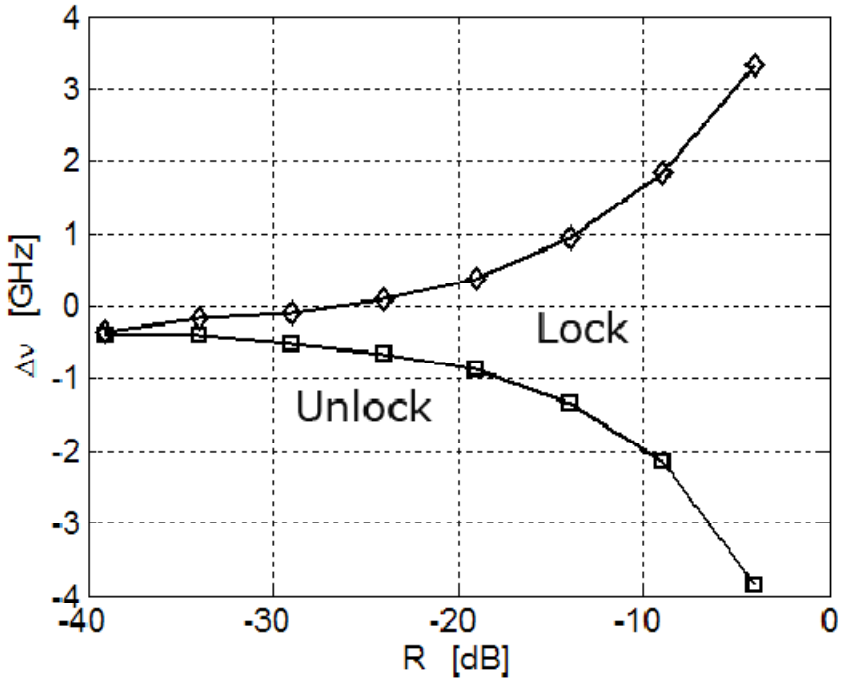

Figure 48: Detuning-R

In the experiment realized in the present project, the Labview software has been modified in order to acquire the value of the power of the principal and secondary mode of the laser that works as master or as slave.

The measurements began with BAR E, device 6. In this measure the optical spectrum of the signal has been taken from the DFB3 side, while changing the DFB1 current between 25 and 180 mA and plotting the behavior of the principal and secondary mode of DFB3 in injection-locking regime. Injection locking happens around 150mA, and this can be identified in the graph of Figure 49 where the maximum graph has a peak. In all measurements carried out on this device the spectrum has been observed from the side of the laser which current hasn't been changed: it means that if, for example, we are observing the spectrum in the DFB3 side with laser DFB3 and 2 on, the current which is changed is DFB2 current.

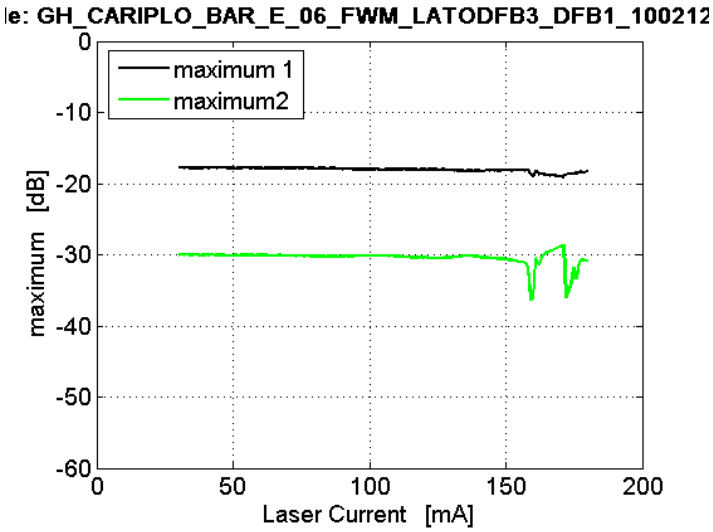

Figure 49: Behavior of the powers of the two modes of DFB3 (BARE, device 6) changing DFB1 current in injection-locking regime observed in DFB3 side.

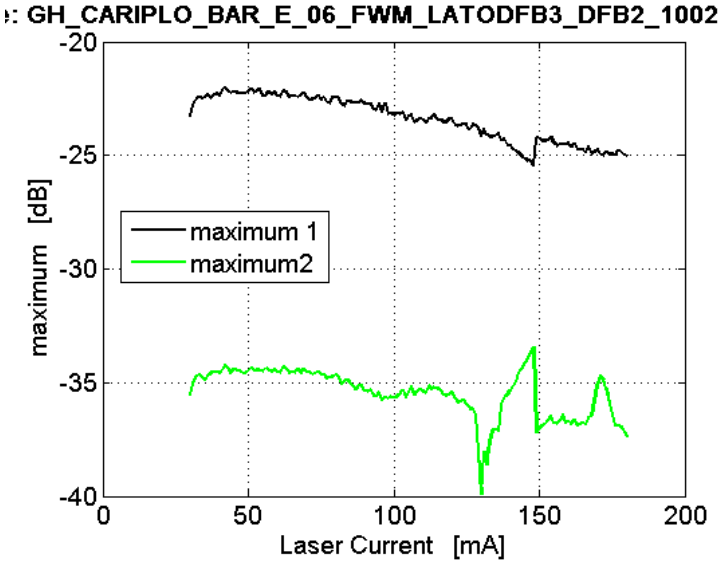

Figure 50: Behavior of the powers of the two modes of DFB3 (BARE, device 6) changing DFB2 current in injection-locking regime observed in DFB3 side.

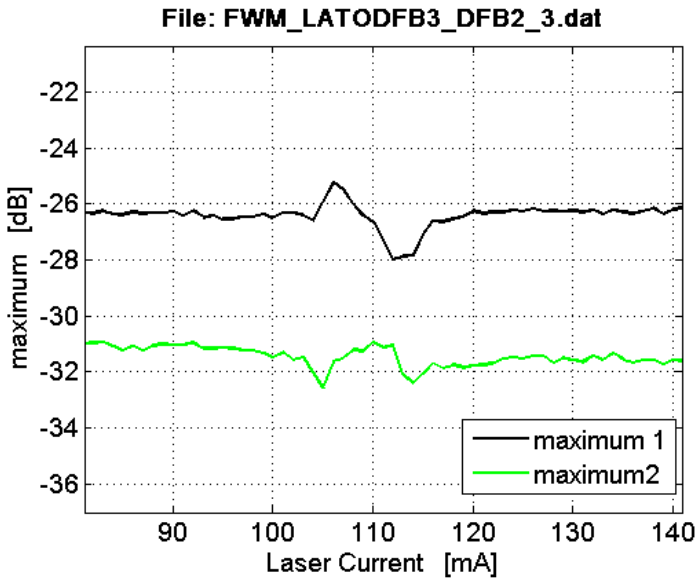

Figure 51: Behavior of the powers of the two modes of DFB2 (BARE, device 2) changing DFB2 current in injection-locking regime observed in DFB3 side.

In the previous graphic the analysis of Device 2, BAR E has been done, with laser DFB2 and DFB3 at the temperature of 24°C. The spectra have been acquired from the OSA (span of 5nm and resolution of 0.01nm) using LabView from the DFB3 side and changing the DFB2 current.

The objective is as it has been explained to study the behavior of the powers of the two modes of DFB2 in injection-locking regime. Injection locking happens around 110mA. It can be seen in the graphic below that there is injection locking between DFB2 and DFB3 at 105.6 mA and is observed a power pick in the maxima graphic. The locking ends at 115 mA where the maxima graphic return to be continue.

A change of 1 mA corresponds to a change of 1 GHz so the locking (the range of frequencies that lasers are locked) is of 9 GHz.

In all graphics shown it is observed a peak in the value of current where the injection-locking is produced due to the fact that when two lasers are locked an only peak is observed with an increment of power therefore Injection locking can also provide a means of gain at a low power cost in certain applications.

CHAPTER 4

INTERFEROMETRIC MEASUREMENT OF THE CORRELATION OF THE MODES OF A FABRY PEROT SEMICONDUCTOR

Light sources capable of generating short optical pulses at high repetition frequencies are key devices in high speed optical transmission systems, optical signal processing, and optical measurements. Harmonic mode-locking technique is widely used to this purpose. Especially, the harmonic colliding-pulse mode-locking technique is advantageous, because no external electro-optic modulator is necessary.

Mode-locking is a technique in optics by which a laser can be made to produce pulses of light of extremely short duration, on the order of picoseconds (10^{-12}s) or femtoseconds (10^{-15}s). The basis of the technique is to induce a fixed phase relationship between the modes of the laser's resonant cavity. The laser is then said to be *phase-locked* or *mode-locked*. Interference between these modes causes the laser light to be produced as a train of pulses. Depending on the properties of the laser, these pulses may be of extremely brief duration, as short as a few femtoseconds.

In a simple laser, each mode will oscillate independently, with no fixed relationship between each other, in essence like a set of independent lasers all emitting light at slightly different frequencies. The individual phase of the light waves in each mode is not fixed, and may vary randomly due to such things as thermal changes in materials of the laser. In lasers with only a few oscillating modes, interference between the modes can cause beating effects in the laser output, leading to random fluctuations in intensity; in

lasers with many thousands of modes, these interference effects tend to average to a near-constant output intensity, and the laser operation is known as a *c.w.* or *continuous wave*.

If instead of oscillating independently, each mode operates with a fixed phase between it and the others modes, the laser output behaves quite differently. Instead of random or constant output intensity, the modes of the laser will periodically all constructively interfere with one another, producing an intense burst or pulse of light. Such a laser is said to be *mode-locked* or *phase-locked*. These pulses occur separated in time by $\tau = 2L/c$, where τ is the time taken for the light to make exactly one round trip of the laser cavity. This time corresponds to a frequency exactly equal to the mode spacing of the laser, $\Delta\nu = 1/\tau$.

Active and passive methods exist to mode-lock a Fabry-Perot laser diode by purely optical or electro-optical means. Passive mode-locking techniques are those that do not use an external electrical signal, but rely on placing some element into the laser cavity which causes self-modulation of the light. Rather, they use the light in the cavity to cause a change in some intracavity element, which will then itself produce a change in the intracavity light. The most common type of device which will do this is a saturable absorber..

A saturable absorber is an optical device that exhibits an intensity-dependent transmission. What this means is that the device behaves differently depending on the intensity of the light passing through it. For passive mode-locking, ideally a saturable absorber will selectively absorb low-intensity light, and transmit light which is of sufficiently high intensity.

In the active optical method two F-P modes are mutually injection-locked with the aid of an injected cw light at the center frequency of the two modes. The other F-P modes are cascadingly mode-locked owing to the cavity-enhanced nondegenerate four-wave mixing in the F-P. By injecting the cw light properly, linewidth narrowing of the lasing longitudinal modes can be observed, and a short optical pulse train at the repetition frequency of one F-P mode spacing is generated.

The principle of the proposed method is shown in figure 52. Narrow-linewidth cw light is injected into an F-P via an optical amplifier. The oscillation frequency of the cw light f_{LD} is adjusted to the center of the frequencies of the two lasing main modes of the F-P, f_{-1} and f_{1}. In this arrangement, the injected cw light acts as a pump source of the nondegenerate FWM, and the FWM sideband components of the modes at f_{-1} and f_{1} are generated at f_{1} and f_{-1}, respectively. The two F-P modes are mutually injection locked owing to these FWM components. Therefore, their relative phases are locked and the linewidths of the F-P modes become narrow.

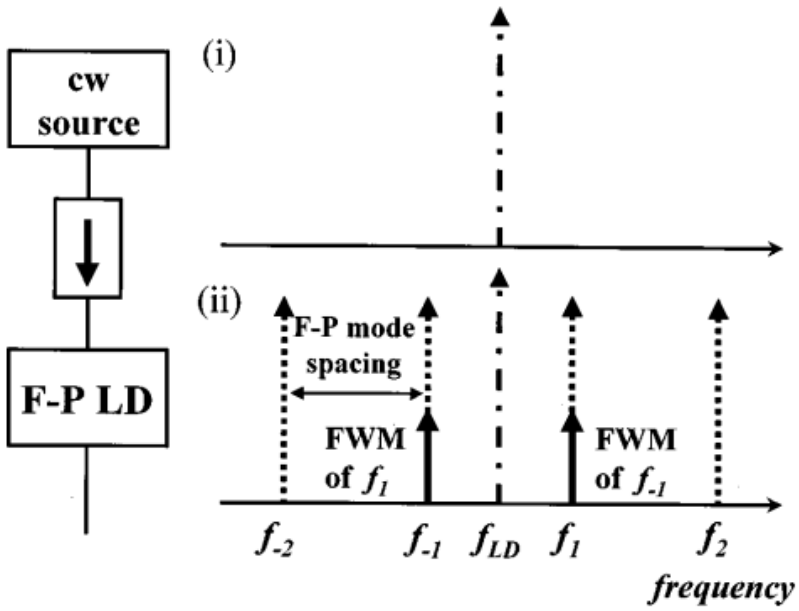

Figure 52: Mutual injection between a Fabry-Perot, ECL lasers

Once this mutual injection locking is established, strong FWM components between the two F-P modes are generated at $f_{\pm 2}$ owing to the cavity-enhanced nondegenerate FWM. Consequently, the F-P modes at $f_{\pm 2}$ are injection locked by these FWM components. This process, that is, the cavity-enhanced nondegenerate FWM between injection locked F-P mode and the

subsequent injection locking of adjacent F-P modes, cascadingly occurs, and the F-P LD is mode locked at the frequency equal to the F-P mode spacing.

In the experiment that implements this active technique (which setup is shown in the figure 53 and it is explained in [11]) it´s demonstrated that the linewidth of a Fabry perot mode laser is reduced when the cw light is injected at the center frequency between two Fabry Perot modes. A commercially available 1.55 mm F-P LD was used whose cavity length is 300 µm. An external cavity tunable laser (ECL) of narrow linewidth (<100 kHz) was used as the cw light source. The cw light power is amplified by an erbium-doped fiber amplifier (EDFA). The amplified cw light passes through a polarization controller (PC) and an optical isolator, and is injected from the output facet of the F-P LD. The output of the F-P LD is observed from the monitor facet through an optical isolator. The output spectrum is measured by an optical spectrum analyzer (resolution 0.01nm). The linewidth of the lasing F-P modes are observed by heterodyning the output of the F-P LD with a DFB-LD of narrow linewidth (<10 MHz). To detect the heterodyne signal and the autocorrelation trace of the pulse train effectively, an EDFA is used. The heterodyne signal is detected by a p-i-n photodetector (PIN-PD, bandwidth520 GHz), and is observed by an RF spectrum analyzer. The judgement whether the mode locking occurs or not is done indirectly by observing the linewidth narrowing of the lasing F±P modes. Concretly the linewidth of the mode at $f_{\pm 3}$ is measure. The pulse train is measured by the autocorrelator in the mode locked condition. The lasing frequency of the DFB-LD for heterodyning was adjusted by controlling the heat sink temperature. Figure 46 a shows the beat spectrum when the frequency of the cw injected light f LD was not exactly adjusted to the center of the two F-P modes at $f \pm_1$.

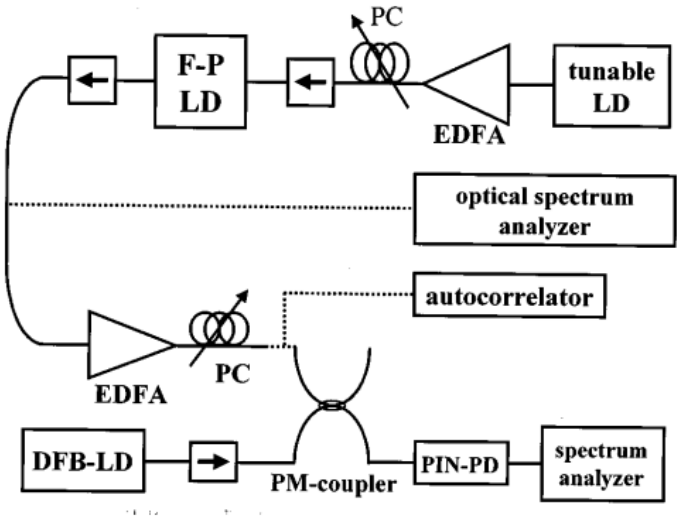

Figure 53: Experimental setup

On the other hand, when f LD was exactly adjusted to $(f_{-1}+ f_1)/2$ by a fine control of the bias current of the F±P LD, the beat spectrum narrowed as shown in Fig. 54 b. Note that the linewidth narrowing of the F±P mode at $f_{\pm3}$ occurs as a consequence of the several-step process; (1) the mutual injection locking of the two F±P modes at $f_{\pm1}$, and (2) The subsequent cascading injection locking of the F±P modes at $f_{\pm2}$ and $f_{\pm3}$ due to the cavity-enhanced nondegenerate FWM between the F±P modes. The mutual injection locking of the two F±P modes at $f_{\pm3}$ may also lead to the linewidth narrowing in Fig. 54 b. But, the FWM eficiency for this process is smaller than for the cascading injection locking mentioned above, because the

wavelength difference between the pump and the signal is larger.

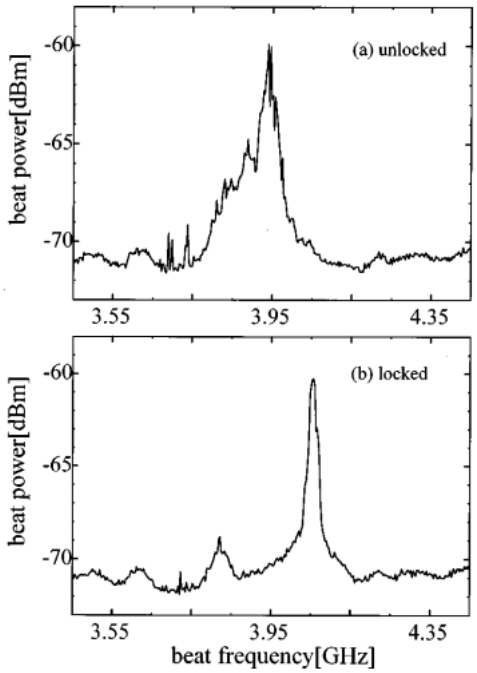

Figure 54: Beat frequency between the F-P laser diode and the mode at 1553nm of the DFB laser diode.

To check if the Fabry Perot modes can be locked without an externally injected signal we have done a similar setup to the previously explained and it is shown in the next figure:

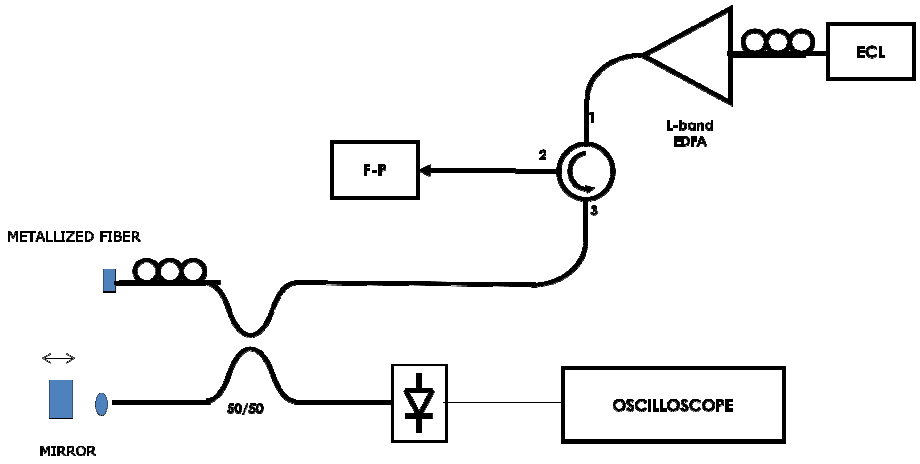

Figure 55: Used setup with a Michelson interferometer's

This setup is composed of: an ECL (external-cavity- laser) laser, an L-band (the L-band EDFA amplifies wavelengths between 1570 nm and 1610nm), a circulator which allows to inject the ECL signal in the Fabry-perot laser and to inject the signal in the interferometer, a Fabry-Perot semiconductor laser, and an interferometer.

The Fabry-Perot (NNT electronics) has a center wavelength of 1585 nm and a maximum work current of 180 mA.

The used interferometer is a Michelson interferometer, the most common configuration for optical interferometry. An interference pattern is produced by splitting a beam of light into two paths, bouncing the beams back and recombining them. The different paths may be of different lengths or be composed of different materials to create alternating interference fringes on a back detector. In this case the interferometer is composed of two paths, one of them relies on a polarization controller, and a metallized fiber, the other one relies on a mirror that let to come back the light that will be detected on the photodiode with the light coming from the metalized fiber.

The analysis of the unbalance between the two branches of a Michelson's interferometer can be achieved by modulating the wavelength of an ECL laser injected in the interferometer, both the mirrors being kept at rest. The different lengths travelled by the light in the two branches give rise to a phase delay in the two signal generated at the interferometer's output. By letting increase the wavelength, an interferometric sinusoidal signal is produced, in which the phase increases because of the nonzero temporal derivative of the wavelength's number rather than that of the unbalance.

The spectra to realize this measurement have been acquired from a FFT electrical spectrum analyzer (span 51kHz, resolution lines 1600).

The power of the ECL laser (TEKTRONIX LPB1100) is 0.5mW in all measurements done and the wavelength modulation is achieved by applying a triangular waveform, 20V peak-peak amplitude and a frequency of 10 Hz.

The initial unbalance is unknown, and different pieces of optical fiber of known length have been added in one of the two branches. To know the initial imbalance we don´t add any fiber in the interferometer branches which correspond to the figure 56. In this case we observe that the frequency peak in the FFT spectrum analyzer is at 2,5kHz which correspond to an imbalance of 1,67m.

To obtain the imbalance measure knowing the beating frequency, we have realized a series of mathematical developments in which the signal that arrives to the photodiode has a phase of $\emptyset = 2k_1s_1 - 2k_2s_2$ being k the wavelength number and s the traveled path for each signal. If we continue developing this equation we obtain that for each meter of added fiber the beat frequency is increased in 1.5 KHz.

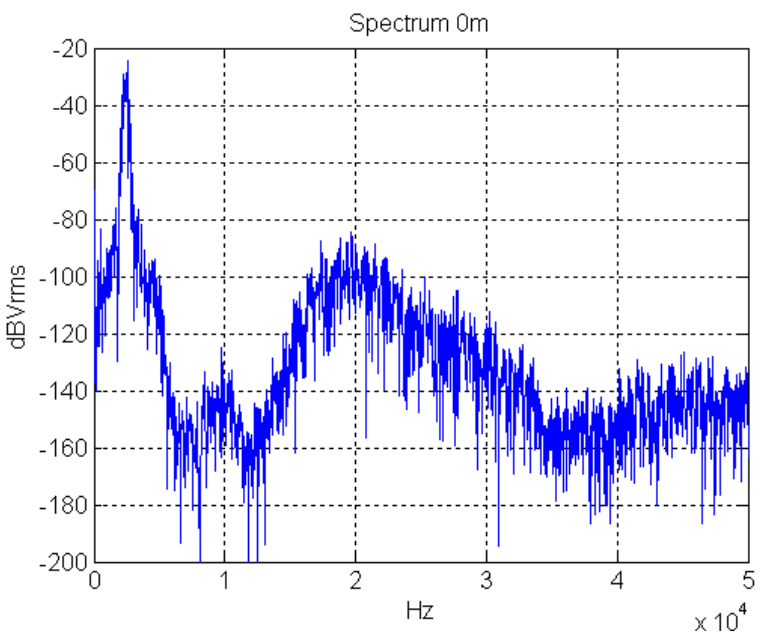

Figure 56: Signal obtained in the FFT spectrum analyzer without added fiber, peak frequency of 2.5KHz

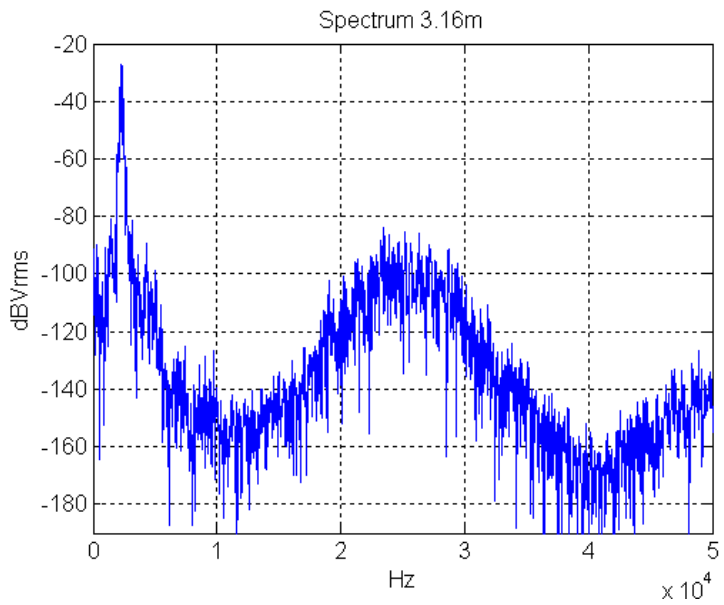

Figure 57: Signal obtained in the FFT spectrum analyzer with 3.16 added fiber meters, peak frequency of 2.3KHz

If 3.16 meters of fiber are added between the polarization controller and the metalized fiber, a beat frequency of 2.3 KHz is observed in the spectrum analyzer, this means that firstly the mirror branch was longer and now the imbalance is due to the metalized fiber branch`s. So we know that the mirror branch's is 1.67 meters longer than the other one and therefore we should to add 1.67 meters of fiber in the metalized fiber branch to balance the two interferometer branches.

Then we know the initial imbalance of the interferometer branches, we pass to measure the fiber length for different fiber introduced between the polarization controller and the metalized fiber. In each plot we can observe that the fact of increase the length of the added fiber leads to a higher beat frequency in the FFT spectrum analyzer.

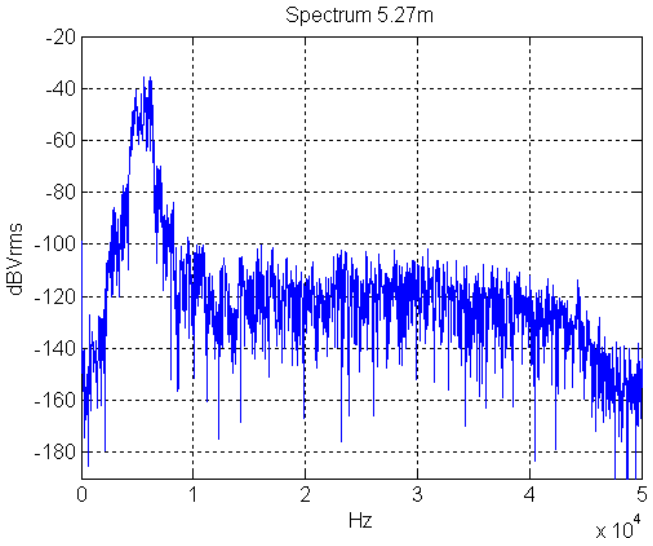

Figure 58: Signal obtained in the FFT spectrum analyzer with 5.27 added fiber meters, peak frequency of 5.6 KHz

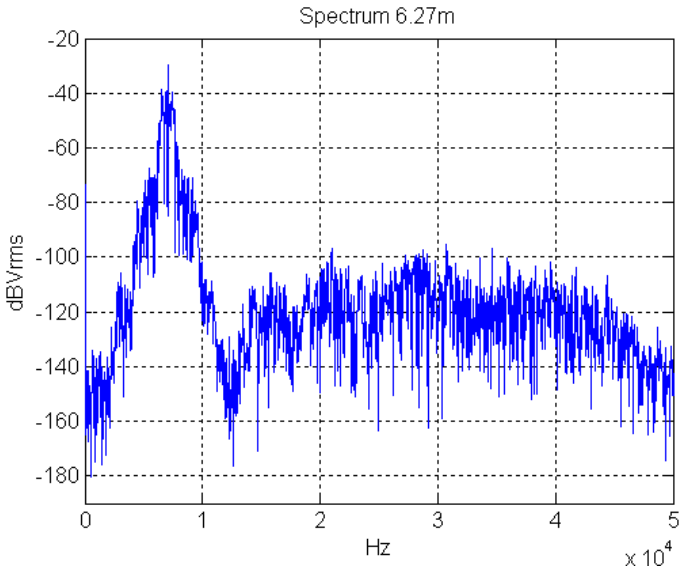

Figure 59: Signal obtained in the FFT spectrum analyzer with 6.27 added fiber meters, peak frequency of 7.1 KHz

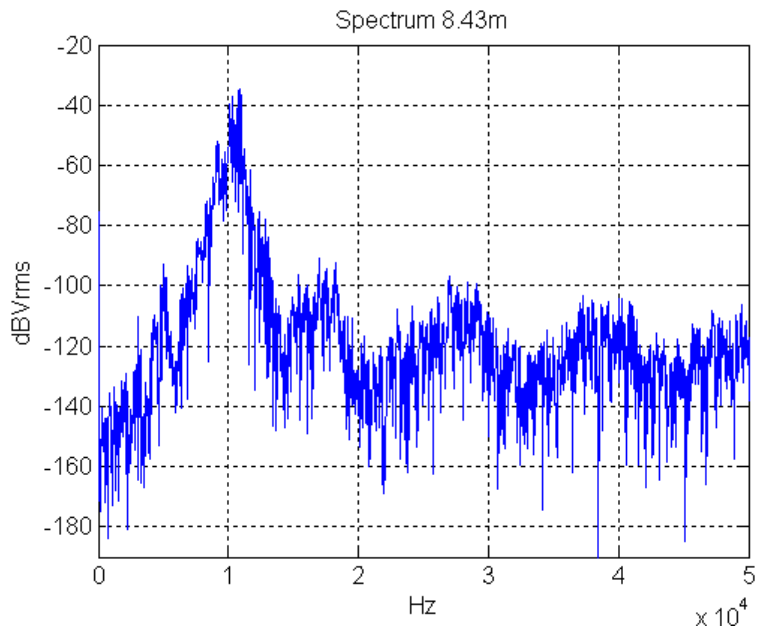

Figure 60: Signal obtained in the FFT spectrum analyzer with 8.43 added fiber meters, peak frequency of 10.3 KHz

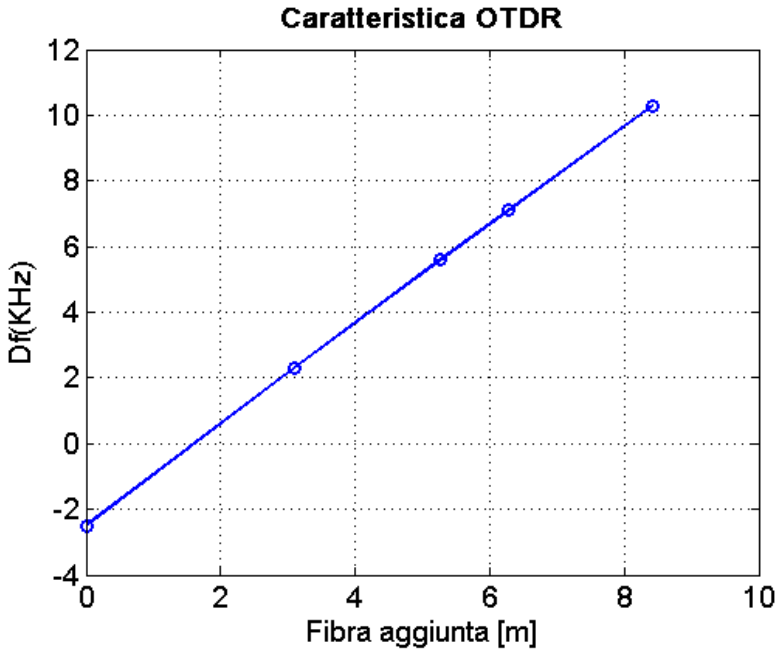

Figure 61: OTDR characteristic

The interferometer characteristic is linear, this is seen in the figure 61 where the x axis represents the added fiber meters and the y axis represents the beat frequency.

After the interferometer has been balanced, we proceeded with the measurement of correlation between the modes of the FP laser. This measurement is performed by displacing the moveable mirror of the interferometer, thus generating interferometric fringes. The contrast of the fringes is measured for different unbalances of the interferometer. By plotting the contrast as a function of the unbalance, the correlation length (related to the correlation time) of the F-P laser modes can be measured.

To carry out these measurements we have lanced the light from the Fabry Perot laser into the interferometer. In the experiment the laser current has been changed between 20 and 160 mA and for each current value the interferometric signal has been obtained by moving the mirror of the interferometer with a small motor which moves the mirror with a constant speed. At the beginning we have done the measurements without inserting any fiber in an interferometer branch, then a fiber of 2.33 and other of 5.66 meter have been introduced in the metalized fiber branch and the same measurements have been done.

For all the interferometric signals measured in the different cases, we were able to measure the contrast of the laser carrier and the contrast of the amplitude modulation caused by the presence of different modes. We can calculate the contrast of the laser as: $C = \frac{C_{max}+C_{min}}{C_{max}-C_{min}}$ where C_{max} is the maximum value of the interference and C_{min} is the minimum value of the interference signal. On the other hand we calculate the contrast of modulation as:$C_m = \frac{A-B}{A}$ where A is the modulation value for each modulation peak and B is the minimum of the modulation.

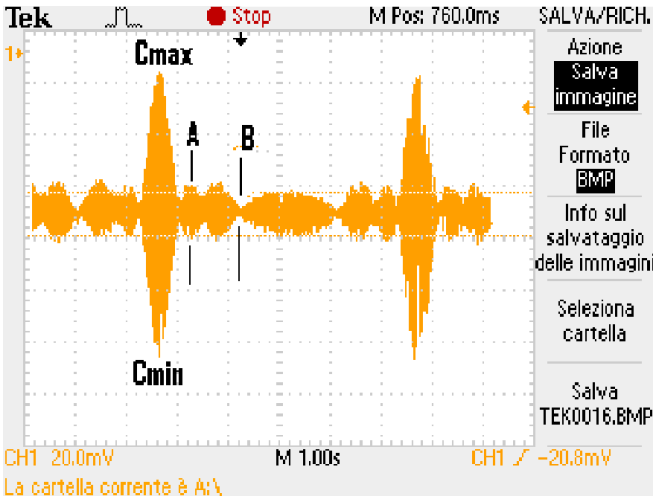

Figure 62: Contrast measurements.

With all this contrast values we realize a plot of the contrast as a function of the injected current for each different unbalance which is depicted in figure 63.

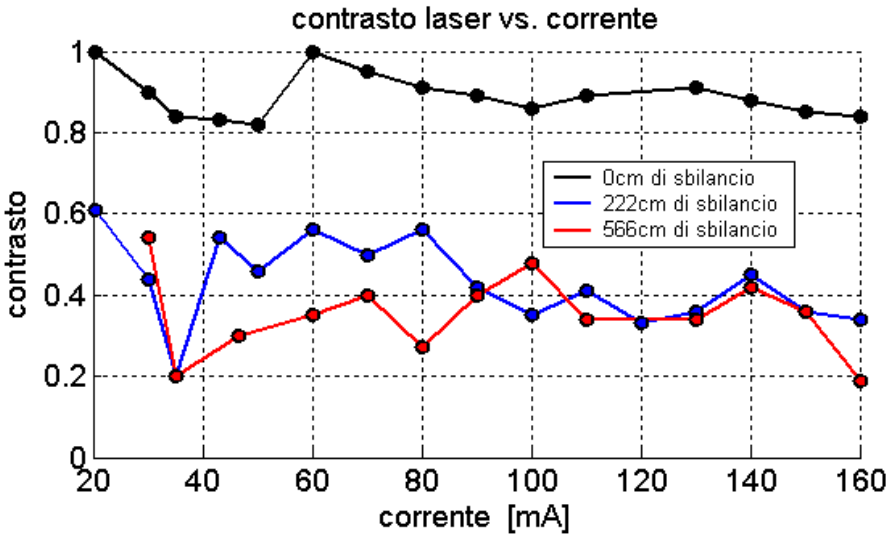

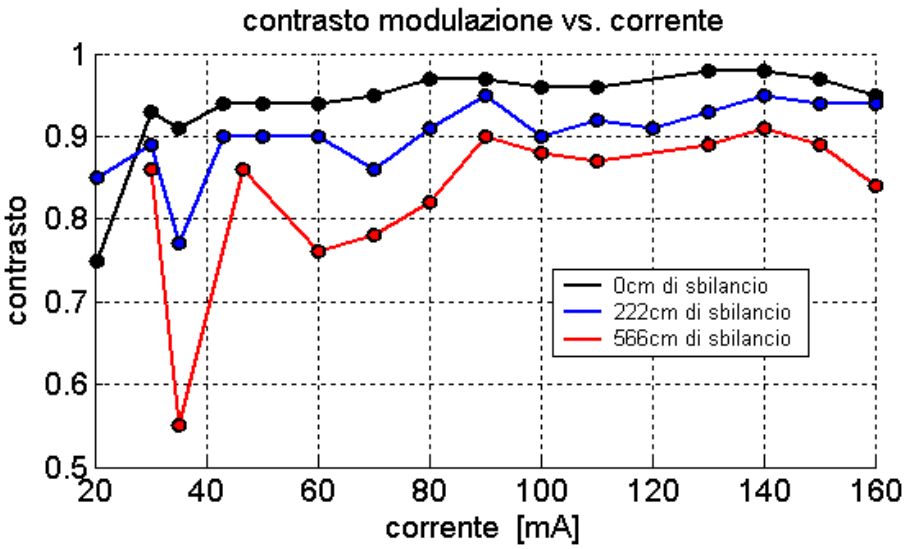

Figure 63 a) Contrast of the laser b) Contrast of modulation

The contrast of the laser is related with the laser linewidth so if the contrast value is close to 1, the linewidth is narrow. By the other side the contrast modulation tell us if the laser modes are correlated. Coherence is one of the most important concepts in optics and is strongly related to the ability of light to exhibit interference effects. A light field is called coherent when there is a fixed phase relationship between the electric field values at different locations or at different times. Partial coherence means that there is some (although not perfect) correlation between phase values. There are various ways of quantifying the degree of coherence, one of these ways is to measure the contrast interference, in this experiment as can be seen in the figure 63 b the contrast of modulation increase slightly with the current.

As conclusion of these measurements we can think that the modes of a Fabry-Perot laser are partially phase-locked without the injection of an external signal. This can be seen because the contrast of modulation is practically between 0.85 and 0.95 for each current value and for each

unbalance value (observe that for example for a 0 meters unbalance the contrast is higher than 0.9 for all current values) so the modes would be correlated and the linewidth of the laser would be narrow. To demonstrate that effectively the modes of the Fabry-Perot laser are correlated we measure the linewidth of a Fabry-Perot mode. As the linewidth of a Fabry-Perot can't be measured by analyzing the beat of two Fabry-Perot modes because this beat coincides with a very high frequency and our instruments don´t work to this frequency, we use a method called heterodyning method which consist in analyzing the beat of a Fabry-Perot mode with the mode of an ECL laser which has a very narrow linewidth and in this case the linewidth of the RF signal will practically correspond to the one of the Fabry-perot mode. The expected linewidth of the beating between modes, in case it could be measured directly is calculated for interpolation of the contrast of modulation plot with this we obtain the straight line equation. With this equation we can know when the contrast of modulation is zero and therefore what the laser correlation length is. The straight line equation is

where u is the unbalance value so the correlation length is 68.57 meters and the linewidth is calculated with:

Where is the linewidth of the Fabry-Perot laser and Lc the correlation length.

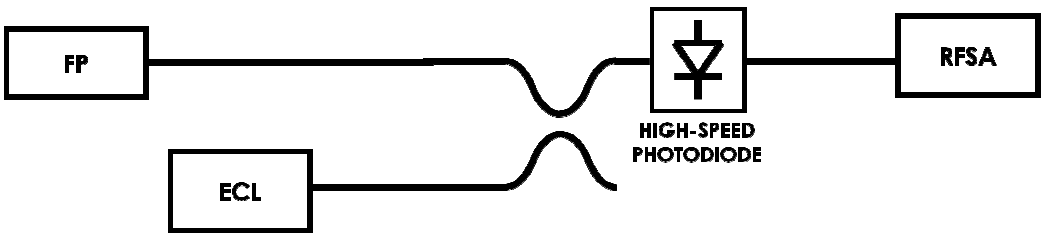

Figure 64: Linewidth measurement's of a Fabry-perot laser with heterodyning method

In this method we inject the Fabry-Perot laser in a coupler branch's and in the other one the ECL laser, the two signals will be beating on a high speed photodiode. Then to measure the linewidth we measure the linewidth of the visualized RF signal in the RFSA (RF spectrum analyzer) and divide this value by a right factor depending on whether the linewidth has been measured at -10 dB or at -30 dB of the maximum of the signal. This is because normally the linewidth is determined measuring the linewidth at -3dB of the maximum (FWHM-full width at half-maximum). To avoid problems due to the fluctuation of the emitted instant frequency of the laser the linewidth has been measured at -10 or -30 dB of the peak. This is a consequence of the form of the line. As this form isn´t Lorentzian the frequency fluctuations produce that in the area near to the peak where the line is narrower the spectrum is longer than it effectively is.

The Lorentzian optical spectrum at a center frequency ν_0 is given by:

$$S_E(\nu) \sim \frac{1}{1+\left[\frac{\nu-\nu_0}{\frac{\Delta\nu}{2}}\right]^2}$$

Where Δν is the FWHM and ν the optic frequency. When $\nu-\nu_0$ is zero $S_E(\nu)$, is maxima. Increasing $\nu-\nu_0$, $S_E(\nu)$ decrease. If the jitter of frequency δν(t) is present , the spectrum vary in the time:

$$S_E(\nu,t) \sim \frac{1}{1+\left[\frac{\nu-\nu_0+\delta\nu(t)}{\frac{\Delta\nu}{2}}\right]^2}$$

When $\nu-\nu_0$ is approximately δν, variations of δν produces important variations of $S_E(\nu)$ and as consequence of the linewidth FWHM. Increasing $\nu-\nu_0$ respect to δν the linewidth depend more on $\nu-\nu_0$ than δν and therefore

the linewidth and amplitude measurements will be closer than the effective values in distant zones to the peak. The measurement mistake is reduced. For a Lorentzian profile the relations for the linewidth and amplitude measurements in distant zones are reported on table 65

Distance of the peak	**Linewidth**
-3 dB	$\Delta\nu$
-10 dB	$\sqrt{9}\Delta\nu$
-20 dB	$\sqrt{99}\Delta\nu$
-30 dB	$\sqrt{999}\Delta\nu$

Figure 65: Relation between the measured RF linewidth and the real value

So we have done the measure of the linewidth for a Fabry-Perot current's of 120 mA and 56 mA, in each case we have done ten measurements and we have calculated the average. The results obtained are: for a current of 120 mA the linewidth is 6.625 MHz and for 56 mA is approximately of 7 MHz so as it is shown in the Figure 66 a the linewidth is similar for a current between 45-90 mA and for a current between 100-160 mA because the contrast average graphs are similar. These curves have been obtained calculating the average and variance of the contrast of the laser and of the contrast of the modulation for a current range of 45-90 mA and 100-160 mA.

The measurement of the linewidth of a single longitudinal mode was important to verify that the correlation between different longitudinal

modes resulted in an estimated bandwidth of the beating signal is roughly one order of magnitude smaller than the above mentioned linewidth.

As conclusion of this chapter we can say that it has been demonstrated that the modes of a Fabry-Perot laser can be partially locked via the FWM phenomenon, also without an externally injected signal. Future measurements will be performed with external light injection, to verify whether the correlation between modes will increase in the case that mode-locking is induced by FWM.

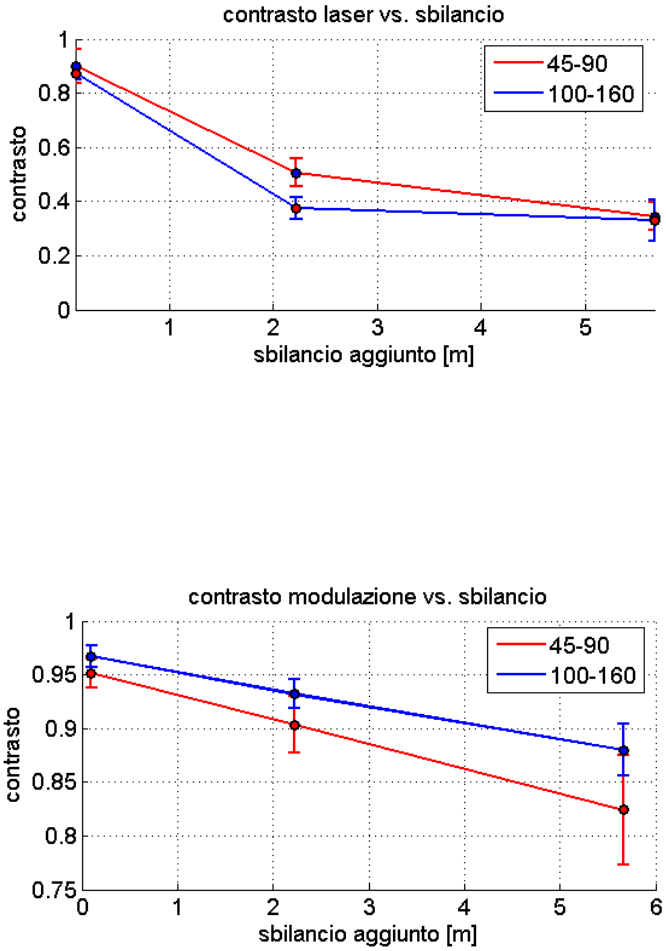

Figure 66: a) Contrast of laser average vs unbalance, b) Contrast of modulation average vs unbalance

CHAPTER 5

CONCLUSION

To conclude the present project we can say that the possibility of generating RF signals with DFB lasers mutually coupled has been verified. These lasers have been incorporated in an integrated device in such a way that the injection of DFB1 and DFB2 in a third laser called DFB-AUX is possible. By means of the FWM phenomenon the DFB1 and 2 are mutually coupled, and they can be phase-locked, so that a spectrally pure RF signal can be generated.

To start the activity all the DFB integrated lasers have been characterized obtaining their curves corresponding to:

Power-Current

SMSR-Current

λ_{peak}-current

Optical Spectra

To continue measurements on the couplers of every chip have been carried out to demonstrate that the coupling value is in effects corresponding the value defined in the specifications and the design of the device.

Then the FWM and injection locking experiments have been realized when 2 laser are on. In the BAR_A device 6 measurements (Chapter 3, paragraph 14) the FWM has been studied with and without attenuation. In the attenuation case the FWM is observed for a detuning value of 10 GHZ while

for a detuning of 5 GHz chaos is observed in the other case for a detuning of 20GHz a single FWM peak is observed, however if we decrease the detuning value to 15 GHz a new peak arise as consequence of FWM. Then demonstrate that FWM is generated between two DFB lasers mutually coupled we measure the FWM Gain. At first the FWM gain of DFB3 (BAR-B, device2) laser inside and outside the stop band of laser 2 has been measure concluding that the gain in the stop band is higher than outside the stop band. Then this FWM gain is measured varying the DFB3 current and maintaining constant the DFB1 current value first and then the DFB2 current, demonstrating that the gain decreases for increasing detuning: it means that when the distance in frequency between the DFB3 laser and the signal generated by FWM increases, the gain decreases. This is in agreement with the fact that the FWM gain is a decreasing function of the detuning.

Another measurement concerned the injection-locking between 2 lasers, now the experiment is realize on BAR E. It has been observed that whether two lasers are on and the current of one of them varies, it exists a point in which injection is produced and an only peak is observed with an increment of power. The locking range (the range of frequencies that lasers are locked) is of 9 GHz.

The last part of the project has been dedicated to the measurements of the contrast of the interferometric signal of a Fabry-Perot laser with the goal of demonstrating that the Fabry-Perot modes can be partially locked without the injection of an external signal. This fact has been demonstrated observing a contrast of modulation between 0.85 and 0.95 for each current value and measuring the linewidth of the laser.

New versions of integrated photonic devices have been fabricated by the University of Glasgow that will be the object of new experiments that will continue investigating the possibility of the generation of RF signal using photonic integrated circuits that realize the idea of the mutual injection-locking via FWM.

Bibliography

[1] Marco Soldo, *Generazione di segnali a onde millimetriche con laser a semiconduttore mutuamente accoppiati tramite Four-Wave-Mixing. Tesi di Laurea, Università degli Studi di Pavia, anno 2007-2008*

[2] Marco Soldo , Nicholas Gibbons, Guido Giuliani*, Narrow Linewidth mm-Wave Signal Generation based on Two Phase-Locked DFB Lasers Mutually Coupled via Four Wave Mixing,* University of Pavia, 2008.

[3] M Bondiou, R Gabet, G M Stéphan and P Besnard, *Linewidth of an optically injected semiconductor laser,* J. Opt. B: Quantum Semiclass, no. 2, pp 41-46, 2000.

[4] R.Goto, T.Goto, H.Kasuya, M.Mori and K.Yamane, *Mutual injection locking between two DFB LDs which lase at frequencies separated by one Fabry-Perot mode spacing,* Electronics Letters. Vol 34, pp. 1669-1670, 1998

[5] Stéphane Blin, Céline Guignard, Pascal Besnard, Renaud Gabet , Guy Michel Stéphan, Marc Bondiou, *Phase and spectral properties of optically injected semiconductor lasers,* C. R. Physique, Vol. 4, pp. 687-699, 2003.

[6] David Wake, Claudio R.Lima, Student Member IEEE and Phillip A. Davies, Member IEEE, *Optical Generation of Millimeter-Wave Signals for Fiber-Radio Systems Using a Dual –Mode DFB Semiconductor Laser*,IEE transactions on microwave theory and techniques, no 9,vol 43, 1995

[7] Hyuk-Kee Sung, *Strong Optical Injection Locking of Edge-Emitting Lasers and Its Applications,* Technical Report No. UCB/EECS-2006-107

[8] C. W. Thiel, *Four-Wave Mixing and its Applications*, http://staff.mbi-berlin.de/breusing/fwmixing.pdf.

[9] Guido Giuliani, *Optoelectronic integrated circuit for generation of tunable and narrow linewidth millimeter-wave signals,* Dipartimento di Elettronica Optoelectronics Group, 2004

[10] P. Bouyer, T. L. Gustavson, K. G. Haritos, and M. A. Kasevich, *Microwave signal generation with optical injection locking*, OPTICS LETTERS, Vol. 21, No. 18, 1996

[11] Hideaki Kasuya and Masakazu Moria, Yakusa-cho, Ryosuke Goto and Toshio Goto, Kazuo Yamane, *All optical mode locking of Fabry-Perot laser diode via mutual injection locking between two longitudinal modes,* App. Ph. Letters, Vol. 75, no. 1, pp.1502-1504, 1999.

[12] M. Al-Mumin, Xinhong Wang, Weiming Mao, *S.A Pappert and Guifang Li, Optical generation and sideband injection locking of tuneable 11-120 GHz microwave/millimeter signals,* Electronics Letters, Vol. 36, no. 18, pp.1547-1548, 2000.

[13] Andreas Stöhr and Dieter Jäger, *Photonic Millimeter-wave and Terahertz Source Technologies*, International Tropical Meeting on Microwave Photonics, 2006.

[14] R. W. TKACH and A. R. CHRAPLYVY, *Regimes of Feedback Effects in 1.5 μm Distributed Feedback Lasers*, Journal of Lightwave Technology, Vol. 4, no. 11, pp. 1655-1661, 1986

[15] R.B.M. Clarke , E. Riis , G.P. Barwood , P. Gill , G. Huang , H.A. Klein , *A sideband-injection locked extended cavity diode laser for interrogating cold trapped Strontium ions,* Optics Communications Vol. 158, p. 36-40, 1998

ACKNOWLEDGEMENTS

Finally I would like to thank all persons that have shared this year with me and have directly or indirectly taken a part in this project.

Firstly to thank Guido Giuliani the offered possibility of realizing my final degree project in the University of Pavia just as his help during these nine months.

To say thank you to Marco Soldo for his unquestionable patience in the days in which nothing worked or for his explications

On the other hand I would like to thank Marcello Simonetta his help in the last months of the project.

Specially thanks to my family for their understanding and advices in all these years and above all in the difficult moments

My friends have been too an important part in these years. Specially to thanks all the Pavia Erasmus group for that unforgettable travels, parties, picnics….I hope this continue the next years.

To finish to thank my “coinquiline” this nine months of life together in which I think I have found two really friends.

Thanks all….

ANEXO-SPANISH VERSION

Los sistemas de comunicación inalámbricos actuales están incrementando su penetración en la sociedad actual, tales sistemas de comunicación tienen elevados requisitos de ancho de banda. Para disponer de anchos de banda elevados es necesario la aparición de nuevos sistemas capaces de operar a frecuencias centradas alrededor de los 40 o 60 GHz. Estas bandas de frecuencia son bandas del espectro sin licencia y por tanto se pueden utilizar libremente.

Tales señales deben tener al mismo tiempo una elevada pureza espectral lo cual viene dado con una anchura de línea menor de 100 KHz y un ruido de fase menor de 100 dBc. Así mismo tales dispositivos deberán ser compactos, sintonizables, con bajo consumo de potencia y bajo coste.

Otras importantes aplicaciones en este campo serían:

1) Radares anti-colision (60GHz)

2) Osciladores locales para investigaciones astronómicas (100-900GHz)

3) Aplicaciones en el rango de los THz (300-3000GHz)

4) Meteorología

Entre las posibles tecnologías para la generación de señales milimétricas, existen actualmente tecnologías microelectrónicas las cuales pueden proveer frecuencias entorno a los 60 GHz (alcanzando incluso frecuencias de cientos de GHz) con la principal desventaja de que no son sintonizables, es decir un diseño realizado para operar a 60 GHz, no puede ser utilizado para operar también a 100GHz.

Como consecuencia de esta restricción surge el presente proyecto final de carrera, donde se pretende estudiar la generación de señales milimétricas mediante una técnica optoelectrónica basada en un efecto conocido como photomixing. Esta técnica resulta de gran interés debido a su sintonizabilidad, escalabilidad y la posibilidad de trasmitir las señales ópticas a lo largo de una fibra para permitir la generación remota de señales de radiofrecuencia. El photomixing es una técnica que consiste en la generación de señales de alta

frecuencia mediante dos láseres los cuales son enfocados en un photomixer el cual genera una radiación a una frecuencia igual a la diferencia de frecuencia entre los dos láseres ($|v1 - v2|$). Una de las restricciones fundamentales de esta técnica es la pureza espectral de la señal generada, puesto que ésta depende de la anchura de línea de los láseres empleados. Por esto es necesaria una nueva técnica cuyo fundamento base parte del photomixing pero que permita crear señales espectralmente puras.

El proyecto realizado en la Universitá degli studi di Pavia, está envuelto en un proyecto de investigación financiado por la fundación Cariplo cuyo principal objetivo es demostrar una nueva aproximación a la generación de señales milimétricas basándose en una modificación del esquema del photomixing. La principal idea en esta modificación es que dos láseres DFB emitiendo a frecuencias ν_1 y ν_2 pueden ser enganchados en fase mediante una inyección mutua asistida de una técnica conocida como FWM (Four Wave Mixing) que tiene lugar en un tercer láser DFB_Aux el cual oscila a una frecuencia $\nu_{AUX} = (\nu_1+\nu_2)/2$.

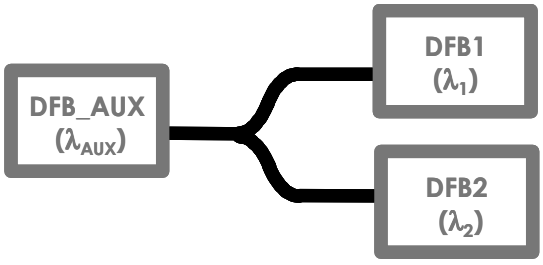

Figura 1: Scheme of mutual injection-locking assisted by FWM.

Un esquema conceptual de lo explicado anteriormente es mostrado en la figura 1. En este esquema las señales procedentes de los láseres 1 y 2 son inyectadas en el laser auxiliar en el cual como consecuencia del FWM se genera un clon de la señal del laser DFB1 a una frecuencia igual a $\nu_{1'}=2\nu_{aux}-\nu_1$ y un clon de la señal procedente del laser 2 a una frecuencia igual a $\nu_{2'}=2\nu_{aux}-\nu_2$. Cuando la señal procedente del laser auxiliar está situada exactamente a una frecuencia igual a la mitad de la frecuencia entre los láseres 1 y 2, se dice que el laser 2 está enganchado por inyección con la señal clon del laser 1 y que el laser 1 esté enganchado con la señal clon del laser 2. En esta condición los láseres DFB1 y DFB2 están mutuamente acoplados y el batido de la señal

generada por los laseres 1 y 2 (a frecuencia $f_{RF}=|f_1-f_2|$) será una señal de radiofrecuencia de una elevada pureza espectral.

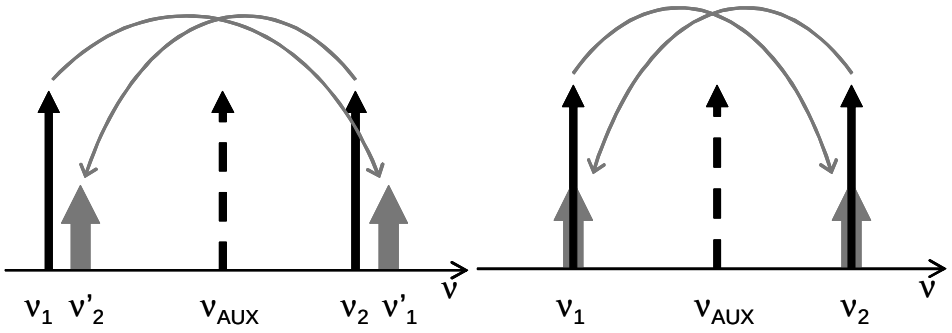

Figura 2 a) unlocking condition. b) mutual injection locking condition

El FWM es producido en el interior del láser DFB_Aux debido a las características no lineales de los materiales semiconductores. Gracias a esta novedosa técnica, la señal de radiofrecuencia generada tendrá una anchura de línea pequeña debido a la relación constante de fase en el tiempo entre los láseres 1 y 2. Otra ventaja introducida por este método es el comportamiento como amplificador del láser auxiliar el cual compensa las pérdidas sufridas por la señal antes de ser inyectada en el mismo.

Para verificar la técnica explicada anteriormente se han realizado pruebas sobre varias barras de dispositivos fabricadas en la universidad de Glasgow. Estas barras cuentan con un gran número de dispositivos cada uno de los cuales tiene una configuración como la observada en la figura 3.

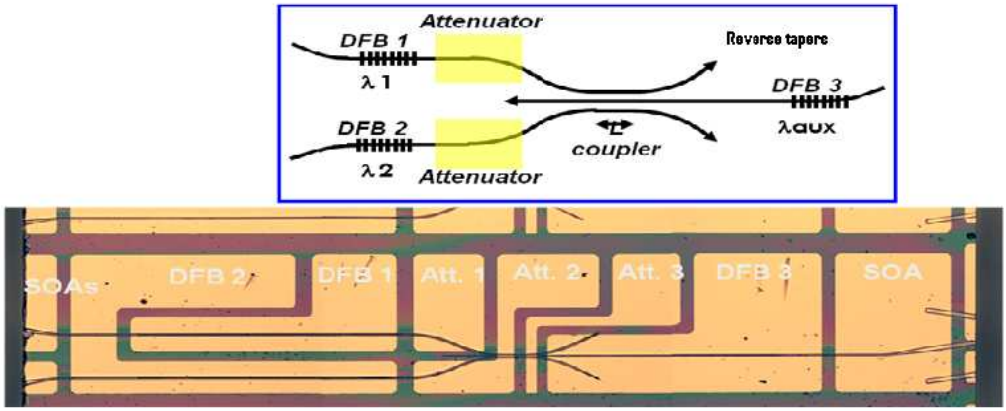

Figura 3: layout of the integrated device

La imagen inferior es una foto de cada dispositivo visto en el microscopio donde como se puede observar, cada hueco corresponde a un laser, atenuador o amplificador óptico. Para la alimentación de cada láser se han utilizado unas puntas móviles de elevada precisión que nos permiten posicionarnos sobre cada uno de los huecos mostrados.

Además de los láseres y atenuadores, el setup cuenta con un acoplador de una determinada longitud L que permite el acoplo de las señales procedentes de los láseres 1 y 2 en la guía del láser 3 y por tanto la generación del efecto del FWM.

Las primeras medidas realizadas en el laboratorio son las referentes a la caracterización individual de cada uno de los láseres, es decir para cada laser hemos obtenido su espectro, la longitud de onda de pico con respecto a la corriente, el SMSR (Side mode suppression ratio) con respecto a la corriente y las gráficas de potencia óptica de salida-corriente inyectada. Para la obtención de cada una de las gráficas se ha empleado el software Laview el cual nos permite obtener ficheros de texto con los valores de medida deseados y mediante Matlab realizar cada una de las gráficas. La temperatura de cada una de las barras ha sido controlada con una peltier que permite mantener el dispositivo a una temperatura constante y un termistor ambos conectados a un TEC (Temperature Electrical Controller).

Como se puede observar en la figura 4 la barra está situada sobre un soporte de metal y esta a su vez está colocada sobre una base móvil que permite desplazar el chip. Del mismo modo las fibras para la visualización de la señal en el OSA (optical spectral analyzer) están colocadas sobre un soporte fijado con tornillos a una base que permite mover la fibra en dirección x, y ,z de manera que se pueda acoplar perfectamente la fibra a cada una de las salidas de los láseres. Uno de los procedimientos iniciales antes de cualquier medida es el alineamiento de la fibra lo cual se realiza moviendo esta base en la dirección oportuna hasta que obtengamos el mayor valor de potencia posible medido mediante un Power Meter.

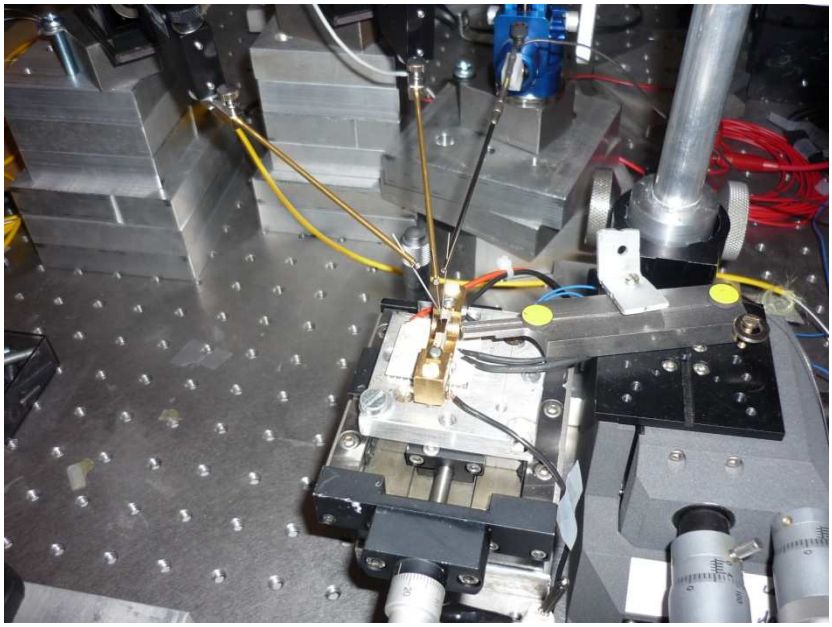

Figura 4: Montaje experimental

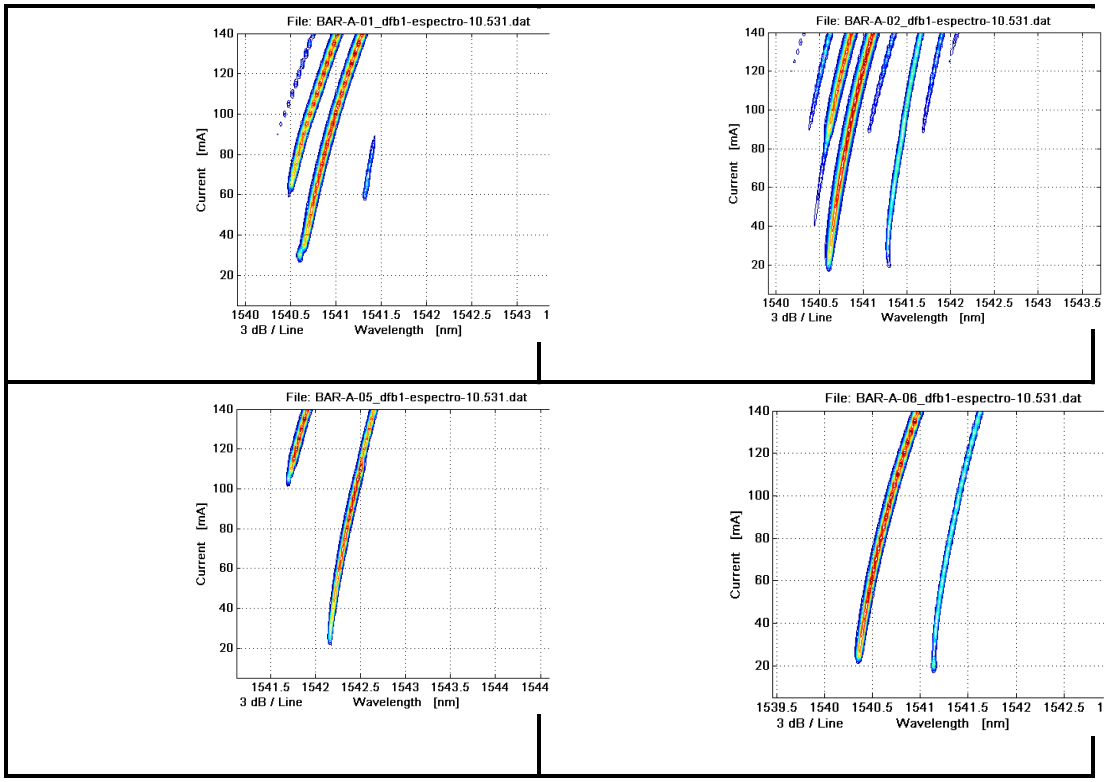

Figura 5: Espectro de los dispositivos 1,2, 5, 6, laser DFB1 de la barra A

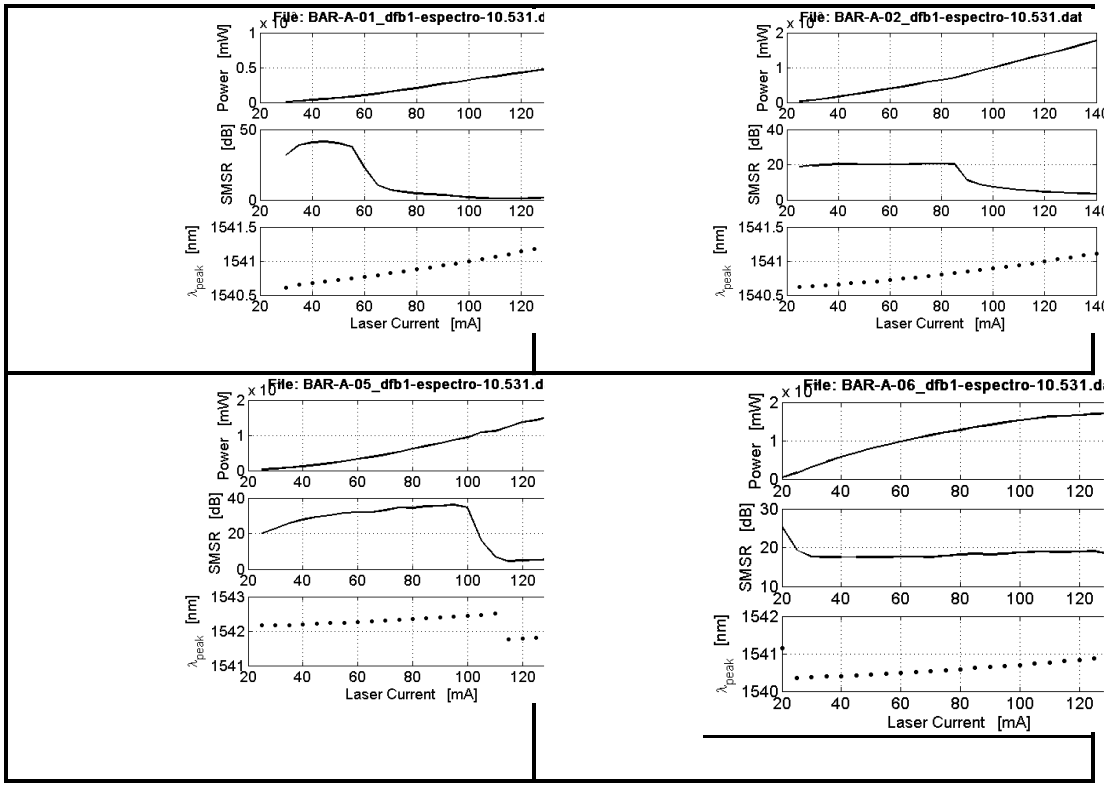

Figura 6: Graficas obtenidas de los dispositivos 1, 2, 5, 6, laser DFB1 de la barra A

En las figuras 5 y 6 se pueden ver las gráficas obtenidas para la caracterización del laser DFB1 de cada uno de los dispositivos que componen la barra A. Esta caracterización ha sido también realizada para los láseres 2 y 3 así como para los láseres de la barra B.

En estos láseres como su nombre indica la realimentación se hace de una manera continua a lo largo de toda una determinada zona del láser, esta zona es toda la longitud que abarca la región activa de los mismos. La manera de conseguir la realimentación no consiste ya en los espejos que forman la cavidad de un laser Fabry-Perot sino mediante una red de difracción de Bragg dispuesta a lo largo de la estructura del dispositivo.

Los espejos a las salidas del dispositivo se suelen eliminar recubriendo las caras de salida del material semiconductor con un material antirreflejante. La red de difracción se forma al variar de forma periódica el índice de refracción a lo largo del je z. Λ define el periodo de dicha variación y $K = \frac{2\pi}{\Lambda}$ es el vector de onda asociado. La perturbación periódica del índice de refracción origina

la aparición de dos modos que se propagan en direcciones opuestas a lo largo de la estructura. Solo en el caso de que la longitud de onda de la señal sea próxima o igual a la longitud de onda de Bragg $\lambda_B = 2\bar{n}\Lambda$ los modos intercambian de forma continua energía.

El problema que surge es que el láser DFB está concebido para ser un laser monomodo y como hemos visto la perturbación periódica del índice de refracción originaría la aparición de dos modos y en el caso de los láseres empleados en el proyecto aparecen en ocasiones más de dos. Para evitar este problema se emplea una estructura DFB ligeramente modificada, donde una zona central en la que no existe perturbación del índice de refracción provoca un desfase $\pi/4$ y en ella los dos modos se desplazan hasta coincidir en uno solo cuya frecuencia de oscilación es $w_{B.}$ Otra forma de conseguir oscilación monomodo es colocar espejos selectivos en frecuencia a la salida del dispositivo que seleccionen uno de los dos modos principales de oscilación. Los nuevos láseres que actualmente se siguen fabricando en la Universidad de Glasgow dispondrán de este conjugador de fase $\lambda/4$.

Una vez caracterizados cada uno de los láseres se han realizado las medidas concernientes a los acopladores que forman cada dispositivo con el objetivo de comprobar si su valor de acoplo coincide con el valor dado en las especificaciones del dispositivo. Efectivamente se demostró que los acopladores funcionaban correctamente con valores de acoplo del 1%.

Seguidamente realizamos el experimento del Four-Wave-Mixing producido entre dos láseres DFB. En esta medida se ha empleado el dispositivo 6 de la barra A porque tiene la longitud de onda más cercana entre los tres láseres y el SMSR mayor y por tanto es más fácil identificar la nueva señal a la nueva frecuencia generada por FWM. Para realizar este experimento hecho con y sin atenuación se mueve la corriente de uno de los láseres mientras la del otro se mantiene fija cambiando por tanto el valor de detuning entre ellos y observando si se produce Four-Wave-Mixing o chaos.

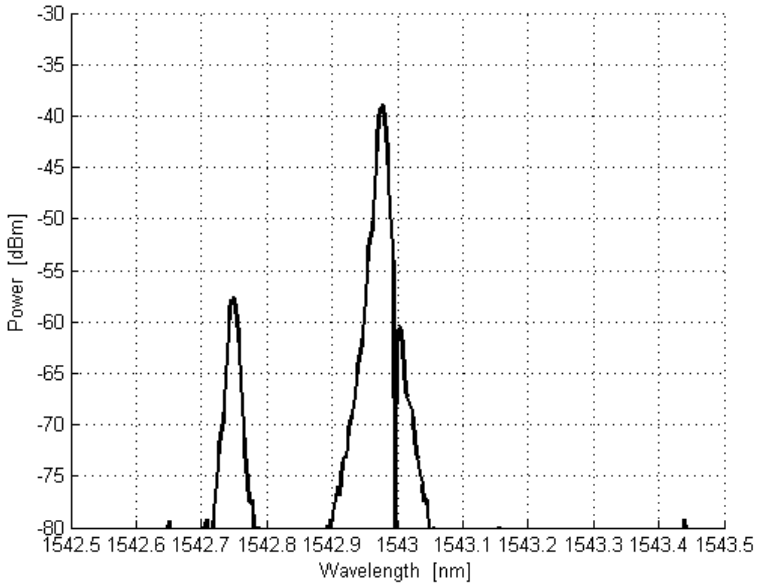

Figura 7: Detuning 30 GHz, con atenuación

En la figura 7 se pueden ver claramente los dos picos correspondientes a el laser DFB3 (izquierda) y DFB2 (derecha), en este caso no se produce un detectable FWM, sin embargo en la figura de abajo cuando el detuning entre los láseres se reduce a 10 GHz aparecen 2 nuevos picos correspondientes al efecto de FWM así los picos observados corresponden al modo el laser DFB2 (194.4342546THz), el modo del laser DFB3 (194.4236699THz), y los dos picos correspondientes al FWM generados a frecuencias $2V_2$-V_3 (194.4452186 THz) y $2V_3$-V_2 (194.4130863THz).

Por último cuando el valor de detuning es reducido hasta 5 GHz el FWM no puede ser observado porque aparece una situación de caos. Esta situación de caos es debida a que la porción de luz inyectada por el laser 3 en el laser 2 y por tanto amplificada y reflejada hacia el laser 3 es muy grande.

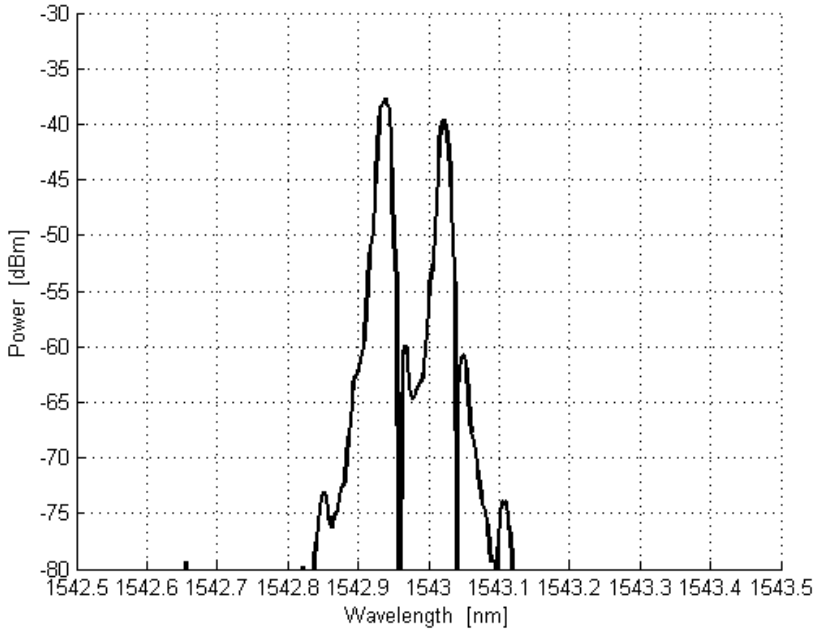

Figura 8: Detuning 10GHz, con atenuación

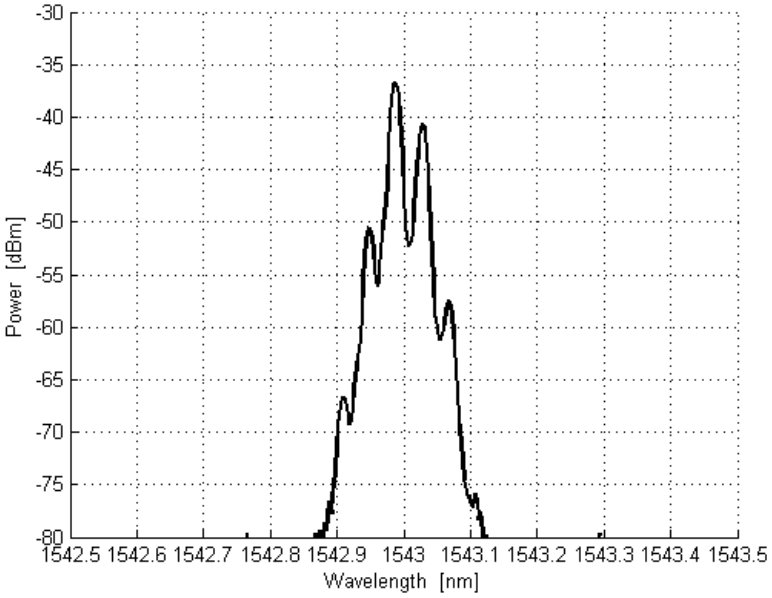

Figura 9: Detuning 5GHz, con atenuación

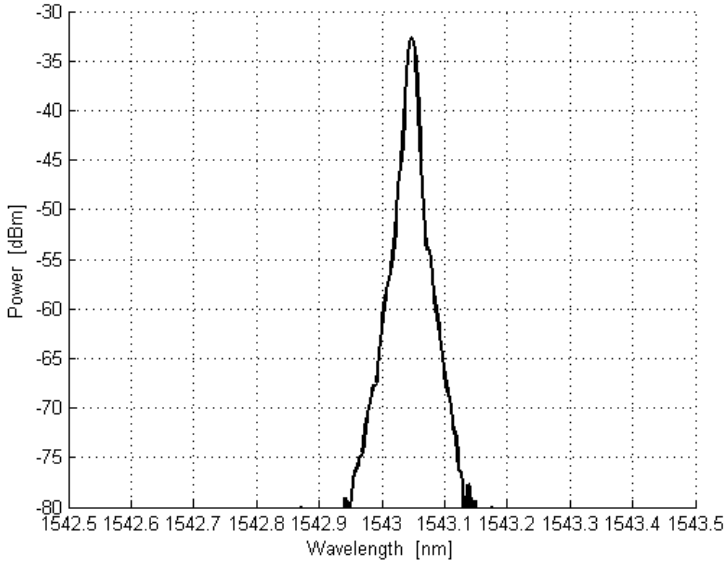

Figura 10: Detuning 0GHz, con atenuación

En el caso de un detuning de 0GHz el efecto mostrado se denomina injection-locking en el cual los dos picos observados inicialmente degeneran en un solo pico.

El injection-locking se refiere a los efectos de frecuencia que pueden ocurrir cuando un oscilador es disturbado por un segundo oscilador operando a una frecuencia cercana.

Cuando el acoplo es suficientemente alto y las frecuencias suficientemente cercanas el segundo oscilador puede capturar al primer oscilador haciendo que tenga una frecuencia idéntica al segundo. Esta técnica puede ser usada para sincronizar un oscilador esclavo con un master, inyectando la luz emitida por el master en el laser esclavo y si ciertas condiciones son cumplidas el laser esclavo emitirá luz a la misma frecuencia y con una relación constante de fase con el laser master.

Existe un cierto valor de R (radio entre la potencia inyectada por el master y la potencia del laser esclavo) para el cual el locking es producido y es mostrado en la grafica 11:

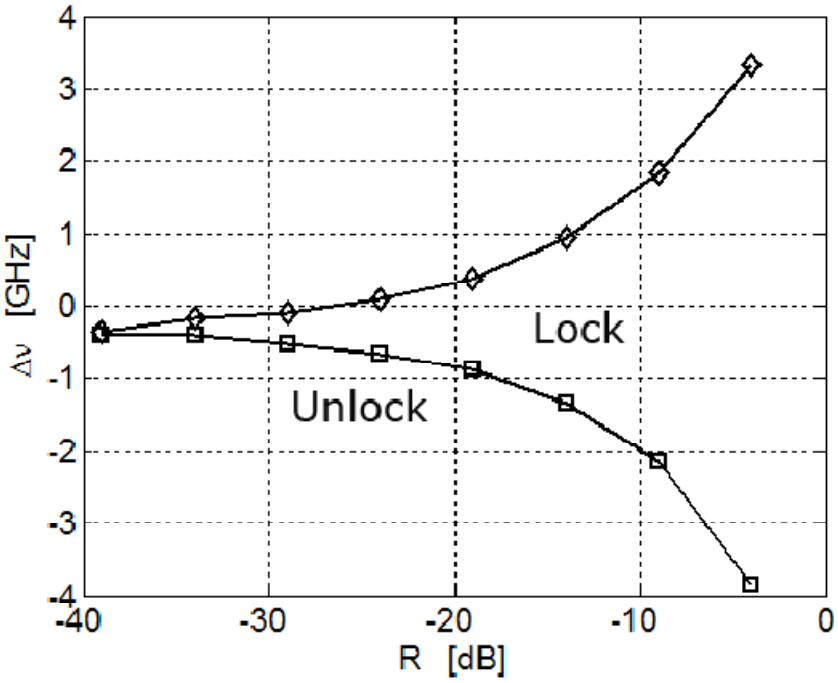

Figura 11: Detuning-R

Otro de los parámetros que pueden ser medidos son la ganancia óptica y la ganancia de FWM del laser AUX usado como amplificador óptico en una configuración en reflexión. La ganancia de FWM nos da una idea de la eficiencia del proceso de FWM. La primera de ellas es obtenida como:

$G_{aux}=P_{out}/P_{in}$;

Donde P_{in} es la potencia inyectada en el laser DFB-AUX y P_{out} es la señal amplificada a la misma longitud de onda de P_{in} que es reflejada por el laser Auxiliar.

La ganancia de FWM puede ser medida como:

$G_{FWM}=P_{FWM}/P_{in}$

Donde P_{FWM} es la potencia de la señal generada por FWM en el laser auxiliar.

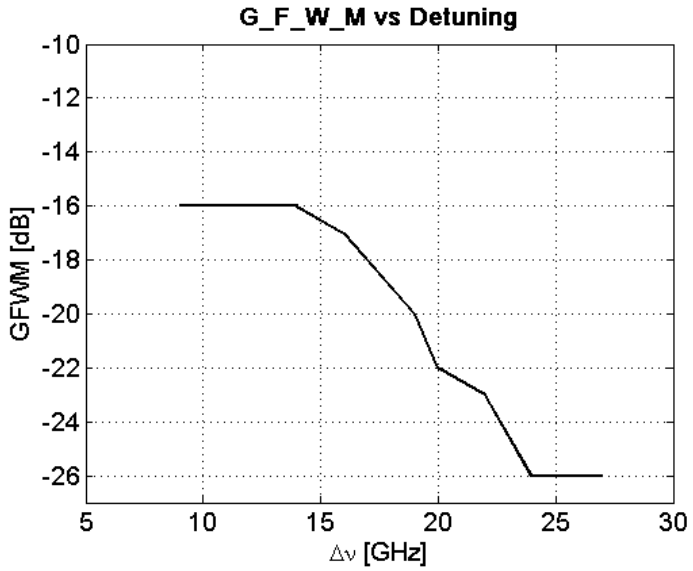

Figura 12: Ganancia de FWM con lasers 2 y 3 encendidos

Como conclusión a estas medidas podemos decir que la ganancia de FWM decrece con el incremento del detuning, es decir cuando la distancia en frecuencia entre el laser AUX (DFB3) y la señal generada por FWM incrementa.

En la última parte del proyecto se ha propuesto un nuevo método para medir la correlación entre los modos de un laser Fabry-Perot mediante un interferómetro. Para comprobar que efectivamente los modos de un Fabry-Perot pueden estar enganchados sin necesidad de la inyección de una señal externa se ha puesto en marcha un setup como el de la figura 13:

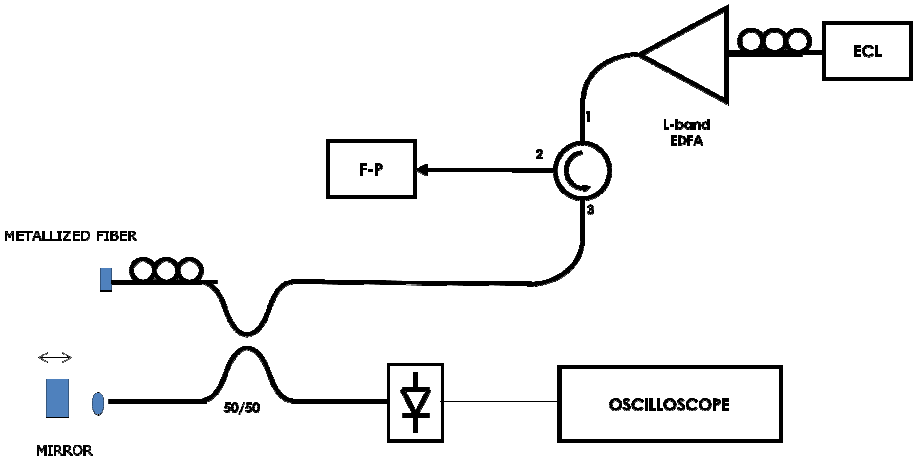

Figura 13: Setup utilizado con un interferómetro de Michelson

Como puede observarse el setup empleado consta de un laser ECL (External-Cavity-Laser), un amplificador óptico que amplifica longitudes de onda entre 1570 nm y 1610 nm, un circulador y un interferómetro.

El interferómetro usado es un interferómetro de Michelson el cual dispone de dos brazos. La luz que llega al interferómetro se divide en dos caminos diferentes y será recombinada para producir un patrón de interferencia. En nuestro caso uno de los brazos del interferómetro está compuesto de un control de polarización y una fibra metalizada que hace volver la luz hacia atrás, y el otro brazo está compuesto de un espejo el cual se mueve mediante un pequeño motor.

Para medir la correlación entre los modos de un Fabry-Perot se desplaza el espejo situado en el interferómetro para crear franjas de interferencia. El contraste de las franjas se mide para diferentes valores de desequilibrio (diferencia de longitud entre los brazos del interferómetro). Pintando el contraste en función del desequilibrio entre los brazos del interferómetro se puede medir la longitud de correlación de los modos del laser Fabry-Perot.

El contraste del laser está relacionado con la anchura de línea del mismo, por lo tanto si su valor es próximo a 1 la anchura de línea es estrecha. Por otro lado el contraste de modulación nos dice si los modos del laser están correlados, como puede observarse en la figura 14 b el contraste de modulación incrementa ligeramente con el incremento de corriente.

Como conclusión de estas medidas podemos pensar que los modos del laser Fabry-Perot están parcialmente enganchados en fase sin la inyección de una señal externa debido a que el contraste de modulación está comprendido prácticamente entre 0.85 y 0.95 para cada valor de corriente. Para demostrar que efectivamente los modos del laser están correlados es necesario realizar la medida del ancho de línea de un modo longitudinal del laser. Para realizar esta medida se utilizó un método llamado heterodino en el cual básicamente se analiza el barrido entre un modo del Fabry-Perot y un modo de un laser ECL el cual tiene una anchura de línea muy pequeña y por lo tanto la anchura de línea medida corresponderá prácticamente a la del modo del Fabry-Perot. La anchura de línea esperada del batido entre los modos de un laser Fabry-Perot en el caso de que pudiera ser directamente medida será 0.696MHz y es obtenida a partir de la gráfica del contraste de modulación en función del desequilibrio entre los brazos del interferómetro.

Sin embargo cuando realizamos las medidas con el método heterodino, para una corriente del Fabry-Perot de 120 mA y de 56 mA se obtienen anchuras de línea de 6.625 MHz y 7 MHz respectivamente y por lo tanto la anchura de línea es similar para el caso de una corriente entre 45-90 y una corriente entre 100-160 tal y como puede observarse en la figura 15 a donde la gráfica del contraste del laser medio en función de la diferencia de caminos entre los brazos del interferómetro son similares.

Por lo tanto queda demostrado que los modos del Fabry-Perot están parcialmente correlados a través del efecto de FWM sin la ayuda de una señal externa inyectada entre los modos del láser, ya que las anchuras de línea obtenidas de las medidas realizadas con el método heterodino están un orden de magnitud por encima de la que se obtendría en caso de que pudiera ser medida directamente tal y como se esperaba y por tanto la aproximación realizada con el método directo es válida.

En un futuro se realizarán medidas que verifiquen si la correlación entre los modos se incrementaría con la inyección de una señal externa y por tanto la generación de un efecto conocido como mode-locking inducido por FWM.

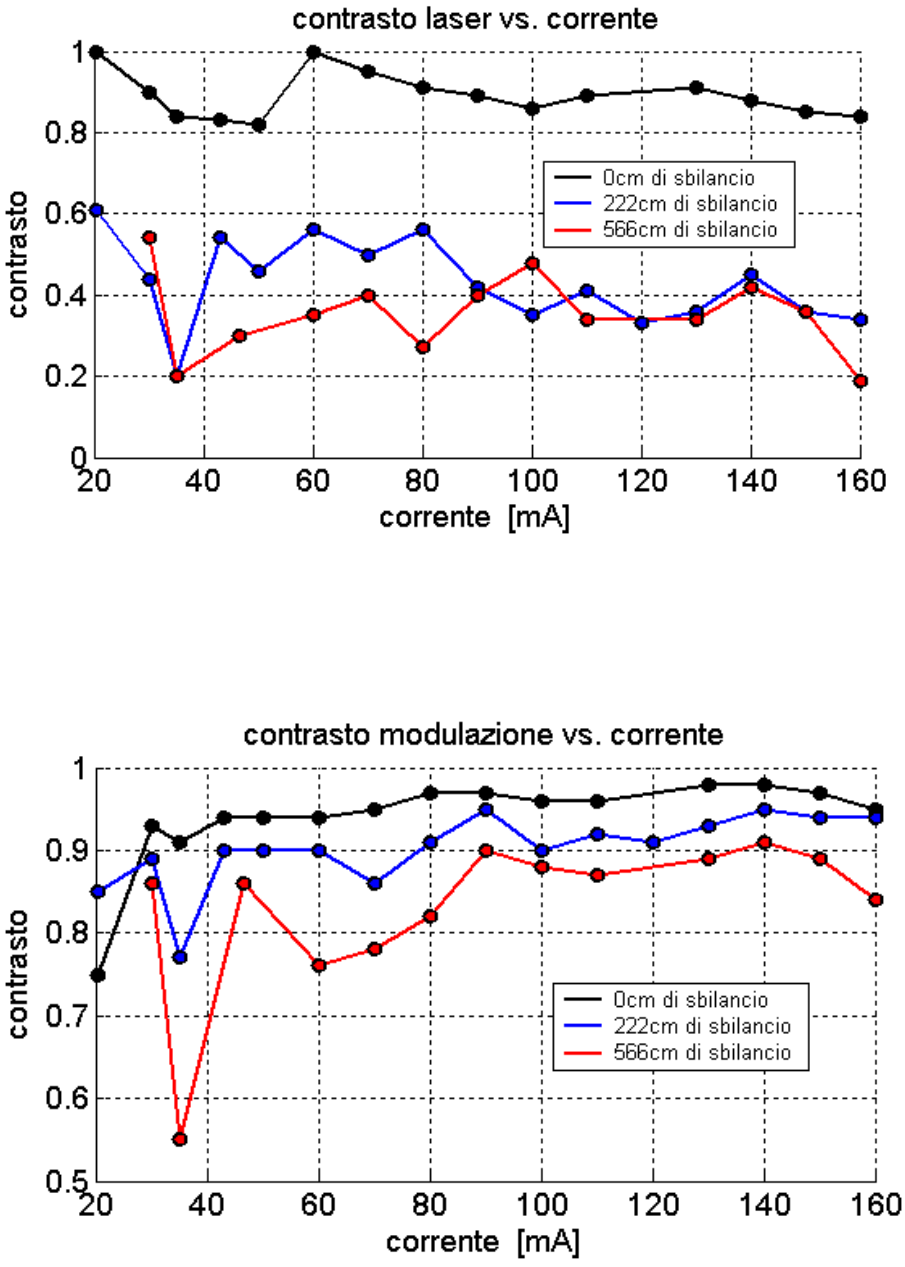

Figura 14 a) Contraste de laser b) Contraste de modulación

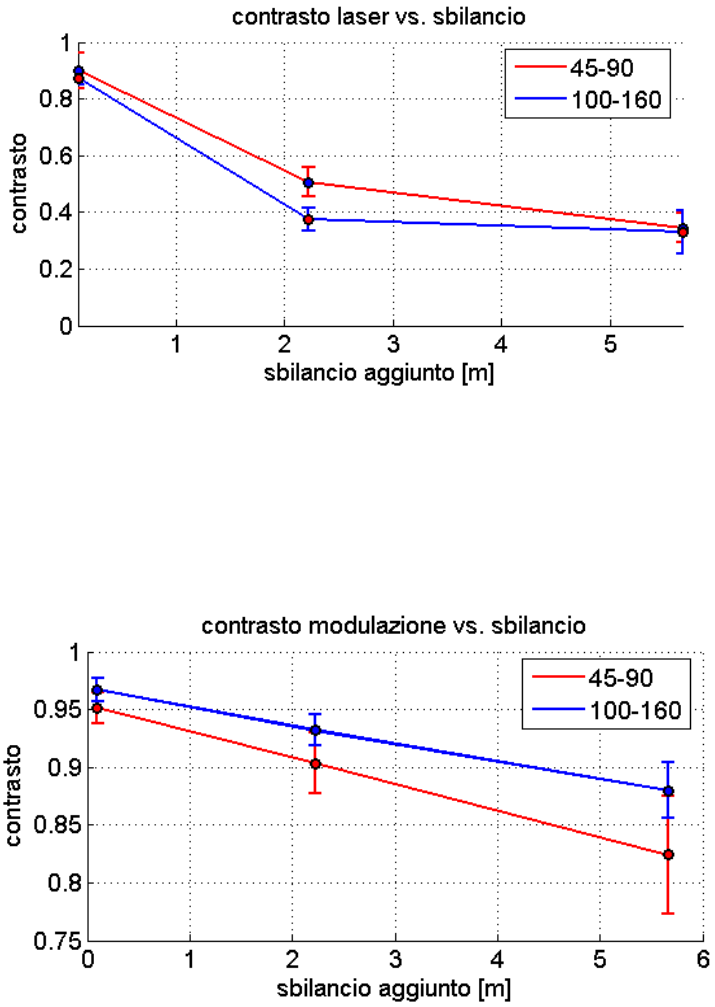

Figura 15: a) Contrast of laser average vs unbalance, b) Contrast of modulation average vs unbalance